

AD-A048 344

LTV AEROSPACE CORP DALLAS TEX VOUGHT SYSTEMS DIV
SEATIDE ANALYSIS PROCESS, VOLUME IIIB, CRUISE MISSILE - CONCEPT--ETC(U)
JAN 74

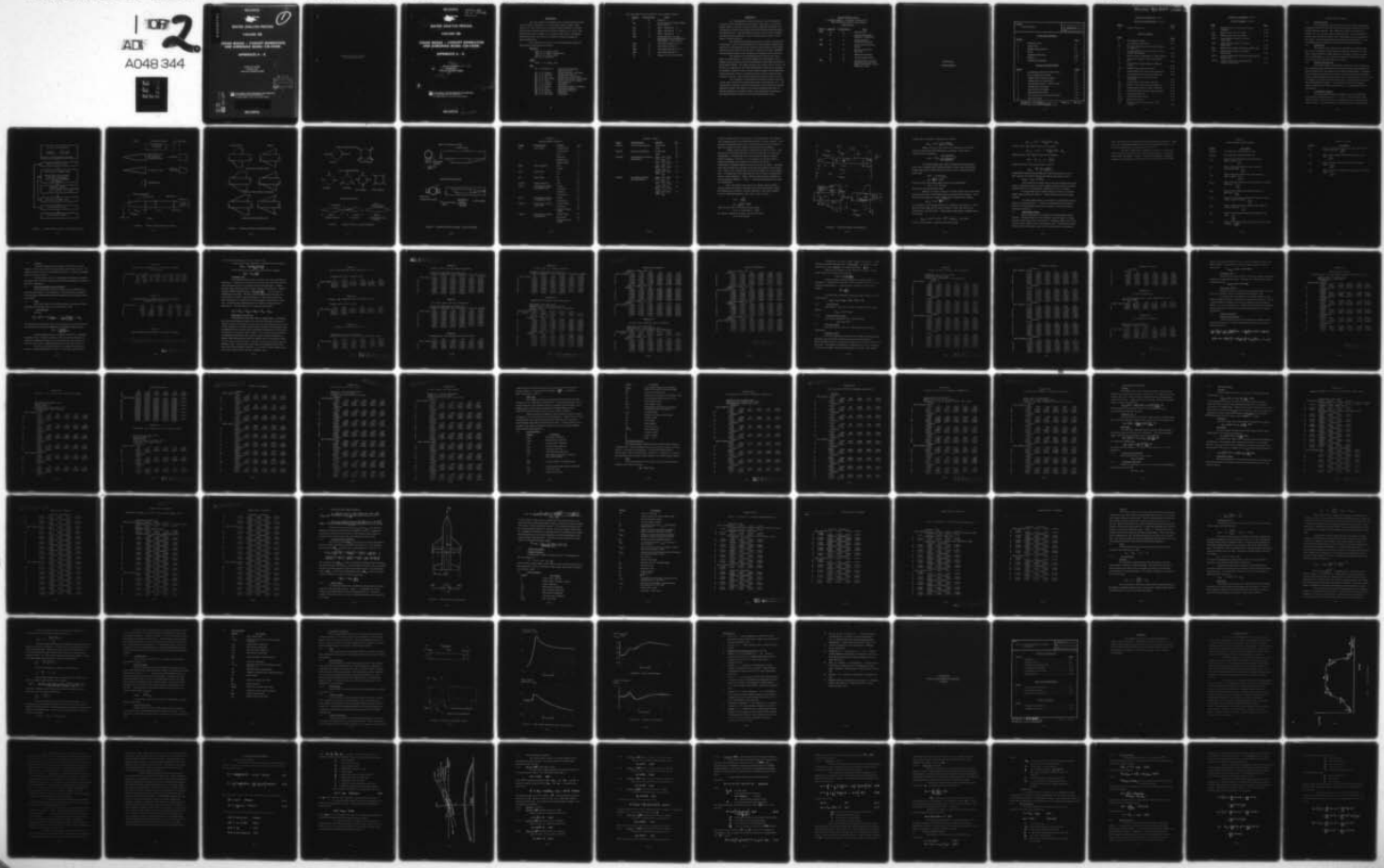
F/G 15/7
DAAB09-72-C-0062

UNCLASSIFIED

VSD-00.1636-VOL-3B

NL

TOP
AD
A048 344



ADA 048344

UNCLASSIFIED

12



B.S.

SEATIDE ANALYSIS PROCESS

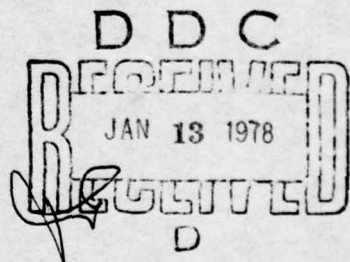
VOLUME IIIB

CRUISE MISSILE – CONCEPT GENERATION AND SCREENING MODEL (CM-CGSM)

APPENDICES A - B

REPORT NO. 00.1636
JANUARY 1974
(CONTRACT DAAB09-72-C-0062)

111D
A048344-365



VOUGHT SYSTEMS DIVISION
LTV AEROSPACE CORPORATION
P.O. BOX 5907 • DALLAS, TEXAS 75222

DISTRIBUTION STATEMENT A
Approved for public release;
Distribution Unlimited

AD 12.
DDC FILE COPY
AD 12.
DDC

UNCLASSIFIED

Approved for public release;
distribution unlimited.

UNCLASSIFIED

VMSC/SEATIDE/ 1108
ITEM 1 COPY NO. 12
FILE _____



6
SEATIDE ANALYSIS PROCESS.

VOLUME IIIB .

**CRUISE MISSILE – CONCEPT GENERATION
AND SCREENING MODEL (CM-CGSM).**

APPENDICES A - B .

ACCESSION NO.	REF ID:		
BTM	DATE ISSUED:		
BTG	DATE ISSUED:		
RECORDED BY:	DATE ISSUED:		
INITIALS	DATE ISSUED:		
BY:			
DISTRIBUTION/AVAILABILITY CODES			
CLASS	TYPE	EXPIRE DATE	SPECIAL
R			

(14) VSD-
REPORT NO. 00.1636 - VOL-3B

(11) JANUARY 1974
(CONTRACT DAAB09-72-C-0062)

(12) H.P.

(15)

D D C
DECLASSIFIED
JAN 18 1978
RELEASER
D



**VOUGHT SYSTEMS DIVISION
LTV AEROSPACE CORPORATION
P.O. BOX 5907 • DALLAS, TEXAS 75222**

DISTRIBUTION STATEMENT A
Approved for public release;
Distribution Unlimited

UNCLASSIFIED

408116

LB

FOREWORD

(U) This report was prepared by the Vought Systems Division, LTV Aerospace Corporation, P.O. Box 6267, Dallas, Texas 75222 under U. S. Army Electronics Command Contract DAAB09-72-C-0062. The work was initiated under the direction of Captain R. A. Dowd, USN and completed under Captain W. A. Greene, USN, Chief, Long Range Forecast Division, Directorate of Estimates, Defense Intelligence Agency (DIA-DE-1).

(U) Persons contributing to the development and testing of the procedure reported herein include:

DIA-DE-1

Capt. W. A. Greene, USN
Capt. R. A. Dowd, USN (Retired)
Capt. R. F. Weiss, USAF
Mr. R. E. McQuiston

ARPA

Cmdr. T. W. Hogan, USN

VSD

Mr. J. S. Smith, Jr.	Chief Project Engineer, Special Projects
Dr. L. D. Gregory	Project Engineer, SEATIDE
Mr. J. R. Matthews	Models and Analysis
Mr. F. E. Dye, Jr.	Technologies (CM-CGSM)
Mr. R. K. McDonough	Models and Analysis (CM-CGSM)
Mr. R. E. Dyer	Models and Analysis (NEM)
Mr. G. G. Johnson	Aerodynamics
Dr. J. A. Bottorff	Propulsion
Mr. A. C. Morris	Electronics (Radar, Guidance)
Mr. H. R. Crow	Operations Research
Mr. G. H. Harris	Operations Research
Mr. G. S. McCorkle	Propulsion
Mr. L. D. Cardwell	Propulsion

(U) This report has been prepared in the following volumes:

<u>Volume</u>	<u>Classification</u>	<u>Title</u>
I	S	Summary
IIA	U	Naval Engagement Model (NEM) - Users Manual
IIB	U	NEM - Appendices A - I
IIC	S	NEM - Appendices J - M
IID	U	NEM - Appendices N
IIIA	U	Cruise Missile - Concept Generation and Screening Model (CM-CGSM) - Users Manual
IIIB	U	CM-CGSM Appendices A-B
IIIC	S	CM-CGSM Appendix C
IID	U	CM-CGSM Appendices D-G
IIIE	U	CM-CGSM Appendix H
IV	S	Relative Worth Model (RWM)

ABSTRACT

(U) The SEATIDE Analysis Process is a semi-automated procedure for the generation of time-phased, high value cruise missile weapon systems concepts, together with the supporting technology and intelligence indicators which would reflect that these technological goals are being achieved. The SEATIDE process can also be used to evaluate the effectiveness of fixed force levels, existing forces in SAL environments, or Naval defenses.

(U) The Defense Intelligence Agency, through its Directorate of Estimates, and The Advanced Research Projects Agency (ARPA) have sponsored the development of this computer based analysis at the weapon system and Naval force structure level. A previous process, RIPTIDE, was developed for DIA for use in analysis of strategic missile systems.

(U) Generic to the SEATIDE Analysis Process are three major computer models: The Naval Engagement Model (NEM), Cruise Missile Concept Generation and Screening Model (CM-CGSM) and Relative Worth Model (RWM). The NEM evaluates force effectiveness, tactics, and task force configurations; the CM-CGSM enables definition and selection of candidate, advanced cruise missile system concepts; and the RWM permits assessment of worth in accordance with a variety of objective and subjective criteria. Each of these models has been checked out by DIA.

(U) In addition to exercising the computer models, there are several other analytical and engineering tasks to be performed, e.g., the identification of areas of current interest and the associated criteria and potential concepts, the creation of a foreign technology data bank in a format needed by the computer models, the engineering of concepts to the required detail, and the use of a verification analysis loop.

TABLE OF CONTENTS :--

CRUISE MISSILE - CONCEPT GENERATION
AND SCREENING MODEL (CM-CGSM) --

APPENDICES -

<u>Volume</u>	<u>Appendix</u>	<u>Classification</u>	<u>Title</u>
IIIB	A	U	Aerodynamics
	B	U	Vehicle Performance Submodel (VEHPER)
IIIC	C	S	Liquid and Solid Propulsion Submodel
IID	D	U	Cruise Missile Booster Sizing
	E	U	Inlet Sizing and Performance
	F	U	Ramjet Sizing Model
	G	U	Turbojet Sizing Model
IIIE	H	U	Cruise Missile - Concept Generation and Screening Model (CM-CGSM) - Source Program Listing

APPENDIX A
AERODYNAMICS

TITLE:

AERODYNAMICS

NO. Appendix A

DATE

TABLE OF CONTENTS

<u>Section</u>		<u>Page</u>
1.	INTRODUCTION	A-5
2.	OBJECTIVE	A-5
3.	MODEL DESCRIPTION	A-5
4.	BODY	A-20
5.	LIFTING SURFACES	A-40
6.	INLETS	A-59
7.	EXTERNAL BOOSTER	A-65

LIST OF ILLUSTRATIONS

<u>Figure</u>		<u>Page</u>
1	Aerodynamics Model Functional Flow	A-6
2	Body Configuration Options	A-7
3	Lifting Surface Planform Option	A-8
4	Lifting Surface Arrangements	A-9
5	Configuration Options - Inlet Systems	A-10
6	Configuration Parameter	A-14
7	Wing Vortices Geometry	A-52
8	External Booster Model	A-66
9	Nose Cone Pressure Drag Coefficient	A-67
10	Lift Curve Slope	A-68

PREPARED BY G.G. Johnson
APPROVED BY L.D. Gregory C.L.D.S.

PAGE 1 OF 70

Preceding Page BLANK - NOT FILMED

TABLE OF CONTENTS (Cont'd.)

LIST OF ILLUSTRATIONS (Cont'd.)

<u>Figure</u>		<u>Page</u>
11	Center of Pressure	A-68

LIST OF TABLES

<u>Table</u>		<u>Page</u>
I	Aerodynamic Options	A-11
II	Aerodynamic Coefficients	A-18
III	Reynold's Number per ft per Mach Number vs. Altitude	A-21
IV	Compressibility Correction Factor vs Mach Number and Altitude	A-21
V	Base Pressure Coefficients vs. Mach Number	A-21
VI	Ogive Nose Pressure Drag Coefficient at $M=1$	A-23
VII	Conical Nose Pressure Drag Coefficient at $M=1$	A-23
VIII	Boattail Drag Coefficient at $M=1$	A-23
IX	Tangent Ogive Nose Wave Drag Coefficient .	A-24
X	Von Karman Nose Wave Drag Coefficient . .	A-24
XI	Hemispherical Nose Pressure Drag Coefficient.	A-24
XII	Conical Nose Wave Drag Coefficient.	A-25
XIII	Blunted Cone Pressure Drag Coefficient. . .	A-25
XIV	Blunted Ogive Pressure Drag Coefficient. . .	A-26
XV	Conical Boattail Pressure Drag Parameter. .	A-29
XVI	Lug Drag Coefficient	A-31
XVII	Munk's Efficiency Factor	A-31
XVIII	Boattail Lift Factor	A-33
XIX	Supersonic Lift Curve Slope for Cone- Cylinders	A-34

TABLE OF CONTENTS (Cont'd.)

LIST OF TABLES (Cont'd.)

<u>Table</u>		<u>Page</u>
XX	Supersonic Lift Curve Slope for Ogive-Cylinders	A-35
XXI	Blunted Cone Lift Curve Slope	A-37
XXII	Blunted Ogive Lift Curve Slope.	A-38
XXIII	Cone-Cylinder Center of Pressure (Supersonic)	A-41
XXIV	Ogive Cylinder Center of Pressure (Supersonic)	A-42
XXV	Blunted Cone Center of Pressure (Supersonic).	A-43
XXVI	Blunted Ogive Center of Pressure (Supersonic)	A-44
XXVII	Subsonic/Supersonic Lift Curve Slope/Surface Aspect Ratio.	A-47
XXVIII	Center of Pressure of Lifting Surface (Subsonic/Supersonic).	A-55

AERODYNAMICS MODEL

1.0 INTRODUCTION

The Aerodynamics Model is designed to provide the aerodynamic parameters required by the CM-CGSM for the general solution to the cruise missile synthesis problem. The coefficients required for performance analysis (C_L , C_D) are the primary output; however, certain elements of the pitch and roll characteristics of the configuration are also computed in the module. The Missile Synthesis and Performance Routine (Ref. 1) was used extensively as a model for the SEATIDE Aerodynamics Model.

2.0 OBJECTIVE

The objective of the program is to provide a description of the basic force coefficients and pitch plane aerodynamic derivatives as a function of vehicle geometry, flight conditions, and center of gravity location. Force coefficients (C_L , C_D) required for mission performance analyses are provided to the Vehicle Performance Model.

3.0 MODEL DESCRIPTION

The model computes aerodynamic coefficients of each element of the configuration and combines these elements along with appropriate interference factors into a description of the complete configuration. Component drag coefficient is computed as a function of both Mach number and altitude, because of the dependency of skin friction drag or altitude while lift curve slope is computed as a function of Mach number only. The general procedure for this is diagrammed in Figure 1. The analysis is limited to the linear angle-of-attack region, Mach numbers from 0 to 5.0 and altitudes below 100,000 feet.

3.1 Configuration Options

The configuration elements available for use in the SEATIDE CM-CGSM are shown in Figures 2, 3, 4, and 5. Body options are illustrated in Figure 2 where the various combinations of nose shape and boattail are shown. The body must have a cylindrical center section with one

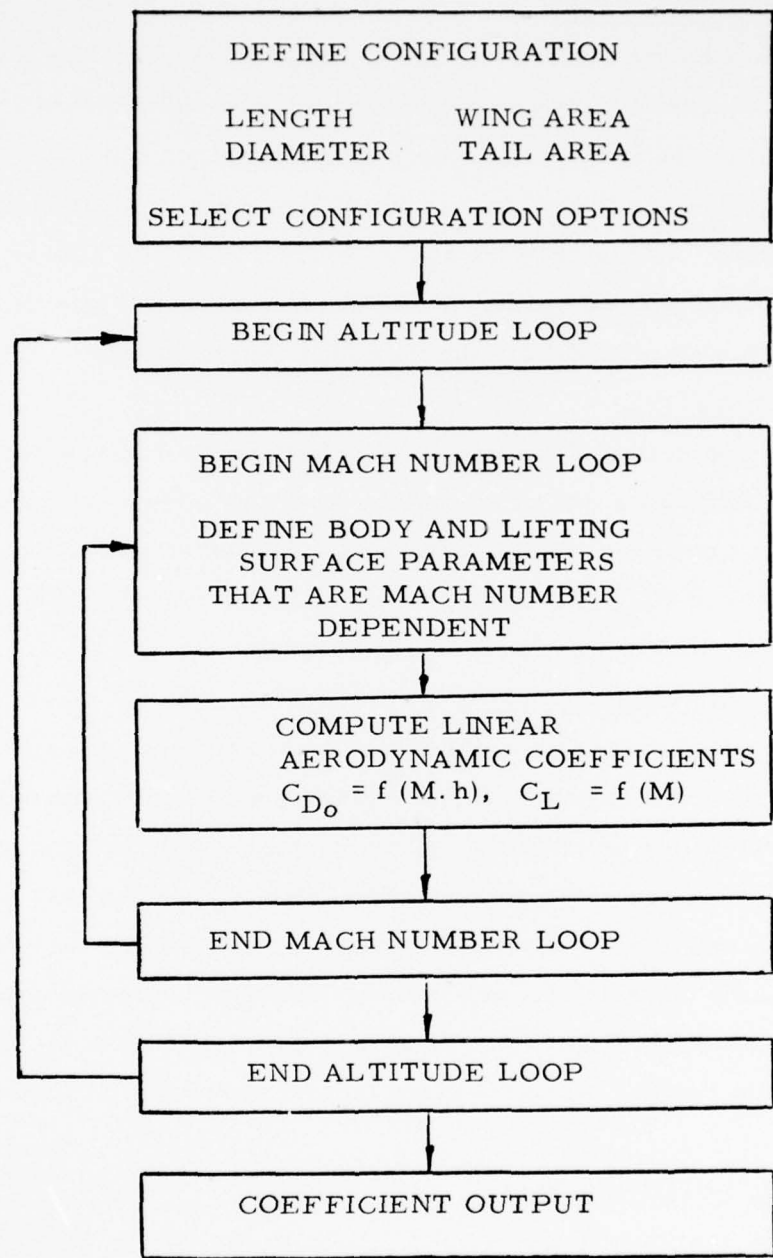


FIGURE 1 AERODYNAMICS MODEL FUNCTIONAL FLOW

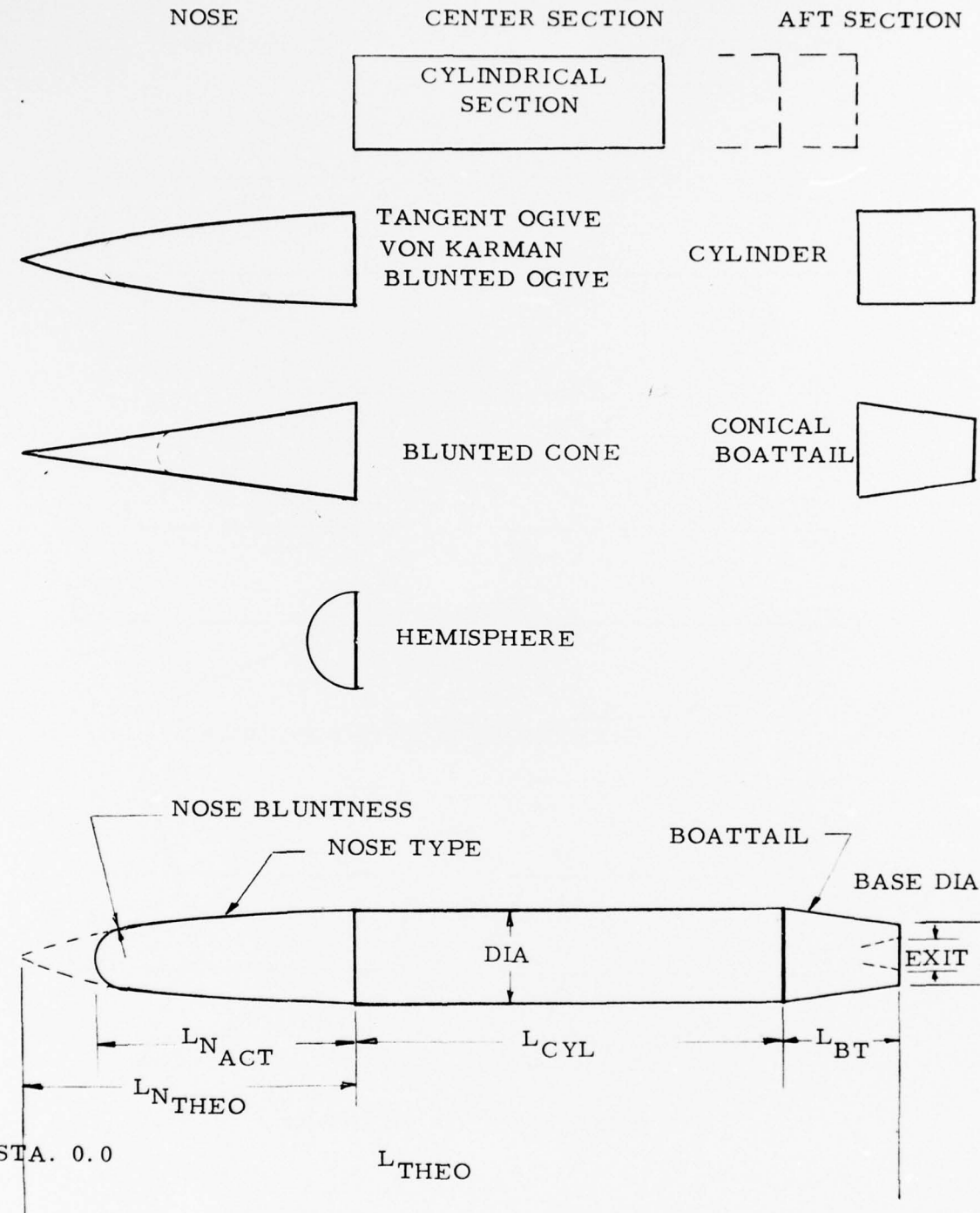
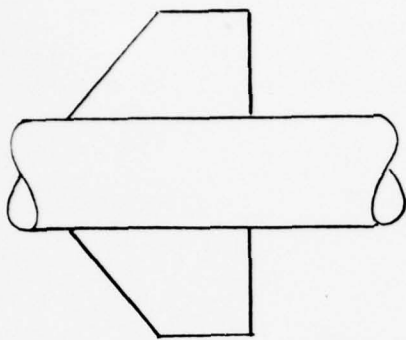
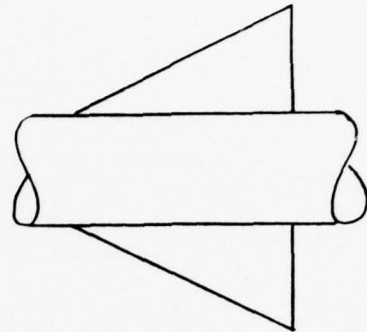


FIGURE 2 BODY CONFIGURATION OPTIONS

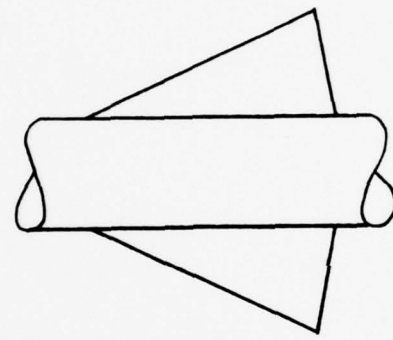
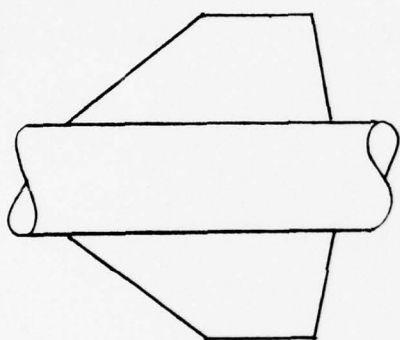
TRAPEZOIDAL



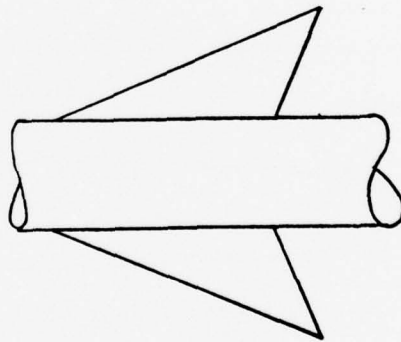
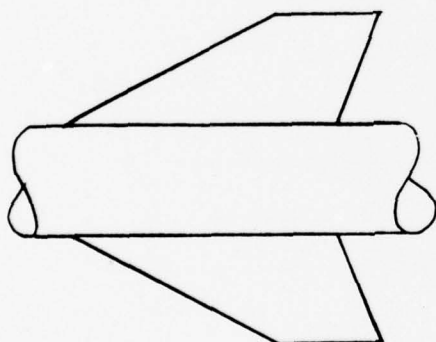
DELTA



STRAIGHT TRAILING EDGE



TRAILING EDGE SWEPT FORWARD



TRAILING EDGE SWEPT AFT

FIGURE 3 LIFTING SURFACE PLANFORM OPTIONS

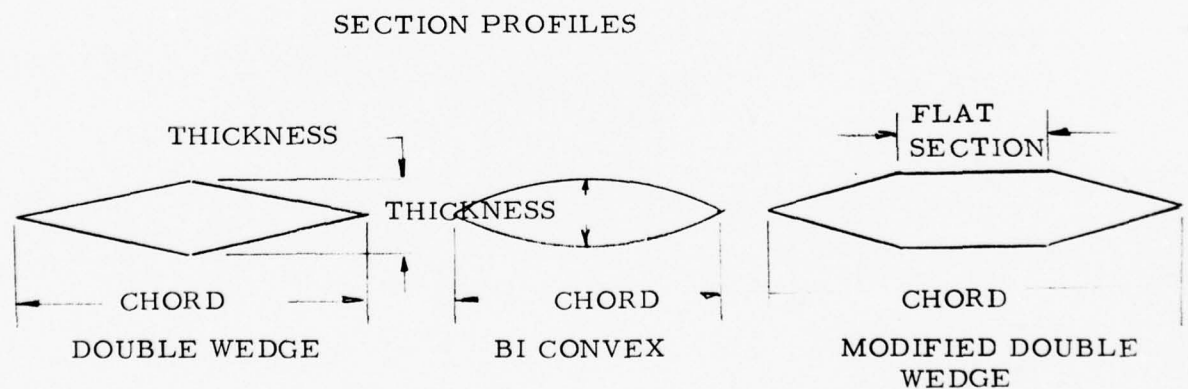
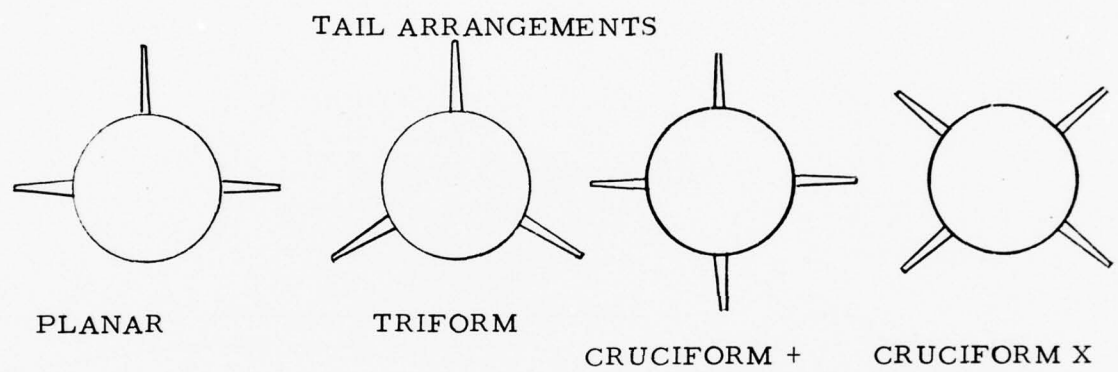
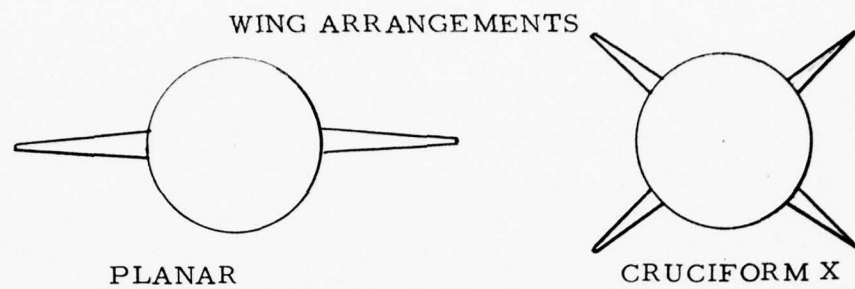


FIGURE 4 LIFTING SURFACE ARRANGEMENTS

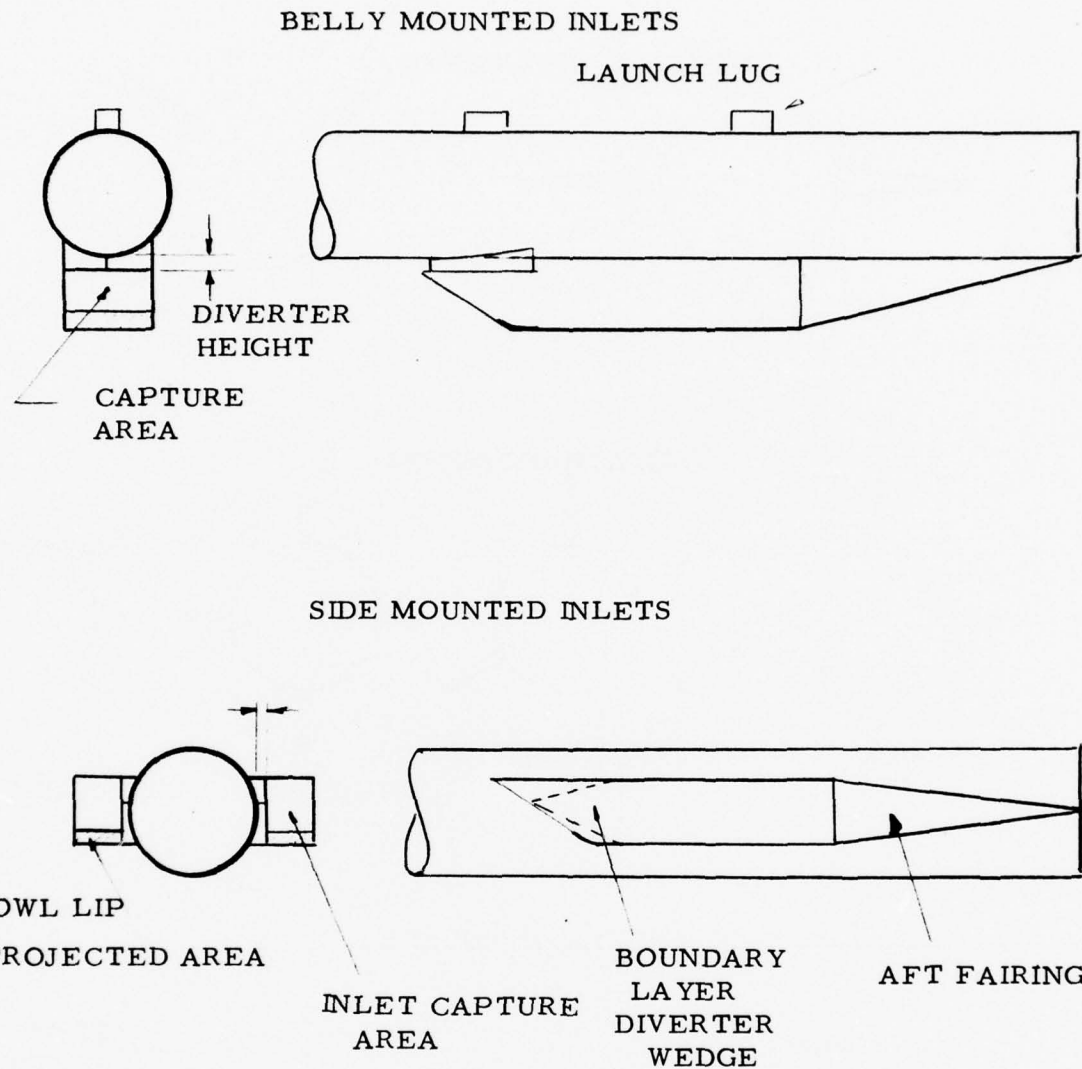


FIGURE 5 CONFIGURATION OPTIONS - INLET SYSTEMS

TABLE I
AERODYNAMIC OPTIONS

<u>NAME</u>	<u>DESCRIPTION</u>	<u>OPTION</u>	<u>NO.</u>
ITN	Type of nose	Tangent Ogive	1
		Von Karman	2
		Cone	3
		Spherical	4
		Blunted Cone	5
		Blunted Ogive	6
IBTL	Type of boattail	None	7
		Conical	8
ILUG	Launch lugs	No	9
		Yes	10
NW	Fixed wings	No	11
		Yes	12
ICNTRL	Control Selection	Tail	13
IART	Aerodynamic Surface Arrangement (Aft)	Planar	14
		Cruciform +	15
		Triform	16
		Cruciform X	17
IARW	Aerodynamic Surface Arrangement (Fwd)	Planar	18
		Cruciform X	19
ITSE CT	Aerodynamic Surface Section (aft)	Double Wedge	20
		Bi-Convex	21
		Modified Double Wedge	22
IWSE CT	Aerodynamic Surface Section (Fwd)	Double Wedge	23
		Bi-Convex	24
		Modified Double Wedge	25

TABLE I (Cont'd.)

<u>NAME</u>	<u>DESCRIPTION</u>	<u>OPTION</u>	<u>NO.</u>
ISURFW	Type of wing planform	Trapezoidal	26
		Delta	27
ISURFT	Type of tail planform	Trapezoidal	28
		Delta	29
IPLANW	Wing planform definition input options	Input: SEW, ARW, TRW, $\Lambda_{TE} = 0.0$	30
		Input: SEW, ARW, $\Lambda_{LE}, \Lambda_{TE} = 0.0$	31
		Input: SEW, ARW, $M_{DES}, \Lambda_{TE} = 0$	32
		Input: SEW, ARW, TRW, Λ_{TE}	33
		Input: SET, ART, TRT, $\Lambda_{TE} = 0.0$	34
IPLANT	Tail planform defini- tion input options	Input: SET, ART, $\Lambda_{LE}, \Lambda_{TE} = 0.0$	35
		Input: SET, ART, $M_{DES}, \Lambda_{TE} = 0.0$	36
		Input: SET, ART, TRW, Λ_{TE}	37

of the nose shapes shown, and may have a conical boattail. Nose fineness ratio, bluntness ratio, and boattail fineness ratio are input variables. The amount of boattailing desired may be selected by an input factor which defines the amount of the base annulus to be removed by boattailing.

Lifting surface options are illustrated in Figures 3 and 4. Lifting surfaces may include two sets of surfaces (wing-tail) or a body-tail configuration. Arrangement of the surfaces may be planar (2 panels),

triform (3 panels), cruciform +, or cruciform X as shown in Figure 4. Wing and tail panels are assumed to be in line in this model.

Trapezoidal or triangular planforms may be specified by input. Wing planform characteristics are specified in all cases by exposed area and aspect ratio. Taper ratio, leading edge sweep, Mach number for a sonic leading edge, or trailing edge sweep angle may be used in various combinations to select a surface planform. Table I shows the input options available for surface planform definition. Figure 6 illustrates the lifting surface planform parameters.

Option 30 requires input values for exposed wing area (SEW), exposed aspect ratio (ARW), and taper ratio of the exposed panel (TRW); the trailing edge is unswept. Exposed span (BW) of the wing is defined from the relationship between aspect ratio, span, and area:

$$ARW = \frac{BW^2}{SEW}$$

$$BW = \sqrt{SEW * ARW}$$

Wing root chord (RCW) is defined by the relation

$$RCW = 2 * SEW / BW / (1 + TRW)$$

Tip chord is defined by the taper ratio and root chord

$$TCW = RCW * (TRW)$$

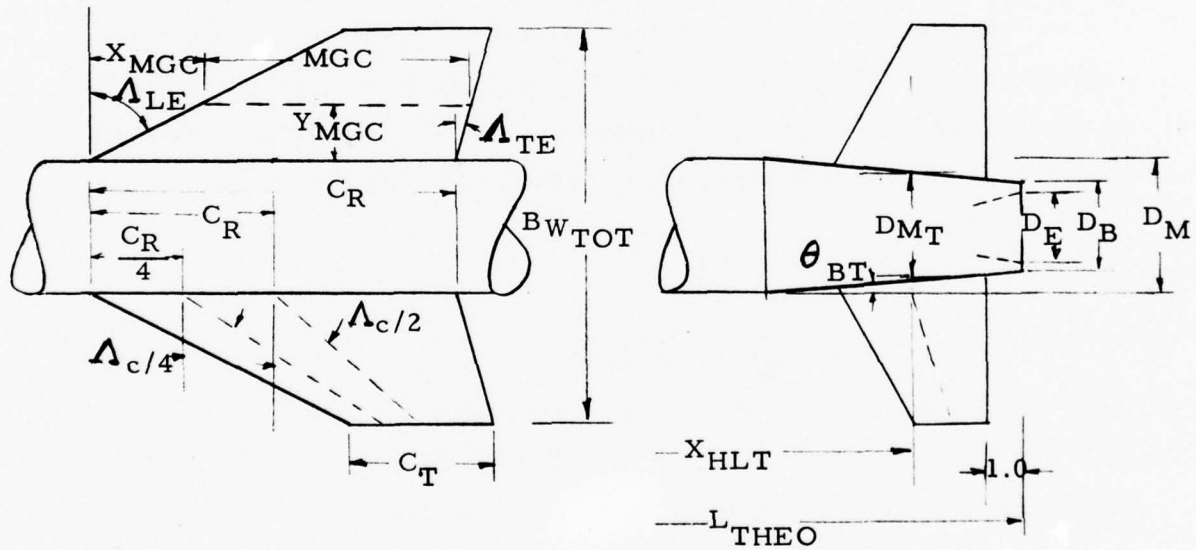
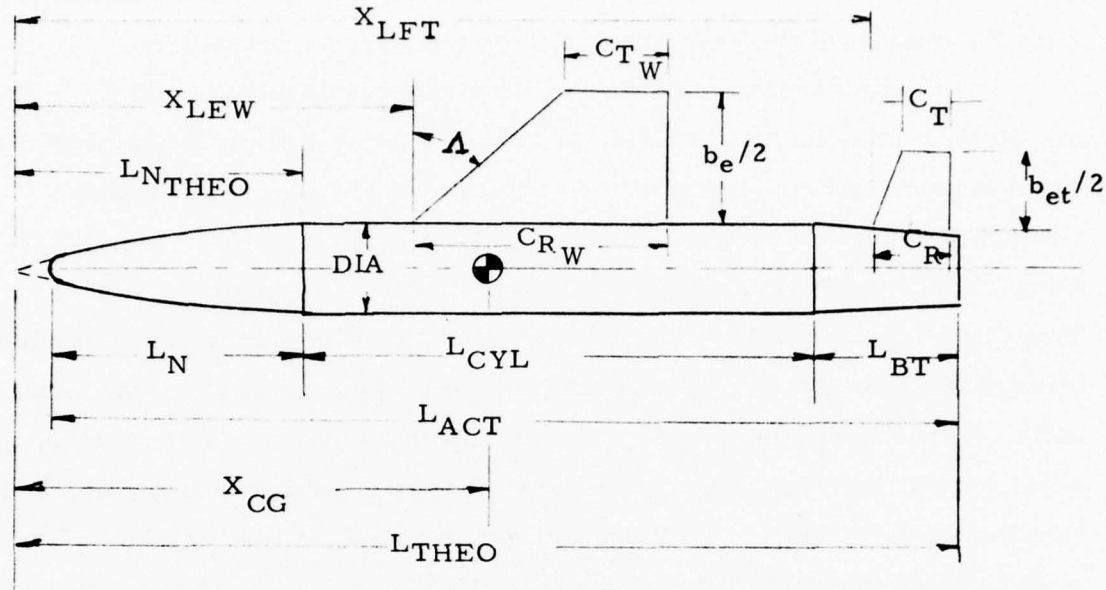


FIGURE 6 CONFIGURATION PARAMETERS

Leading edge sweep angle is defined by the relation

$$\Lambda_{LE} = \tan^{-1} \frac{4(1. - TRW)}{ARW(1. + TRW)}$$

Option 31 requires input values for leading edge sweep angle rather than taper ratio; the trailing edge is unswept. Taper ratio is computed from the following

$$TRW = \frac{(1. - \frac{4}{ARW \tan \Lambda_{LE}})}{\frac{1. + \frac{4}{ARW \tan \Lambda_{LE}}}{4}}$$

If the input leading edge sweep combined with the input aspect ratio is not consistent with a trapezoidal wing, a delta wing with the input leading edge sweep is defined from the input area and a computed value of aspect ratio.

$$ARW = 4.0 / \tan \Lambda_{LE}$$

$$BW = \sqrt{SW * ARW}$$

Wing root chord for the delta wing is based on the relationship

$$RCW = 2.0 * SEW / BW$$

Tip chord is zero for the delta wing.

Option 32 is similar to Option 31 with the leading edge sweep angle being set to provide a sonic leading edge at a specified Mach number. Leading edge sweep angle for a sonic leading edge is defined by the relation

$$\Lambda_{LE} = \tan^{-1} \sqrt{M^2 - 1}$$

The remainder of the wing parameters are computed as in Option 31. Trailing edge sweep angle must be input in Option 33 along with aspect ratio, exposed area, and taper ratio. Leading edge sweep angle is computed from the relation

$$\Lambda_{LE} = \tan^{-1} (2(RCW + \frac{BW}{2} \tan \Lambda_{TE} - TCW) / BW)$$

Midchord sweep angle is computed from the following

$$\Lambda_{C/2} = \tan^{-1} \frac{RCW - TCW}{BW} + \Lambda_{TE}$$

Quarter chord sweep angle is based on the relation

$$\Lambda_{C/4} = \tan^{-1} \frac{1.5 (RCW - TCW)}{BW} + \Lambda_{TE}$$

Mean geometric chord length is based on the relation

$$MGC = \frac{2}{3} (C_R + C_T - \frac{C_R C_T}{C_R + C_T})$$

Spanwise location of the mean geometric chord is

$$Y_{MGC} = \frac{BW}{6} \left(\frac{1. + 2 TRW}{1. + TRW} \right)$$

Longitudinal location of the leading edge of the mean geometric chord with respect to the surface leading edge intersection with the body is

$$X_{MGL} = Y_{MGC} \tan \Lambda_{LE}$$

The location of the intersection of the wing leading edge may be input or computed to satisfy a desired stability margin at either a subsonic condition ($M = 0.8$) or a supersonic condition ($M = 2.0$) for example.

Section profile may be double wedge, bi-convex, or modified double wedge as shown in Figure 4. Surface thickness ratio is an input variable.

Two inlet configurations are provided for airbreathing configurations as shown in Figure 5. A single two-dimensional belly mounted inlet or dual side mounted inlets may be selected. Launch lugs may be specified as required.

3.2 Input-Output Options

Input requirements are related to the configuration options selected. The basic inputs are body diameter, missile length or weight, wing area, wing aspect ratio, and tail area. Modifying inputs for the body are nose shape, fineness ratio, and bluntness ratio. Wing and tail modifications include sweep angle, taper ratio, section profile, and thickness

ratio. Inlet type must be specified for the airbreathing configuration. Table I lists the configuration option switches for the Aerodynamics Model. Detailed input instructions are discussed in Volume IIIA.

The basic output of the aerodynamics model is zero-lift drag coefficient and lift curve slope of a specified configuration as a function of Mach number and altitude. Table II lists the aerodynamic coefficients computed in aerodynamics model and included in the lift/drag coefficients.

TABLE II
AERODYNAMIC COEFFICIENTS

<u>Symbol</u>	<u>Description</u>
$C_{DO_{OFF}}$	Zero-lift drag coefficient (power-off)
$C_{DO_{ON}}$	Zero-lift drag coefficient (power-on)
C_{L_α}	Slope of lift coefficient curve with respect to angle of attack $\frac{d C_L}{d \alpha}$
C_{L_δ}	Slope of lift coefficient curve with respect to surface deflection $\frac{d C_L}{d \delta}$
C_{m_α}	Slope of pitching moment curve with respect to angle of attack $\frac{d C_m}{d \alpha}$
$C_{m_\delta T}$	Slope of pitching moment curve with respect to surface deflection $\frac{d C_m}{d \delta_T}$
C_{m_Q}	Slope of pitch damping moment with respect to pitch rate $\frac{d C_m}{d Q}$
$C_{m \dot{\alpha}}$	Slope of pitch damping moment with respect to rate of change of angle of attack $\frac{d C_m}{d \dot{\alpha}}$
C_{l_δ}	Slope of rolling moment coefficient with respect to surface deflection $\frac{d C_l}{d \delta}$
C_{l_P}	Slope of roll damping moment with respect to roll rate $\frac{d C_l}{d \frac{pb}{2V}}$
C_{h_α}	Slope of tail hinge moment curve with respect to angle of attack $\frac{d (HM)}{d \alpha}$

TABLE II (Cont'd.)

<u>Symbol</u>	<u>Description</u>
$C_h \delta$	Slope of tail hinge moment curve with respect to tail surface deflection $\frac{d (HM)}{d \delta}$
C_{N_R}	Slope of yaw damping moment with respect to yaw rate $\frac{d C_N}{d R}$
$C_N \beta$	Slope of yawing moment with respect to sideslip angle $\frac{d C_N}{d \beta}$
$C_Y \beta$	Slope of side force coefficient with respect to sideslip angle $\frac{d C_Y}{d \beta}$

3.3 Analysis

Complete configuration aerodynamic coefficients are determined by a build-up procedure with appropriate interference factors. The general procedure for this is diagrammed in Figure 1 using the component options described in Table I.

The procedures used for computing the component coefficients and interference factors are outlined in the following paragraphs, along with the source references.

4.0 Body Aerodynamics Characteristics

The vehicle body consists of a right circular cylinder with a forebody and possibly a conical afterbody. Forebody shape and fineness ratio are input variables while afterbody fineness ratio and diameter ratio are variable.

4.1 Drag

Body drag consists of skin friction drag, nose pressure drag, afterbody pressure drag, base drag, and drag due to lift.

4.1.1 Zero-lift Drag

Subsonic

$$C_{D_0} = \left\{ C_F + C_F \left[\frac{1.5}{(FRB)^{1.5}} + \frac{7.0}{(FRB)^3} \right] \right\} \frac{S_{NET}}{S_{REF}} + C_{D_B}$$

The flat plate incompressible skin friction coefficient (C_{F_i}) is based on the modified Prandtl-Schlichting relationship for turbulent boundary layers.

$$C_{F_i} = \frac{0.482}{(\log_{10} R_n)^{2.62}}$$

Body Reynold's number is computed from 1962 U.S. Standard Atmosphere data. Reynold's number per foot per Mach number data vs. altitude is presented in Table III. The incompressible skin friction coefficient is corrected for compressibility effects by the data of Table IV.

Base drag at all Mach numbers is computed from the base pressure coefficients presented in Table V. Base drag coefficients are

TABLE III
REYNOLD'S NUMBER PER FT. PER MACH NUMBER
VS ALTITUDE

	DATA FRCTN1/	0.,	7.088,	5.,	6.171,	10.,	5.348,	15.,	4.611,
★		20.,	3.954,	25.,	3.370,	30.,	2.655,	35.,	2.401,
★		40.,	1.914,	45.,	1.505,	50.,	1.184,	55.,	.931,
★		60.,	.732,	65.,	.576,	70.,	.453,	75.,	.356,
★		80.,	.280,	85.,	.220,	90.,	.173,	95.,	.136,
★		100.,	.107/						

TABLE IV
COMPRESSIBILITY CORRECTION FACTOR VS MACH
NUMBER AND ALTITUDE

	DATA FRCTN3/	0.0,	0.0,	1.0,	0.5,	0.973,	0.75,
1		0.945,	1.0,	0.915,	1.5,	0.834,	2.5,
2		0.65,	3.0,	0.574,	4.0,	0.445,	5.0,
3		0.353,	6.0,	0.29,	80.0,	0.0,	1.0,
4		0.5,	0.978,	0.75,	0.96,	1.0,	0.933,
5		1.5,	0.858,	2.5,	0.68,	3.0,	0.61,
6		4.0,	0.491,	5.0,	0.4,	6.0,	0.347/

TABLE V
BASE PRESSURE COEFFICIENTS VS MACH NUMBER

	DATA BASECPR/						
1		0.0,	-0.137,	0.8,	-0.137,	0.9,	-0.145,
1		1.0,	-0.195,	1.2,	-0.191,		
1		1.5,	-0.172,	2.0,	-0.141,	3.0,	-0.092,
1		4.0,	-0.062,	5.0,	-0.046/		

BEST AVAILABLE COPY

corrected for boattailing by the base diameter ratio.

Power-on base drag coefficient is computed from the relation:

$$C_{D_B} = -C_{P_B} \left(\frac{D_B^2 - D_E^2}{D_M^2} \right) \frac{D_B}{D_M}$$

Power-off base drag coefficient is based on the relation:

$$C_{D_B} = -C_{P_B} \left(\frac{D_B}{D_M} \right)^3$$

Transonic, M=1

Nose pressure drag at M=1 is based on curve fits of the data of Reference 3. Tables II and III present ogival nose and conical nose pressure drag coefficients at M=1 as a function of nose apex half angle. Boattail pressure drag coefficient at M=1 is based on data of Reference 4. Table III presents boattail drag parameter $C_{D_{BT}} \left(\frac{L}{D} \right)^2 \frac{\theta_{BR}}{B}$ as a function of boattail base area ratio. The effect of nose bluntness on nose drag coefficient at M=1 is based on data of Reference 5. Base drag and friction drag coefficients are computed in the same manner as the subsonic condition. Launch lug drag coefficient at M=1 is based on empirical data of Reference 6. Zero-lift drag at M=1 is given by the relation:

$$C_{D_C} = C_{D_N} + C_{D_{BT}} + C_{D_B} + C_{D_L} + C_{D_F}$$

Supersonic, M = 1.25 - 5

Nose pressure drag coefficients for tangent ogive, von Karman, and conical nose shapes are based on a curve fit of the data of Reference 7. Tables IX through XI present nose pressure drag coefficient times the square of Mach number as a function of Mach number divided by nose-fineness ratio. Hemispherical nose pressure drag coefficient from Reference 8 is presented in Table XII as a function of Mach number. Nose pressure drag coefficient of hemispherically blunted conical noses is based on data of Reference 1. Tabular data of nose pressure drag for blunted cones is presented in Table XIII as a function of Mach number, theoretical nose fineness ratio, and nose bluntness ratio. Pressure drag coefficients for hemispherically blunted ogive noses is presented in Table XIV, as a function of Mach number, theoretical nose fineness ratio, and nose bluntness ratio.

TABLE VI
OGIVE NOSE PRESSURE DRAG COEFFICIENT AT M=1

$$TN = ARCSIN(FR/(0.25 + FR*FR)) * 57.3$$

	TN	COPN	TN	COPN	TN	COPN	
	DATA COP50/	0.000,	0.000,	10.000,	0.010,	20.000,	0.040,
1		30.000,	0.080,	40.000,	0.130,	50.000,	0.170,
2		60.000,	0.210,	70.000,	0.250,	80.000,	0.280,
3		90.000,	0.310/				

TABLE VII
CONICAL NOSE PRESSURE DRAG COEFFICIENT AT M=1

$$TN = \text{CONE HALF ANGLE IN DEG.}$$

	TN	COPN	TN	COPN	TN	COPN	
	DATA COP51/	0.000,	0.000,	10.000,	0.200,	20.000,	0.370,
1		30.000,	0.500,	40.000,	0.670,	50.000,	0.800,
2		60.000,	0.870,	70.000,	0.920,	80.000,	0.960,
3		90.000,	1.000/				

TABLE VIII
BOATTAIL DRAG PARAMETER AT M=1

$$DD2 = (\text{BASE DIA.} / \text{MAX. DIA.})^{**2}$$

$$CDPRT1 = CDPRT1(M=1) * (L/D)^{**2} * (\text{BT. ANG. (DEG.)}) / R_0$$

	DD2	CDPRT1	DD2	CDPRT1	DD2	CDPRT1	
	DATA CDP53/	0.000,	1.170,	0.100,	0.880,	0.150,	0.670,
1		0.200,	0.520,	0.250,	0.390,	0.300,	0.300,
2		0.350,	0.230,	0.400,	0.180,	0.450,	0.140,
3		0.500,	0.110,	0.550,	0.085,	0.600,	0.060,
4		0.800,	0.012,	1.000,	0.000/		

BEST AVAILABLE COPY

BEST AVAILABLE COPY

TABLE IX
TANGENT OGIVE NOSE WAVE DRAG COEFFICIENT

	DML=MACH NUMBER/NOSE FINENESS RATIO CDKM2=NOSE PRESSURE DRAG COEFFICIENT TIMES MACH SQUARED					
	DMI	CDKM2	DML	CDWM2	DML	CDWM2
DATA CDNOG/	0.000,	0.000,	0.050,	0.008,	0.100,	0.017,
1	0.150,	0.033,	0.200,	0.053,	0.250,	0.078,
2	0.300,	0.107,	0.350,	0.134,	0.400,	0.166,
3	0.450,	0.201,	0.500,	0.241,	0.550,	0.281,
4	0.600,	0.326,	0.650,	0.375,	0.700,	0.430,
5	0.750,	0.484,	0.800,	0.542,	0.850,	0.640,
6	0.900,	0.665,	0.950,	0.731,	1.000,	0.797,
7	1.050,	0.867,	1.100,	0.940,	1.150,	1.016,
8	1.200,	1.104,	1.600,	1.850,	2.000,	2.700,
9	2.600,	4.450,	4.000,	9.800/		

TABLE X
VON KARMAN NOSE WAVE DRAG COEFFICIENT

	DML=MACH NUMBER/NOSE FINENESS RATIO CDKM2=NOSE PRESSURE DRAG COEFFICIENT TIMES MACH SQUARED					
	DMI	CDKM2	DML	CDWM2	DML	CDWM2
DATA CDNVK/	0.000,	0.000,	0.050,	0.007,	0.100,	0.016,
1	0.150,	0.029,	0.200,	0.042,	0.250,	0.060,
2	0.300,	0.083,	0.350,	0.106,	0.400,	0.132,
3	0.450,	0.160,	0.500,	0.190,	0.550,	0.223,
4	0.600,	0.260,	0.650,	0.297,	0.700,	0.341,
5	0.750,	0.384,	0.800,	0.433,	0.850,	0.480,
6	0.900,	0.531,	0.950,	0.581,	1.000,	0.637,
7	1.050,	0.701,	1.100,	0.769,	1.150,	0.834,
8	1.200,	0.901,	1.600,	1.450,	2.000,	2.050,
9	2.600,	3.300,	4.000,	7.500/		

TABLE XI
HEMISPHERICAL NOSE PRESSURE DRAG COEFFICIENT

	MACH	CDPN	MACH	CDPN	MACH	CDPN
DATA CDSPH/	0.000,	0.200,	0.250,	0.200,	0.500,	0.220,
1	0.750,	0.240,	1.000,	0.310,	1.250,	0.525,
2	1.500,	0.660,	1.750,	0.730,	2.000,	0.775,
3	2.500,	0.830,	3.000,	0.845,	4.000,	0.860,
4	5.000,	0.870,	6.000,	0.880,	10.000,	0.890/

TABLE XII
CONICAL NOSE WAVE DRAG COEFFICIENT

	CDL=MACH NUMBER/NOSE FINENESS RATIO		CDWMPENOSE PRESSURE DRAG COEFFICIENT		TIMES MACH SQUARED	
	DML	CDWM2	DML	CDWM2	DML	CDWM2
DATA CDNCO/	0.000,	0.000,	0.050,	0.016,	0.100,	0.029,
1	0.150,	0.050,	0.200,	0.071,	0.250,	0.098,
2	0.300,	0.122,	0.350,	0.151,	0.400,	0.180,
3	0.450,	0.212,	0.500,	0.247,	0.550,	0.283,
4	0.600,	0.317,	0.650,	0.360,	0.700,	0.406,
5	0.750,	0.450,	0.800,	0.503,	0.850,	0.554,
6	0.900,	0.606,	0.950,	0.667,	1.000,	0.730,
7	1.050,	0.794,	1.100,	0.864,	1.150,	0.931,
8	1.200,	1.005,	1.600,	1.400,	2.000,	2.350,
9	2.600,	3.750,	4.000,	8.500/		

TABLE XIII
BLUNTED CONE PRESSURE DRAG COEFFICIENT

	FCAP=NOSE BLUNTNES RATIO		CDP=THEORETICAL NOSE FINENESS RATIO		CDPN=BLUNTED CONE PRESSURE DRAG COEFFICIENT	
	RM=MACH NUMBER	CDP	FCAP	CDPN	FCAP	CDP
DATA CDP701/	1.250,	1.500,	2.000,	3.000,	4.000,	
1	2.000,	3.000,	4.000,	5.000,	6.000,	7.000,
2	0.000,	0.200,	0.400,	0.600,	0.800,	1.000,
	RM=1.25, FR=2.0 THRU 8.0					
X	FCAP=0.0	0.20	0.40	0.60	0.80	1.00
X	0.255,	0.210,	0.190,	0.213,	0.320,	0.520,
X	0.125,	0.110,	0.115,	0.170,	0.300,	0.520,
X	0.078,	0.070,	0.095,	0.160,	0.290,	0.520,
X	0.050,	0.050,	0.080,	0.155,	0.290,	0.520,
X	0.035,	0.040,	0.075,	0.152,	0.290,	0.520,
X	0.030,	0.035,	0.070,	0.151,	0.290,	0.520,
X	0.025,	0.030,	0.068,	0.150,	0.290,	0.520,
	RM=1.50, FR=2.0 THRU 8.0					
X	FCAP=0.0	0.20	0.40	0.60	0.80	1.00
3	0.212,	0.202,	0.233,	0.311,	0.456,	0.669,
4	0.111,	0.117,	0.164,	0.263,	0.429,	0.669,
5	0.071,	0.082,	0.135,	0.245,	0.413,	0.669,
6	0.049,	0.060,	0.123,	0.232,	0.408,	0.669,
7	0.036,	0.050,	0.114,	0.230,	0.405,	0.669,
8	0.028,	0.045,	0.110,	0.227,	0.405,	0.669,
9	0.023,	0.042,	0.106,	0.227,	0.402,	0.669/

BEST AVAILABLE COPY

TABLE XIII (Continued)

RM=2.00, FR=2.0 THRU 8.0						
FCAP=0.0						
DATA CDP702/	0.180,	0.188,	0.236,	0.348,	0.518,	0.758,
B	0.095,	0.112,	0.181,	0.306,	0.403,	0.758,
C	0.059,	0.080,	0.156,	0.288,	0.400,	0.758,
D	0.041,	0.063,	0.140,	0.280,	0.479,	0.758,
E	0.027,	0.050,	0.133,	0.275,	0.477,	0.758,
F	0.022,	0.045,	0.132,	0.270,	0.476,	0.759,
G	0.016,	0.042,	0.130,	0.268,	0.475,	0.758,
RM=3.00, FR=2.0 THRU 8.0						
FCAP=0.0						
X	0.154,	0.180,	0.258,	0.385,	0.582,	0.843,
1	0.079,	0.112,	0.200,	0.350,	0.568,	0.843,
2	0.049,	0.083,	0.175,	0.333,	0.558,	0.844,
3	0.034,	0.067,	0.163,	0.324,	0.550,	0.843,
4	0.025,	0.058,	0.156,	0.318,	0.549,	0.844,
5	0.019,	0.052,	0.150,	0.315,	0.545,	0.843,
6	0.017,	0.050,	0.150,	0.313,	0.545,	0.843/
RM=4.00, FR=2.0 THRU 8.0						
FCAP=0.0						
DATA CDP703/	0.142,	0.171,	0.262,	0.408,	0.613,	0.868,
B	0.073,	0.112,	0.210,	0.369,	0.590,	0.868,
9	0.044,	0.083,	0.185,	0.350,	0.582,	0.869,
A	0.031,	0.068,	0.172,	0.340,	0.572,	0.869,
R	0.022,	0.063,	0.164,	0.340,	0.570,	0.869,
C	0.016,	0.055,	0.160,	0.333,	0.568,	0.869,
D	0.013,	0.054,	0.160,	0.332,	0.565,	0.869/

TABLE XIV

BLUNTED OGIVE PRESSURE DRAG COEFFICIENT

FCAP=NOSE BLUNTNES RATIO						
FR=THEORETICAL NOSE FINENESS RATIO						
CDPNE=BLUNTED OGIVE PRESSURE DRAG COEFFICIENT						
DATA CDP711/	1.250,	1.500,	2.000,	3.000,	4.000,	
1	2.000,	3.000,	4.000,	5.000,	6.000,	7.000,
2	0.000,	0.200,	0.400,	0.600,	0.800,	1.000,
RM=1.25, FR=2.0 THRU 8.0						
FCAP=0.0						
Z	0.220,	0.125,	0.090,	0.125,	0.270,	0.520,
Z	0.110,	0.065,	0.070,	0.125,	0.270,	0.520,
Z	0.065,	0.040,	0.045,	0.125,	0.270,	0.520,
Z	0.045,	0.030,	0.045,	0.125,	0.275,	0.520,
Z	0.035,	0.025,	0.045,	0.130,	0.280,	0.520,
Z	0.025,	0.020,	0.045,	0.135,	0.285,	0.520,
Z	0.020,	0.015,	0.050,	0.140,	0.290,	0.520,

TABLE XIV(Continued)

RM=1.50, FR=2.0 THRU 8.0						
	FCAP=0.0	0.20	0.40	0.60	0.80	1.00
3		0.220,	0.140,	0.153,	0.235,	0.395,
4		0.105,	0.093,	0.128,	0.220,	0.395,
5		0.065,	0.060,	0.110,	0.215,	0.396,
6		0.040,	0.048,	0.100,	0.212,	0.400,
7		0.030,	0.038,	0.098,	0.210,	0.400,
8		0.030,	0.033,	0.095,	0.210,	0.400,
9		0.018,	0.030,	0.093,	0.210,	0.400,
RM=2.00, FR=2.0 THRU 8.0						
	FCAP=0.0	0.20	0.40	0.60	0.80	1.00
DATA CDP712/	0.197,	0.179,	0.205,	0.306,	0.478,	0.754,
B		0.095,	0.100,	0.153,	0.281,	0.473,
C		0.055,	0.068,	0.134,	0.269,	0.465,
D		0.035,	0.052,	0.125,	0.263,	0.469,
E		0.025,	0.042,	0.124,	0.260,	0.479,
F		0.018,	0.039,	0.115,	0.257,	0.468,
G		0.015,	0.036,	0.115,	0.258,	0.469,
RM=3.00, FR=2.0 THRU 8.0						
	FCAP=0.0	0.20	0.40	0.60	0.80	1.00
X		0.173,	0.178,	0.235,	0.360,	0.564,
1		0.088,	0.111,	0.185,	0.331,	0.549,
2		0.053,	0.080,	0.169,	0.323,	0.541,
3		0.036,	0.068,	0.156,	0.317,	0.538,
4		0.026,	0.055,	0.150,	0.313,	0.539,
5		0.019,	0.050,	0.145,	0.308,	0.538,
6		0.014,	0.049,	0.142,	0.306,	0.537,
RM=4.00, FR=2.0 THRU 8.0						
	FCAP=0.0	0.20	0.40	0.60	0.80	1.00
DATA CDP713/	0.163,	0.173,	0.240,	0.380,	0.590,	0.868,
B		0.081,	0.111,	0.200,	0.355,	0.577,
9		0.050,	0.082,	0.180,	0.340,	0.568,
A		0.032,	0.070,	0.170,	0.335,	0.565,
H		0.022,	0.063,	0.162,	0.333,	0.561,
C		0.016,	0.058,	0.160,	0.330,	0.560,
D		0.011,	0.055,	0.156,	0.325,	0.560,

BEST AVAILABLE COPY

Boattail pressure drag is based on data of Reference 1. Table XV presents boattail drag parameter $4C_{D_{BT}}(\frac{L}{D})^2$ as a function of boattail base area ratio (D_B^2/D_M^2) and boattail parameter $\frac{L}{B} \frac{L}{D}$.

Base drag is computed as described in the subsonic region.

Body friction drag is based on the relation

$$C_{DF} = 1.1 C_F \frac{C_F}{C_{FL}} \frac{S_{NET}}{S_{REF}}$$

Launch lug drag coefficient is based on empirical data of Reference 6. Table XVI presents launch lug equivalent flat plate area as a function of Mach number. Launch lug drag coefficient is based on the relation

$$C_{DL} = \frac{F_L}{S_{REF}}$$

Zero-lift drag coefficient at supersonic Mach number is based on the relation

$$C_{Dc} = C_{DN} + C_{DST} + C_{DB} + C_{DF} + C_{DL}$$

4.1.2 Induced Drag

Induced drag coefficient at all Mach numbers is based on the relation

$$C_{DI} = C_L \tan \alpha$$

4.1.3 Total Drag Coefficient

Total drag coefficient is based on the relation

$$C_D = C_{Dc} + C_{DI}$$

4.2 Lift Curve Slope

Body lift consists of the nose contribution and the boattail contribution.

Subsonic, M $\leq .9$

Nose and cylindrical section lift curve shape is based on potential theory and uses Munk's apparent mass factor from Reference 1.

Munk's efficiency factor is presented in Table XVII as a function of body fineness ratio. The boattail contribution is equivalent to the nose contribution corrected for boattail volume and boattail base area ratio. The boattail

TABLE XV
CONICAL BOATTAIL PRESSURE DRAG PARAMETER

DATA CRABT1/ 1.000,						
	DD2	CDA	DD2	CDA	DD2	CDA
1	0.000,	0.480,	0.025,	0.570,	0.050,	0.600,
2	0.075,	0.620,	0.100,	0.680,	0.150,	0.580,
3	0.200,	0.510,	0.250,	0.480,	0.300,	0.440,
4	0.350,	0.380,	0.400,	0.320,	0.450,	0.250,
5	0.500,	0.210,	0.550,	0.160,	0.600,	0.130,
6	0.650,	0.110,	0.700,	0.090,	0.800,	0.060,
7	0.850,	0.040,	0.950,	0.000,	1.000,	0.000,
	RLDR=1.0					
8	2.000,					
9	0.000,	1.740,	0.025,	1.640,	0.050,	1.540,
A	0.075,	1.440,	0.100,	1.340,	0.150,	1.200,
B	0.200,	1.070,	0.250,	0.940,	0.300,	0.810,
C	0.350,	0.700,	0.400,	0.590,	0.450,	0.500,
D	0.500,	0.420,	0.550,	0.350,	0.600,	0.280,
E	0.650,	0.210,	0.700,	0.170,	0.800,	0.080,
F	0.900,	0.020,	0.950,	0.010,	1.000,	0.000,
	RLDR=2.0					
8	3.000,					
9	0.000,	2.460,	0.025,	2.250,	0.050,	2.020,
A	0.075,	1.890,	0.100,	1.760,	0.150,	1.540,
B	0.200,	1.340,	0.250,	1.170,	0.300,	1.010,
C	0.350,	0.870,	0.400,	0.720,	0.450,	0.600,
D	0.500,	0.500,	0.550,	0.410,	0.600,	0.320,
E	0.650,	0.250,	0.700,	0.200,	0.800,	0.090,
F	0.900,	0.020,	0.950,	0.010,	1.000,	0.000,
	RLDR=3.0					
8	4.000,					
9	0.000,	2.990,	0.025,	2.600,	0.050,	2.380,
A	0.075,	2.220,	0.100,	2.060,	0.150,	1.780,
B	0.200,	1.560,	0.250,	1.350,	0.300,	1.170,
C	0.350,	1.000,	0.400,	0.860,	0.450,	0.700,
D	0.500,	0.570,	0.550,	0.460,	0.600,	0.360,
E	0.650,	0.220,	0.700,	0.240,	0.800,	0.090,
F	0.900,	0.020,	0.950,	0.010,	1.000,	0.000,
	RLDR=4.0					

BEST AVAILABLE COPY

TABLE XV (Cont'd.)

RLDR=5.0

DATA CDART3/ 5.000,

	DD2	CDA	DD2	CDA	DD2	CDA
1	0.000,	3.320,	0.025,	3.010,	0.050,	2.650,
2	0.075,	2.460,	0.100,	2.270,	0.150,	1.970,
3	0.200,	1.710,	0.250,	1.480,	0.300,	1.260,
4	0.350,	1.080,	0.400,	0.910,	0.450,	0.770,
5	0.500,	0.620,	0.550,	0.510,	0.600,	0.410,
6	0.650,	0.310,	0.700,	0.240,	0.800,	0.110,
7	0.900,	0.030,	0.950,	0.020,	1.000,	0.000,

RLDR=6.0

DATA CDART3/ 6.000,

	DD2	CDA	DD2	CDA	DD2	CDA
1	0.000,	3.720,	0.050,	2.960,	0.100,	2.470,
2	0.150,	2.110,	0.200,	1.840,	0.250,	1.600,
3	0.300,	1.390,	0.350,	1.170,	0.400,	0.990,
4	0.450,	0.840,	0.500,	0.700,	0.550,	0.540,
5	0.600,	0.450,	0.650,	0.340,	0.700,	0.240,
6	0.750,	0.160,	0.800,	0.110,	0.850,	0.060,
7	0.900,	0.030,	0.950,	0.020,	1.000,	0.000/

RLDR=8.0

DATA CDART4/ 8.000,

	DD2	CDA	DD2	CDA	DD2	CDA
1	0.000,	4.250,	0.025,	3.750,	0.050,	3.270,
2	0.075,	3.020,	0.100,	2.760,	0.150,	2.380,
3	0.200,	2.040,	0.250,	1.760,	0.300,	1.520,
4	0.350,	1.300,	0.400,	1.090,	0.450,	0.910,
5	0.500,	0.760,	0.550,	0.600,	0.600,	0.480,
6	0.650,	0.370,	0.700,	0.270,	0.800,	0.130,
7	0.900,	0.040,	0.950,	0.010,	1.000,	0.000,

RLDR=10.0

DATA CDART4/ 10.000,

	DD2	CDA	DD2	CDA	DD2	CDA
1	0.000,	5.000,	0.025,	4.270,	0.050,	3.560,
2	0.075,	3.280,	0.100,	2.990,	0.150,	2.560,
3	0.200,	2.210,	0.250,	1.910,	0.300,	1.630,
4	0.350,	1.390,	0.400,	1.160,	0.450,	0.970,
5	0.500,	0.820,	0.550,	0.660,	0.600,	0.520,
6	0.650,	0.410,	0.700,	0.270,	0.800,	0.140,
7	0.900,	0.040,	0.950,	0.010,	1.000,	0.000/

RLDR=16.0

DATA CDART5/16.000,

	DD2	CDA	DD2	CDA	DD2	CDA
1	0.000,	5.600,	0.025,	5.000,	0.050,	4.100,
2	0.075,	3.700,	0.100,	3.340,	0.150,	2.910,
3	0.200,	2.500,	0.250,	2.160,	0.300,	1.860,
4	0.350,	1.630,	0.400,	1.360,	0.450,	1.140,
5	0.500,	0.920,	0.550,	0.750,	0.600,	0.580,
6	0.650,	0.440,	0.700,	0.320,	0.800,	0.140,
7	0.900,	0.040,	0.950,	0.010,	1.000,	0.000,

BEST AVAILABLE COPY

TABLE XV (Cont'd.)

	RLDR=20.0	DD2	CDA	DD2	CDA	DD2	CDA
8	20.000						
9	0.025,	4.990,	0.050,	4.500,	0.100,	3.750,	
A	0.150,	3.150,	0.200,	2.750,	0.250,	2.380,	
B	0.300,	2.040,	0.350,	1.740,	0.400,	1.470,	
C	0.450,	1.200,	0.500,	1.000,	0.550,	0.800,	
D	0.600,	0.630,	0.650,	0.490,	0.700,	0.360,	
E	0.750,	0.250,	0.800,	0.150,	0.850,	0.080,	
F	0.900,	0.040,	0.950,	0.010,	1.000,	0.000/	

TABLE XVI

LUG DRAG COEFFICIENT

FL = LUG EQUIVALENT FLAT PLATE AREA-SQUARE INCHES
 RM = MACH NUMBER

	RM	FL	RM	FL	RM	FL
DATA FLRM7/	1.200,	18.200,	1.250,	18.400,	1.300,	18.400,
1	1.400,	18.100,	1.600,	16.900,	2.000,	14.900,
2	2.400,	13.200,	2.800,	11.600,	3.200,	10.300,
3	3.600,	9.100,	4.000,	8.100/		

TABLE XVII

MUNK'S EFFICIENCY FACTOR

FRB = BODY FITNESS RATIO
 EK=MUNK'S EFFICIENCY FACTOR

	FRB	EK	FRB	EK	FRB	EK
DATA EKFRB/	4.000,	0.780,	5.000,	0.830,	6.000,	0.870,
1	7.000,	0.890,	8.000,	0.920,	9.000,	0.930,
2	10.000,	0.940,	11.000,	0.950,	12.000,	0.960,
3	13.000,	0.965,	14.000,	0.970,	15.000,	0.975,
4	16.000,	0.980,	17.000,	0.984,	18.000,	0.985,
5	19.000,	0.985,	20.000,	0.988/		

BEST AVAILABLE COPY

factor is presented in Table XVIII as a function of boattail geometry and angle of attack. Body lift curve slope at subsonic speeds is based on the relation

$$C_{L\alpha_B} = 2EK + 2EK(K_{BT})$$

Transonic, M=1

Body lift curve slope at Mach 1 is based on slender body theory adjusted for experimental results. Body lift curve slope is given by the following relation

$$C_{L\alpha_B} = 2.41 + 2.41K_{BT}$$

Supersonic, M>1.2

Supersonic lift curve slope for nose-cylinder bodies is a function of nose fineness ratio to cylindrical section fineness ratio.

Supersonic lift curve slope for cone-cylinder bodies is presented in Table XIX. Ogive-cylinder data is presented in Table XX. Effects of nose bluntness on blunted cone lift curve slope are based on data of Figure 4.2.1.1-24 of Reference 1. Tables XXI and XXII present bluntness effects for blunted conical nose shapes and blunted ogival nose shapes, respectively.

4.3 Center of Pressure

Subsonic and Transonic

Center of pressure for nose and boattail at subsonic speeds and transonic speeds according to potential flow theory is given by the following relation:

$$\frac{CP}{DR} = \left\{ \frac{LN}{DR} \left(1 - \frac{V}{S_{REF} L_N} \right) \left(\frac{CP_{AB}}{CP_C} \right) C_{L\alpha_N} + \frac{L_{BT}}{DR} \left\{ [DR + 2(D_B + \frac{0.2 L_M}{12})] / \right. \right. \\ \left. \left. 3(D_R + D_B + \frac{0.2 L_M}{12}) \right] + \left(\frac{L_N + L_C}{DR} \right) \right\} C_{L\alpha_{BT}} \right\} / (C_{L\alpha_N} + C_{L\alpha_{BT}})$$

TABLE XVIII
BOATTAIL LIFT FACTOR
VOLRATERBOATTAIL VOLUME(1.-BASE AREA/REF. AREA)/NOSE VOLUME

ALPHA= ANGLE OF ATTACK = DEG RBTON=BOATTAIL LIFT FACTOR ALPHA=0.0						
DATA VOLRA/ 0.000, VOLRAT RBTON VOLRAT RBTON VOLRAT RBTON						
1 0.000, 0.000, 0.200, -0.515, 0.400, -0.861,						
2	0.600, -0.973,	0.800, -1.000,			1.000, -1.000,	
ALPHA=5.0 3 5.000, VOLRAT RBTON VOLRAT RBTON VOLRAT RBTON						
4	0.000, 0.000, 0.200, -0.500,	0.400, -0.845,				
5	0.600, -0.958,	0.800, -0.980,	1.000, -0.985,			
ALPHA=10.0 6 10.000, VOLRAT RBTON VOLRAT RBTON VOLRAT RBTON						
7	0.000, 0.000, 0.200, -0.465,	0.400, -0.802,				
8	0.600, -0.905,	0.800, -0.925,	1.000, -0.930,			
ALPHA=15.0 9 15.000, VOLRAT RBTON VOLRAT RBTON VOLRAT RBTON						
A	0.000, 0.000, 0.200, -0.400,	0.400, -0.695,				
B	0.600, -0.810,	0.800, -0.835,	1.000, -0.840,			
ALPHA=20.0 C 20.000, VOLRAT RBTON VOLRAT RBTON VOLRAT RBTON						
D	0.000, 0.000, 0.200, -0.280,	0.400, -0.502,				
E	0.600, -0.630,	0.800, -0.671,	1.000, -0.680,			
ALPHA=30.0 F 30.000, VOLRAT RBTON VOLRAT RBTON VOLRAT RBTON						
G	0.000, 0.000, 0.200, 0.000,	0.400, 0.000,				
H	0.600, 0.000, 0.800, 0.000,	1.000, 0.000/				

BEST AVAILABLE COPY

BEST AVAILABLE COPY

TABLE XIX
SUPERSONIC LIFT CURVE SLOPE FOR CONE-CYLINDERS

REF. FIG. 4.2.1.1-21B, PFF.1
BFN=BETA/NOSE L/D
BFN=1.0/BFN
FAFN=CYLINDER (L/D)/NOSE (L/D)
CLA=LIFT CURVE SLOPE -(1/RAD)
FAFN=0.0

DATA CNA231/0.000,

	BFN	CLA	BFN	CLA	BFN	CLA
2	0.300,	1.930,	0.400,	1.900,	0.600,	1.880,
3	0.700,	1.870,	0.800,	1.860,	0.900,	1.860,
4	1.000,	1.860,				
	FAFN=0.5					
5	0.500,					
	BFN	CLA	BFN	CLA	BFN	CLA
6	0.300,	2.580,	0.400,	2.600,	0.600,	2.620,
7	0.700,	2.610,	0.800,	2.605,	0.900,	2.600,
8	1.000,	2.580,				
	FAFN=1.0					
9	1.000,					
	BFN	CLA	BFN	CLA	BFN	CLA
A	0.300,	2.690,	0.400,	2.790,	0.600,	2.910,
B	0.700,	2.940,	0.800,	2.980,	0.900,	2.990,
C	1.000,	3.000,				
	FAFN=2.0					
D	2.000,					
	BFN	CLA	BFN	CLA	BFN	CLA
E	0.300,	2.730,	0.400,	2.860,	0.600,	3.060,
F	0.700,	3.130,	0.800,	3.200,	0.900,	3.240,
G	1.000,	3.290/				
	FAFN=3.0					

DATA CNA232/3.000,

	BFN	CLA	BFN	CLA	BFN	CLA
1	0.300,	2.760,	0.400,	2.910,	0.600,	3.140,
2	0.700,	3.220,	0.800,	3.290,	0.900,	3.360,
3	1.000,	3.430,				
	FAFN=4.0					
4	4.000,					
	BFN	CLA	BFN	CLA	BFN	CLA
5	0.300,	2.770,	0.400,	2.920,	0.600,	3.160,
6	0.700,	3.240,	0.800,	3.320,	0.900,	3.380,
7	1.000,	3.475,				
	FAFN=5.0					
8	5.000,					

TABLE XIX (Cont'd.)

	BFN	CLA	BFN	CLA	BFN	CLA
9	0.300,	2.790,	0.400,	2.940,	0.600,	3.165,
A	0.700,	3.245,	0.800,	3.325,	0.900,	3.408,
B	1.000,	3.475/				
DATA CNA24/	0.000,	0.300,	1.850,	0.500,	1.855,	0.600,
1	1.860,	0.800,	1.860,	1.000,	1.860,	
2	0.500,	0.300,	2.230,	0.500,	2.420,	0.600,
3	2.460,	0.800,	2.540,	1.000,	2.580,	
4	1.000,	0.300,	2.560,	0.500,	2.780,	0.600,
5	2.850,	0.800,	2.940,	1.000,	2.990,	
6	2.000,	0.300,	2.970,	0.500,	3.220,	0.600,
7	3.280,	0.800,	3.320,	1.000,	3.290,	
8	3.000,	0.300,	3.230,	0.500,	3.440,	0.600,
9	3.490,	0.800,	3.490,	1.000,	3.430,	
A	4.000,	0.300,	3.340,	0.500,	3.530,	0.600,
B	3.590,	0.800,	3.560,	1.000,	3.460,	
C	5.000,	0.300,	3.435,	0.500,	3.620,	0.600,
D	3.633,	0.800,	3.600,	1.000,	3.475/	

TABLE XX

SUPERSONIC LIFT CURVE SLOPE FOR OGIVE-CYLINDERS

REF. FIG.4.2.1.21A, REF.1

BFN=BETA/NOSE L/D

RBFN=1.0/BFN

FAFN=CYLINDER L/D/NOSE L/D

CLAE=LIFT CURVE SLOPE=(1/RADI)

FAFN=0.0

DATA CNA211/0.000,

	BFN	CLA	BFN	CLA	BFN	CLA
1	0.200,	2.430,	0.300,	2.410,	0.400,	2.380,
2	0.500,	2.360,	0.600,	2.340,	0.800,	2.290,
3	1.000,	2.220,				
		FAFN=0.5				
4	0.500,					
	BFN	CLA	BFN	CLA	BFN	CLA
5	0.200,	2.780,	0.300,	2.810,	0.400,	2.820,
6	0.500,	2.825,	0.600,	2.830,	0.800,	2.800,
7	1.000,	2.760,				
		FAFN=1.0				
8	1.000,					
	BFN	CLA	BFN	CLA	BFN	CLA
9	0.200,	2.890,	0.300,	2.920,	0.400,	2.960,
A	0.500,	2.990,	0.600,	3.020,	0.800,	3.040,
B	1.000,	3.045/				

BEST AVAILABLE COPY

TABLE XX (Continued)

FAFN=2.0						
DATA CNA212/2.000,						
	RFN	CLA	RFN	CLA	RFN	CLA
1	0.200,	2.880,	0.300,	2.950,	0.400,	3.020,
2	0.500,	3.090,	0.600,	3.140,	0.800,	3.220,
3	1.000,	3.290,				
	FAFN=3.0					
4	3.000,					
	RFN	CLA	RFN	CLA	RFN	CLA
5	0.200,	2.860,	0.300,	2.950,	0.400,	3.030,
6	0.500,	3.120,	0.600,	3.190,	0.800,	3.320,
7	1.000,	3.390,				
	FAFN=4.0					
8	4.000,					
	RFN	CLA	RFN	CLA	RFN	CLA
9	0.200,	2.840,	0.300,	2.930,	0.400,	3.030,
A	0.500,	3.140,	0.600,	3.220,	0.800,	3.350,
B	1.000,	3.410/				
	FAFN=0.0					
	DATA CNA22/0.000,					
	PPFN	CLA	PPFN	CLA	PPFN	CLA
1	0.200,	1.250,	0.300,	1.530,	0.400,	1.730,
2	0.600,	1.960,	0.800,	2.110,	1.000,	2.220,
	FAFN=0.5					
3	0.500,					
	PPFN	CLA	PPFN	CLA	PPFN	CLA
4	0.200,	1.560,	0.300,	1.900,	0.400,	2.160,
5	0.600,	2.470,	0.800,	2.650,	1.000,	2.760,
	FAFN=1.0					
6	1.000,					
	PPFN	CLA	PPFN	CLA	PPFN	CLA
7	0.200,	1.630,	0.300,	2.040,	0.400,	2.380,
8	0.600,	2.820,	0.800,	3.020,	1.000,	3.060,
	FAFN=2.0					
9	2.000,					
	PPFN	CLA	PPFN	CLA	PPFN	CLA
A	0.200,	1.720,	0.300,	2.200,	0.400,	2.580,
B	0.600,	3.070,	0.800,	3.290,	1.000,	3.290,
	FAFN=3.0					
C	3.000,					
	PPFN	CLA	PPFN	CLA	PPFN	CLA
D	0.200,	1.790,	0.300,	2.280,	0.400,	2.670,
E	0.600,	3.180,	0.800,	3.390,	1.000,	3.390,
	FAFN=4.0					
F	4.000,					
	PPFN	CLA	PPFN	CLA	PPFN	CLA
G	0.200,	1.800,	0.300,	2.300,	0.400,	2.690,
H	0.600,	3.190,	0.800,	3.430,	1.000,	3.410/

TABLE XXI
BLUNTED CONE LIFT CURVE SLOPE

BEST AVAILABLE COPY

$FR_1 = \text{ACTUAL NOSE FINENESS RATIO}$

$FCAP = \text{NOSE BLUNTNES RATIO}$

$CNAB = \text{BLUNTED CONE LIFT CURVE SLOPE}$

$FR_1 = 1.0$

DATA CNA721/1.000,

	FCAP	CNAB	FCAP	CNAB	FCAP	CNAB
1	0.000,	1.600,	0.100,	1.670,	0.200,	1.685,
2	0.300,	1.680,	0.400,	1.640,	0.500,	1.590,
3	0.600,	1.530,	0.700,	1.450,	0.800,	1.340,

$FR_1 = 1.5$

4

1.500,

	FCAP	CNAB	FCAP	CNAB	FCAP	CNAB
5	0.000,	1.800,	0.100,	1.875,	0.200,	1.865,
6	0.300,	1.790,	0.400,	1.745,	0.500,	1.685,
7	0.600,	1.605,	0.700,	1.490,	0.800,	1.350,

$FR_1 = 2.0$

8

2.000,

	FCAP	CNAB	FCAP	CNAB	FCAP	CNAB
9	0.000,	1.885,	0.100,	1.887,	0.200,	1.875,
A	0.300,	1.843,	0.400,	1.795,	0.500,	1.718,
B	0.600,	1.620,	0.700,	1.500,	0.800,	1.355,

$FR_1 = 3.0$

C

3.000,

	FCAP	CNAB	FCAP	CNAB	FCAP	CNAB
D	0.000,	1.945,	0.100,	1.943,	0.200,	1.922,
E	0.300,	1.882,	0.400,	1.818,	0.500,	1.738,
F	0.600,	1.635,	0.700,	1.505,	0.800,	1.358/

$FR_1 = 4.0$

DATA CNA722/4.000,

	FCAP	CNAB	FCAP	CNAB	FCAP	CNAB
1	0.000,	1.965,	0.100,	1.962,	0.200,	1.940,
2	0.300,	1.893,	0.400,	1.831,	0.500,	1.740,
3	0.600,	1.638,	0.700,	1.508,	0.800,	1.358,

$FR_1 = 5.0$

4

5.000,

	FCAP	CNAB	FCAP	CNAB	FCAP	CNAB
5	0.000,	1.980,	0.100,	1.972,	0.200,	1.945,
6	0.300,	1.903,	0.400,	1.835,	0.500,	1.745,
7	0.600,	1.640,	0.700,	1.509,	0.800,	1.358,

$FR_1 = 6.0$

8

6.000,

	FCAP	CNAB	FCAP	CNAB	FCAP	CNAB
9	0.000,	1.989,	0.100,	1.975,	0.200,	1.950,
A	0.300,	1.906,	0.400,	1.838,	0.500,	1.748,
B	0.600,	1.641,	0.700,	1.510,	0.800,	1.358,

$FR_1 = 7.0$

C

7.000,

	FCAP	CNAB	FCAP	CNAB	FCAP	CNAB
D	0.000,	1.990,	0.100,	1.978,	0.200,	1.950,
E	0.300,	1.905,	0.400,	1.835,	0.500,	1.748,
F	0.600,	1.642,	0.700,	1.510,	0.800,	1.358/

BEST AVAILABLE COPY

TABLE XXII
BLUNTED OGIVE LIFT CURVE SLOPE

FR1=ACTUAL NOSE FINENESS RATIO

FCAPENOSE BLUNTNES RATIO

CNAB=BLUNTED OGIVE LIFT CURVE SLOPE

FR1=1.0

DATA CNA731/1.000,

	FCAP	CNAB	FCAP	CNAB	FCAP	CNAB
1	0.000,	1.600,	0.100,	1.600,	0.200,	1.59,
2	0.300,	1.580,	0.400,	1.560,	0.500,	1.530,
3	0.600,	1.485,	0.700,	1.415,	0.800,	1.320,

FR1=1.5

4 1.500,

	FCAP	CNAB	FCAP	CNAB	FCAP	CNAB
5	0.000,	1.762,	0.100,	1.761,	0.200,	1.756,
6	0.300,	1.740,	0.400,	1.709,	0.500,	1.650,
7	0.600,	1.563,	0.700,	1.462,	0.800,	1.335,

FR1=2.0

8 2.000,

	FCAP	CNAB	FCAP	CNAB	FCAP	CNAB
9	0.000,	1.850,	0.100,	1.850,	0.200,	1.841,
A	0.300,	1.812,	0.400,	1.762,	0.500,	1.693,
B	0.600,	1.605,	0.700,	1.439,	0.800,	1.342,

FR1=3.0

C 3.000,

	FCAP	CNAB	FCAP	CNAB	FCAP	CNAB
D	0.000,	1.930,	0.100,	1.920,	0.200,	1.905,
E	0.300,	1.863,	0.400,	1.808,	0.500,	1.730,
F	0.600,	1.630,	0.700,	1.508,	0.800,	1.353,

FR1=4.0

DATA CNA732/4.000,

	FCAP	CNAB	FCAP	CNAB	FCAP	CNAB
1	0.000,	1.960,	0.100,	1.950,	0.200,	1.930,
2	0.300,	1.888,	0.400,	1.822,	0.500,	1.738,
3	0.600,	1.638,	0.700,	1.512,	0.800,	1.360,

FR1=5.0

4 5.000,

	FCAP	CNAB	FCAP	CNAB	FCAP	CNAB
5	0.000,	1.972,	0.100,	1.965,	0.200,	1.942,
6	0.300,	1.900,	0.400,	1.830,	0.500,	1.745,
7	0.600,	1.640,	0.700,	1.512,	0.800,	1.362,

FR1=6.0

8 6.000,

	FCAP	CNAB	FCAP	CNAB	FCAP	CNAB
9	0.000,	1.986,	0.100,	1.975,	0.200,	1.950,
A	0.300,	1.902,	0.400,	1.835,	0.500,	1.750,
B	0.600,	1.643,	0.700,	1.515,	0.800,	1.364,

FR1=7.0

C 7.000,

	FCAP	CNAB	FCAP	CNAB	FCAP	CNAB
D	0.000,	1.990,	0.100,	1.978,	0.200,	1.950,
E	0.300,	1.900,	0.400,	1.835,	0.500,	1.750,
F	0.600,	1.642,	0.700,	1.510,	0.800,	1.358,

Center of pressure of the nose alone is assumed to be at the centroid of the nose volume. A correction for afterbody ($\frac{CP_{AB}}{CP_c}$) is based on data of References 9 and 10.

Supersonic

Nose center of pressure at supersonic speeds is based on data of Figures 4.2.2.1-18a and b of Reference 1. Table XXIII presents center of pressure data for cone-cylinder bodies as a function of Mach number, nose fineness ratio, and the ratio of afterbody to forebody fineness ratio.

Table XXIV presents similar data for ogive-cylinder or bodies.

Center of pressure of blunted cones and ogives is based on data of Figures 4.2.2.1-21 and 4.2.2.1-22 of Reference 1. Tables XXV and XXVI present center of pressure for blunted cones and ogives as a function of nose bluntness ratio and actual non-fineness ratio. At Mach numbers greater than 4, the center of pressure is based on a curve fit of data obtained from modified Newtonian theory.

4.4

List of Symbols

<u>Symbol</u>	<u>Description</u>
C_{D_B}	Base drag coefficient
$C_{D_{BT}}$	Boattail drag coefficient
C_{D_F}	Friction drag coefficient
C_{D_i}	Induced drag coefficient
C_{D_L}	Lug drag coefficient
C_{D_O}	Zero-lift drag coefficient
C_F	Skin friction coefficient (corrected for compressibility)
$\frac{C_F}{C_{F_I}}$	Compressibility correction factor
C_{F_I}	Incompressible skin friction coefficient
$C_{L\alpha}$	Lift curve slope
CP	Center of pressure

<u>Symbol</u>	<u>Description</u>
$\frac{CP_{AB}}{CP_o}$	Nose center of pressure correction factor to account for afterbody length
EK	Munk's efficiency factor
FA	Afterbody (body minus nose) fineness ratio
FL	Launch lug equivalent flat plate area
FN	Nose fineness ratio
FRB	Body fineness ratio
K_{BT}	Boattail lift correlation factor based on boattail volume and geometry
L_{BT}	Boattail length
LC	Cylindrical center section length
LM	Missile length
LN	Nose length
M	Mach number
S_{Ref}	Reference area
Swet B	Body wetted area
V	Volume of nose
α	Angle of attack
β	Beta = $M^2 - 1$

5. LIFTING SURFACES

The lifting surfaces planform may be either the basic delta or a clipped delta. The fixed lifting surfaces may be either a planar arrangement or a cruciform X arrangement. The movable lifting surfaces may be planar with a vertical panel, cruciform +, cruciform X, or triform. Section profile may be double wedge, biconvex, or modified double wedge.

5.1 Drag

Drag of the lifting surfaces consists of pressure drag due to thickness and skin friction drag

$$C_D = C_{DP} + C_{DF}$$

TABLE XXIII
CONE-CYLINDER CENTER OF PRESSURE (SUPERSONIC)

BFN=BETA/NOSE FINENESS RATIO XCPDL=C.P. IN PERCENT BODY LENGTH FAFN=AFTERBODY (L/D1)/NOSE (L/D) FAFN=1.0						
DATA XCPRFN/1.000, BFN XCPDL BFN XCPDL BFN XCPDL						
1	0.200,	0.397,	0.600,	0.454,	0.800,	0.467,
2	1.000,	0.472,				
	FAFN=2.0					
3	2.000,					
	BFN XCPDL BFN XCPDL BFN XCPDL					
4	0.200,	0.258,	0.600,	0.332,	0.800,	0.350,
5	1.000,	0.365,				
	FAFN=3.0					
6	3.000,					
	BFN XCPDL BFN XCPDL BFN XCPDL					
7	0.200,	0.195,	0.600,	0.265,	0.800,	0.285,
8	1.000,	0.297,				
	FAFN=5.0					
9	5.000,					
A	0.200,	0.126,	0.600,	0.180,	0.800,	0.197,
B	1.000,	0.209/				
	FAFN=1.0					
DATA XCPRPP/1.000, BPPFN XCPDL BPPFN XCPDL BPPFN XCPDL						
1	0.200,	0.453,	0.600,	0.478,	0.800,	0.480,
2	1.000,	0.475,				
	FAFN=2.0					
3	2.000,					
	BPPFN XCPDL BPPFN XCPDL BPPFN XCPDL					
4	0.200,	0.383,	0.600,	0.385,	0.800,	0.375,
5	1.000,	0.365,				
	FAFN=3.0					
6	3.000,					
	BPPFN XCPDL BPPFN XCPDL BPPFN XCPDL					
7	0.200,	0.330,	0.600,	0.315,	0.800,	0.308,
8	1.000,	0.297,				
	FAFN=5.0					
9	5.000,					
A	0.200,	0.273,	0.600,	0.239,	0.800,	0.223,
B	1.000,	0.209/				

BEST AVAILABLE COPY

TABLE XXIV
OGIVE CYLINDER CENTER OF PRESSURE (SUPERSONIC)

		FAFN=1.0			
		FAFN=1.0			
	DATA XCP64/	1.000,			
1		BFN	YCPDL	BFN	XCPDL
		0.200,	0.294,	0.400,	0.335,
2		1.000,	0.380,		0.700,
			FAFN=2.0		0.366,
3		2.000,			
		BFN	YCPDL	BFN	XCPDL
4		0.200,	0.178,	0.400,	0.232,
5		1.000,	0.288,		0.700,
			FAFN=3.0		0.270,
6		3.000,			
		BFN	YCPDL	BFN	XCPDL
7		0.200,	0.125,	0.400,	0.178,
8		1.000,	0.233,		0.700,
			FAFN=4.0		0.215,
9		4.000,			
A		BFN	YCPDL	BFN	XCPDL
B		0.200,	0.095,	0.400,	0.144,
		1.000,	0.197,		0.700,
C		5.000,			
D		BFN	YCPDL	BFN	XCPDL
E		0.200,	0.080,	0.400,	0.121,
		1.000,	0.167,		0.700,
			FAFN=1.0		0.150,
	DATA XCP65/	1.000,			
1		RPPFN	YCPDL	RPPFN	XCPDL
		0.300,	0.333,	0.500,	0.373,
2		1.000,	0.380,		0.700,
			FAFN=2.0		0.381,
3		2.000,			
		RPPFN	YCPDL	RPPFN	XCPDL
4		0.300,	0.277,	0.500,	0.295,
5		1.000,	0.285,		0.700,
			FAFN=3.0		0.297,
6		3.000,			
		RPPFN	YCPDL	RPPFN	XCPDL
7		0.300,	0.235,	0.500,	0.246,
8		1.000,	0.232,		0.700,
			FAFN=4.0		0.243,
9		4.000,			
A		RPPFN	YCPDL	RPPFN	XCPDL
B		0.300,	0.204,	0.500,	0.213,
		1.000,	0.197,		0.700,
C		5.000,			
D		RPPFN	YCPDL	RPPFN	XCPDL
E		0.300,	0.177,	0.500,	0.186,
		1.000,	0.167,		0.700,

TABLE XXV
BLUNTED CONE CENTER OF PRESSURE (SUPERSONIC)

$FCAP = \text{NOSE BLUNTNES RATIO}$

$FR1 = \text{ACTUAL NOSE FINENESS RATIO}$

$XCPN = C.P. \text{ OF NOSE IN PERCENT ACTUAL NOSE LENGTH}$

$FR1=1.0$

DATA XCPNC1/1.000,

	FCAP	XCPN	FCAP	XCPN	FCAP	XCPN
1	0.000,	0.830,	0.100,	0.805,	0.200,	0.780,
2	0.300,	0.753,	0.400,	0.727,	0.500,	0.698,
3	0.600,	0.670,	0.700,	0.640,	0.800,	0.613,

$FR1=2.0$

2.000,

	FCAP	XCPN	FCAP	XCPN	FCAP	XCPN
5	0.000,	0.668,	0.100,	0.642,	0.200,	0.615,
6	0.300,	0.589,	0.400,	0.560,	0.500,	0.525,
7	0.600,	0.485,	0.700,	0.435,	0.800,	0.365,

$FR1=3.0$

3.000,

	FCAP	XCPN	FCAP	XCPN	FCAP	XCPN
9	0.000,	0.667,	0.100,	0.639,	0.200,	0.611,
A	0.300,	0.580,	0.400,	0.548,	0.500,	0.510,
B	0.600,	0.466,	0.700,	0.410,	0.800,	0.338,

$FR1=4.0$

4.000,

	FCAP	XCPN	FCAP	XCPN	FCAP	XCPN
D	0.000,	0.666,	0.100,	0.637,	0.200,	0.610,
E	0.300,	0.576,	0.400,	0.543,	0.500,	0.503,
F	0.600,	0.456,	0.700,	0.398,	0.800,	0.321/

$FR1=5.0$

DATA XCPNC2/5.000,

	FCAP	XCPN	FCAP	XCPN	FCAP	XCPN
1	0.000,	0.666,	0.100,	0.636,	0.200,	0.607,
2	0.300,	0.573,	0.400,	0.539,	0.500,	0.498,
3	0.600,	0.448,	0.700,	0.390,	0.800,	0.311,

$FR1=6.0$

6.000,

	FCAP	XCPN	FCAP	XCPN	FCAP	XCPN
5	0.000,	0.666,	0.100,	0.635,	0.200,	0.606,
6	0.300,	0.572,	0.400,	0.536,	0.500,	0.495,
7	0.600,	0.444,	0.700,	0.386,	0.800,	0.305,

$FR1=7.0$

7.000,

	FCAP	XCPN	FCAP	XCPN	FCAP	XCPN
9	0.000,	0.666,	0.100,	0.635,	0.200,	0.605,
A	0.300,	0.570,	0.400,	0.535,	0.500,	0.493,
B	0.600,	0.443,	0.700,	0.385/		

BEST AVAILABLE COPY

TABLE XXVI
BLUNTED NOSE CENTER OF PRESSURE (SUPERSONIC)

FCAP = NOSE BLUNTNES RATIO

FR1 = ACTUAL NOSE FINENESS RATIO

XCPN = C.P. OF NOSE IN PERCENT ACTUAL NOSE LENGTH

FR1=1.0

DATA XCP751/1.000,

	FCAP	XCPN	FCAP	XCPN	FCAP	XCPN
--	------	------	------	------	------	------

1	0.000	0.496	0.100	0.487	0.200	0.475
---	-------	-------	-------	-------	-------	-------

2	0.300	0.463	0.400	0.451	0.500	0.438
---	-------	-------	-------	-------	-------	-------

3	0.600	0.422	0.700	0.405	0.800	0.381
---	-------	-------	-------	-------	-------	-------

FR1=2.0

2.000,

	FCAP	XCPN	FCAP	XCPN	FCAP	XCPN
--	------	------	------	------	------	------

5	0.000	0.470	0.100	0.457	0.200	0.441
---	-------	-------	-------	-------	-------	-------

6	0.300	0.426	0.400	0.409	0.500	0.390
---	-------	-------	-------	-------	-------	-------

7	0.600	0.368	0.700	0.318	0.800	0.297
---	-------	-------	-------	-------	-------	-------

FR1=3.0

3.000,

	FCAP	XCPN	FCAP	XCPN	FCAP	XCPN
--	------	------	------	------	------	------

9	0.000	0.469	0.100	0.453	0.200	0.434
---	-------	-------	-------	-------	-------	-------

A	0.300	0.419	0.400	0.400	0.500	0.379
---	-------	-------	-------	-------	-------	-------

B	0.600	0.353	0.700	0.317	0.800	0.273
---	-------	-------	-------	-------	-------	-------

FR1=4.0

4.000,

	FCAP	XCPN	FCAP	XCPN	FCAP	XCPN
--	------	------	------	------	------	------

D	0.000	0.468	0.100	0.451	0.200	0.433
---	-------	-------	-------	-------	-------	-------

E	0.300	0.415	0.400	0.394	0.500	0.371
---	-------	-------	-------	-------	-------	-------

F	0.600	0.344	0.700	0.305	0.800	0.260
---	-------	-------	-------	-------	-------	-------

FR1=5.0

DATA XCP752/5.000,

	FCAP	XCPN	FCAP	XCPN	FCAP	XCPN
--	------	------	------	------	------	------

1	0.000	0.467	0.100	0.450	0.200	0.430
---	-------	-------	-------	-------	-------	-------

2	0.300	0.410	0.400	0.389	0.500	0.364
---	-------	-------	-------	-------	-------	-------

3	0.600	0.336	0.700	0.298	0.800	0.250
---	-------	-------	-------	-------	-------	-------

FR1=6.0

6.000,

	FCAP	XCPN	FCAP	XCPN	FCAP	XCPN
--	------	------	------	------	------	------

5	0.000	0.467	0.100	0.449	0.200	0.428
---	-------	-------	-------	-------	-------	-------

6	0.300	0.408	0.400	0.385	0.500	0.360
---	-------	-------	-------	-------	-------	-------

7	0.600	0.330	0.700	0.291	0.800	0.243
---	-------	-------	-------	-------	-------	-------

FR1=7.0

7.000,

	FCAP	XCPN	FCAP	XCPN	FCAP	XCPN
--	------	------	------	------	------	------

9	0.000	0.467	0.100	0.447	0.200	0.427
---	-------	-------	-------	-------	-------	-------

A	0.300	0.405	0.400	0.382	0.500	0.356
---	-------	-------	-------	-------	-------	-------

B	0.600	0.325	0.700	0.285	0.800	0.236
---	-------	-------	-------	-------	-------	-------

5.1.1 Zero-Lift Drag Coefficient

Subsonic

The lifting surface drag at subsonic speeds is based on skin friction drag corrected for thickness ratio effects. The skin friction coefficient is based on Reynold's number computed from the mean geometric chord of the surface. Lifting surface zero lift drag coefficient at subsonic speeds is given by the following:

$$C_{D_0} = \left\{ 2C_F + 2C_F \left[2\left(\frac{t}{c}\right) + 100\left(\frac{t}{c}\right)^4 \right] \right\} \frac{S_p}{S_{REF}} N_p$$

Surface wetted area is assumed to be twice the planform area S_p . N_p accounts for the number of panels.

Transonic, M = 1

Zero-lift drag in the transonic region consists of friction drag plus a pressure drag term derived from a curve fit of data of Reference 2.

$$C_{D_0} = \left[2C_F + \left(\frac{C_{DP}}{A(\frac{t}{c})} \right) A\left(\frac{t}{c}\right) \right] \frac{S_p}{S_{REF}} N_p$$

Supersonic

Zero-lift drag coefficient in the supersonic region consists of friction drag and pressure drag due to thickness. For subsonic leading edges, zero-lift drag coefficient is given by the following:

$$C_{D_0} = \left[2C_F + K \cot \Lambda_{LE} \left(\frac{t}{c} \right) \right] \frac{S_p}{S_{REF}} N_p$$

For supersonic leading edges

$$C_{D_0} = \left[2C_F + \frac{K}{\beta} \left(\frac{t}{c} \right)^2 \right] \frac{S_p}{S_{REF}} N_p$$

The airfoil section constant, K, is based on data of page 4.1.5.1-15 of Reference 1.

5.1.2 Induced Drag Coefficient

Induced drag is based on the relation

$$C_{D_L} = C_L \tan \alpha$$

5.1.3 Total Drag Coefficient

Total drag coefficient consists of zero-lift drag coefficient plus the induced drag coefficient

$$C_D = C_{D_0} + C_{D_L}$$

5.2

Lift Curve SlopesSubsonic

Isolated lifting surface lift curve slope is obtained from data of Reference 11.

$$C_{L\alpha} = f(A, \tan \Lambda_{1/2}, \beta) \frac{S_P}{S_{REF}} N_P K_F$$

The arrangement factor K_F accounts for the reduced effective angle of attack and rotates the lift vector into the pitch plume for tri-form and cruciform "X" configurations. Table XXVII presents isolated surface lift curve slope divided by aspect ratio $C_{L\alpha}/A$ as a function of surface taper ratio (λ), the product of aspect ratio and the tangent of the midchord sweep angle $A \tan \Lambda_{1/2}$ and the product of aspect ratio and $\beta \sqrt{M^2 - 1}$. (BAR)

Transonic

Lift curve slope of the isolated panel is defined by the relation

$$C_{L\alpha} = f(A, \tan \Lambda_{1/2}, \beta) \frac{S_P}{S_{REF}} N_P K_F$$

Supersonic

Lift curve slope of lifting surfaces with exposed aspect ratios greater than 1.0 is based on the relation.

$$C_{L\alpha} = f(A, \tan \Lambda_{1/2}, \beta) \frac{S_P}{S_{REF}} N_P K_F$$

Low aspect ratio wings ($A \leq 1.0$) produce more lift than indicated by Reference 11 according to data of Reference 10 and 12. A correction factor $(1 + K_A K_M)$ was developed by Martin to account for aspect ratio and Mach number. This factor is applied to the $C_{L\alpha}$ obtained from Reference 11.

$$C_{L\alpha} = [f(A, \tan \Lambda_{1/2}, \beta)](1 + K_A K_M) \frac{S_P}{S_{REF}} N_P K_F$$

5.3

Interference Effects

The mutual interference effects of the wing/body, tail/body, and tail in the presence of the wing are based on the methods described in References 1 and 13.

TABLE XXVII
SURSONIC SURFACE LIFT CURVE SLOPE/SURFACE ASPECT RATIO

TRI=SURFACE TAPER RATIO										
DATA AIC601/0.000, .00.250, .0.500, 1.000,										
ATNS2I=ASPECT RATIO TIMES TANGENT OF MIDCHORD SWEEP										
1	0.000,	1.000,	2.000,	3.000,	4.000,	5.000,	6.000,			
	BARI=RETA TIMES ASPFCT RATIO									
2	0.000,	0.500,	1.000,	1.500,	2.000,					
3	3.000,	4.000,	5.000,	6.000,	7.000,					
ATCLI=SURFACE LIFT CURVE SLOPE/ASPECT RATIO										
	TRI=0.0	ATNS2I=0.0								
4	1.570,	1.500,	1.425,	1.320,	1.210,					
5	1.030,	0.900,	0.780,	0.700,	0.640,					
	TRI=0.0	ATNS2I=1.0								
6	1.570,	1.490,	1.400,	1.285,	1.170,					
7	1.010,	0.880,	0.770,	0.690,	0.620,					
	TRI=0.0	ATNS2I=2.0								
8	1.570,	1.440,	1.310,	1.180,	1.080,					
9	0.950,	0.840,	0.750,	0.670,	0.610,					
	TRI=0.0	ATNS2I=3.0								
A	1.260,	1.190,	1.120,	1.055,	0.990,					
B	0.890,	0.800,	0.720,	0.650,	0.600,					
	TRI=0.0	ATNS2I=4.0								
C	1.045,	1.015,	0.975,	0.935,	0.890,					
D	0.810,	0.740,	0.670,	0.620,	0.580,					
	TRI=0.0	ATNS2I=5.0								
E	0.900,	0.888,	0.860,	0.883,	0.800,					
F	0.740,	0.690,	0.640,	0.590,	0.550,					
	TRI=0.0	ATNS2I=6.0								
G	0.790,	0.783,	0.770,	0.750,	0.730,					
H	0.680,	0.630,	0.590,	0.560,	0.520/					
	TRI=0.25	ATNS2I=0.0								
DATA AIC602/1.570,						1.520,	1.440,	1.345,	1.250,	
1		1.070,	0.930,	0.820,	0.730,	0.660,				
	TRI=0.25	ATNS2I=1.0								
2		1.570,	1.510,	1.420,	1.325,	1.220,				
3		1.040,	0.910,	0.790,	0.720,	0.650,				
	TRI=0.25	ATNS2I=2.0								
4		1.570,	1.440,	1.330,	1.220,	1.135,				
5		0.980,	0.870,	0.770,	0.690,	0.630,				
	TRI=0.25	ATNS2I=3.0								
6		1.265,	1.200,	1.130,	1.065,	1.000,				
7		0.910,	0.810,	0.730,	0.660,	0.510,				
	TRI=0.25	ATNS2I=4.0								
8		1.050,	1.010,	0.970,	0.930,	0.890,				
9		0.830,	0.760,	0.690,	0.660,	0.580,				

BEST AVAILABLE COPY

TABLE XXVII (Continued)

			TRI=0.25 ATNSPI=5.0	
A	0.900,	0.870, 0.840, 0.810,	0.780,	
B	0.740,	0.690, 0.640, 0.600,	0.560,	
		TRI=0.25 ATNSPI=6.0		
C	0.790,	0.765, 0.740, 0.720,	0.700,	
D	0.670,	0.640, 0.600, 0.560,	0.530/	
		TRI=0.50 ATNSPI=0.0		
	DATA AIR603/1.570,	1.520, 1.430, 1.340,	1.240,	
1	1.080,	0.940, 0.820, 0.730,	0.660,	
		TRI=0.50 ATNSPI=1.0		
2	1.570,	1.500, 1.405, 1.300,	1.200,	
3	1.040,	0.920, 0.800, 0.720,	0.640,	
		TRI=0.50 ATNSPI=2.0		
4	1.570,	1.430, 1.310, 1.200,	1.120,	
5	0.980,	0.870, 0.770, 0.690,	0.630,	
		TRI=0.50 ATNSPI=3.0		
6	1.260,	1.200, 1.130, 1.060,	1.010,	
7	0.910,	0.820, 0.730, 0.660,	0.600,	
		TRI=0.50 ATNSPI=4.0		
8	1.060,	1.017, 0.975, 0.940,	0.900,	
9	0.830,	0.750, 0.680, 0.620,	0.580,	
		TRI=0.50 ATNSPI=5.0		
A	0.910,	0.875, 0.850, 0.815,	0.785,	
B	0.740,	0.680, 0.630, 0.590,	0.550,	
		TRI=0.50 ATNSPI=6.0		
C	0.780,	0.760, 0.740, 0.715,	0.690,	
D	0.660,	0.630, 0.580, 0.550,	0.520/	
		TRI=1.00 ATNSPI=0.0		
	DATA AIR604/1.570,	1.525, 1.445, 1.340,	1.220,	
1	1.040,	0.900, 0.790, 0.700,	0.640,	
		TRI=1.00 ATNSPI=1.0		
2	1.570,	1.510, 1.420, 1.305,	1.180,	
3	1.000,	0.880, 0.770, 0.690,	0.620,	
		TRI=1.00 ATNSPI=2.0		
4	1.570,	1.473, 1.350, 1.220,	1.106,	
5	0.950,	0.820, 0.730, 0.660,	0.610,	
		TRI=1.00 ATNSPI=3.0		
6	1.260,	1.170, 1.093, 1.020,	0.960,	
7	0.860,	0.770, 0.690, 0.630,	0.580,	
		TRI=1.00 ATNSPI=4.0		
8	1.050,	0.992, 0.940, 0.886,	0.845,	
9	0.780,	0.710, 0.650, 0.600,	0.560,	
		TRI=1.00 ATNSPI=5.0		
A	0.905,	0.853, 0.803, 0.765,	0.740,	
B	0.700,	0.650, 0.600, 0.560,	0.540,	
		TRI=1.00 ATNSPI=6.0		
C	0.790,	0.740, 0.705, 0.670,	0.650,	
D	0.620,	0.590, 0.560, 0.530,	0.500/	

BEST AVAILABLE COPY

TABLE XXVII (Continued)

SUPERSONIC SURFACE LIFT CURVE SLOPE/SURFACE ASPECT RATIO

TRI=SURFACE TAPER RATIO
DATA AIC611/0.000, 0.250, 0.500, 1.000,
ATNS2I=ASPECT RATIO TIMES TANGENT OF MIDCHORD SWEEP
1 0.000, 1.000, 2.000, 3.000, 4.000,
2 5.000, 6.000,
BARJ=BETA TIMES ASPECT RATIO
3 0.000, 0.500, 1.000, 1.500, 2.000,
4 3.000, 4.000, 5.000, 6.000, 7.000,
AICLI=SURFACE LIFT CURVE SLOPE/ASPECT RATIO
TRI=0.00 ATNS2I=0.0
5 1.570, 1.700, 1.750, 1.730, 1.700,
6 1.210, 0.950, 0.770, 0.650, 0.550,
TRI=0.00 ATNS2I=1.0
7 1.570, 1.740, 1.745, 1.630, 1.490,
8 1.260, 0.960, 0.790, 0.660, 0.560,
TRI=0.00 ATNS2I=2.0
9 1.570, 1.530, 1.460, 1.380, 1.300,
A 1.140, 1.010, 0.820, 0.680, 0.580,
TRI=0.00 ATNS2I=3.0
B 1.260, 1.300, 1.275, 1.230, 1.170,
C 1.050, 0.950, 0.860, 0.710, 0.600,
TRI=0.00 ATNS2I=4.0
D 1.040, 1.066, 1.080, 1.075, 1.060,
E 0.980, 0.900, 0.830, 0.760, 0.630,
TRI=0.00 ATNS2I=5.0
F 0.900, 0.915, 0.930, 0.935, 0.940,
G 0.910, 0.840, 0.780, 0.730, 0.680,
TRI=0.00 ATNS2I=6.0
H 0.800, 0.800, 0.800, 0.800, 0.800,
X 0.800, 0.810, 0.750, 0.710, 0.660/
TRI=0.25 ATNS2I=0.0
DATA AIC612/1.570, 1.400, 1.890, 1.830, 1.640,
1 1.220, 0.940, 0.770, 0.650, 0.560,
TRI=0.25 ATNS2I=1.0
2 1.570, 1.350, 1.840, 1.710, 1.580,
3 1.220, 0.940, 0.770, 0.650, 0.560,
TRI=0.25 ATNS2I=2.0
4 1.570, 1.120, 1.480, 1.470, 1.410,
5 1.230, 0.990, 0.810, 0.680, 0.580,
TRI=0.25 ATNS2I=3.0
6 1.265, 1.180, 1.090, 1.240, 1.280,
7 1.130, 1.020, 0.850, 0.720, 0.610,
TRI=0.25 ATNS2I=4.0
8 1.055, 1.053, 1.050, 1.048, 1.045,
9 1.040, 0.960, 0.870, 0.750, 0.640,

BEST AVAILABLE COPY

TABLE XXVII (Continued)

			TRT=0.25	ATNS2I=5.0
A	0.900,	0.910,	0.920,	0.930,
B	0.950,	0.910,	0.850,	0.780,
			TRT=0.25	ATNS2I=6.0
C	0.793,	0.785,	0.780,	0.780,
D	0.800,	0.830,	0.820,	0.760,
			TRT=0.50	ATNS2I=0.0
	DATA AIC613/1.570,	1.860,	1.960,	1.830,
1	1.200,	0.930,	0.760,	0.640,
			TRT=0.50	ATNS2I=1.0
2	1.570,	1.780,	1.930,	1.780,
3	1.200,	0.940,	0.770,	0.660,
			TRT=0.50	ATNS2I=2.0
4	1.570,	1.480,	1.360,	1.430,
5	1.210,	0.980,	0.800,	0.670,
			TRT=0.50	ATNS2I=3.0
6	1.270,	1.255,	1.240,	1.225,
7	1.150,	1.010,	0.840,	0.700,
			TRT=0.50	ATNS2I=4.0
8	1.060,	1.060,	1.060,	1.060,
9	1.065,	0.980,	0.870,	0.750,
			TRT=0.50	ATNS2I=5.0
A	0.910,	0.910,	0.910,	0.910,
B	0.920,	0.910,	0.860,	0.770,
			TRT=0.50	ATNS2I=6.0
C	0.780,	0.790,	0.800,	0.810,
D	0.825,	0.830,	0.820,	0.770,
			TRT=1.00	ATNS2I=0.0
	DATA AIC614/1.570,	1.790,	1.990,	1.800,
1	1.120,	0.980,	0.730,	0.620,
			TRT=1.00	ATNS2I=1.0
2	1.570,	1.547,	2.010,	1.720,
3	1.130,	0.900,	0.740,	0.630,
			TRT=1.00	ATNS2I=2.0
4	1.570,	1.537,	1.520,	1.480,
5	1.140,	0.930,	0.760,	0.650,
			TRT=1.00	ATNS2I=3.0
6	1.250,	1.300,	1.300,	1.275,
7	1.140,	0.960,	0.800,	0.680,
			TRT=1.00	ATNS2I=4.0
8	1.050,	1.050,	1.050,	1.040,
9	0.980,	0.970,	0.830,	0.710,
			TRT=1.00	ATNS2I=5.0
A	0.910,	0.900,	0.880,	0.873,
B	0.860,	0.860,	0.840,	0.740,
			TRT=1.00	ATNS2I=6.0
C	0.790,	0.785,	0.780,	0.770,
D	0.760,	0.750,	0.760,	0.780,

5.3.1

Carryover Due to Angle of Attack

$$K_{S(B)} = \frac{z}{\pi} \cdot \frac{\left\{ \left(1 + \frac{r^4}{s^4} \right) \left[\frac{1}{2} \tan^{-1} \frac{1}{2} \left(\frac{s}{r} - \frac{r}{s} \right) + \frac{\pi}{4} \right] - \frac{r^2}{s^2} \left[\left(\frac{s}{r} - \frac{r}{s} \right) + 2 \tan^{-1} \frac{r}{s} \right] \right\}}{\left(1 - \frac{r^2}{s^2} \right)^2}$$

$$K_{B(S)} = \frac{\left(1 - \frac{r^2}{s^2} \right)^2 - \frac{z}{\pi} \left\{ \left(1 + \frac{r^4}{s^4} \right) \left[\frac{1}{2} \tan^{-1} \frac{1}{2} \left(\frac{s}{r} - \frac{r}{s} \right) + \frac{\pi}{4} \right] - \frac{r^2}{s^2} \left[\left(\frac{s}{r} - \frac{r}{s} \right) + 2 \tan^{-1} \frac{r}{s} \right] \right\}}{\left(1 - \frac{r^2}{s^2} \right)^2}$$

The basic carryover factors, $K_{S(B)}$ and $K_{B(S)}$, are based on slender body theory as presented in References 1 and 13. At supersonic speeds the carryover from the surface to the body has been modified to account for the aft movement of the area influenced by the surface.

5.3.2

Carryover Due to Incidence

The carryover factor $k_{S(B)}$ for the case of surface deflection is based on slender body theory as derived in Reference 13. The following expression gives $k_{S(B)}$ in terms of the semi-span-ratios ratio ($\tau = s/r$)

$$k_{S(B)} = \frac{1}{\pi^2} \left[\frac{\pi^2}{4} \frac{(\tau+1)^2}{\tau^2} + \frac{\pi (\tau^2+1)^2}{\tau^2(\tau+1)^2} \sin^{-1} \left(\frac{\tau^2-1}{\tau^2+1} \right) - \frac{z \pi (\tau+1)}{\tau(\tau-1)} + \frac{(\tau^2+1)^2}{\tau^2(\tau-1)^2} \left(\sin^{-1} \frac{\tau^2-1}{\tau^2+1} \right)^2 - \frac{4(\tau+1)}{\tau(\tau-1)} \sin^{-1} \frac{\tau^2-1}{\tau^2+1} + \frac{8}{(\tau-1)^2} \log \left(\frac{\tau^2+1}{2\tau} \right) \right]$$

The carryover factor $k_{B(S)}$ is based on slender body theory and the assumption that the surface transmits a certain fraction of its lift to the body whether the lift is developed by angle of attack or incidence angle. An approximate value for $k_{B(S)}$ is given by multiplying the value of $k_{S(B)}$ by the ratio of the carryover factor due to angle of attack $K_{B(S)}/K_{S(B)}$

$$k_{B(S)} = k_{S(B)} \frac{K_{B(S)}}{K_{S(B)}}$$

5.3.3

Wing Vortices

The wing-tail interference results from downwash in the region of the tail caused by wing vortices. Figure 7 illustrates the vortex model used in determination of the wing-tail interference. The lateral location of the wing vortices is based on slender body theory and is given by the relation:

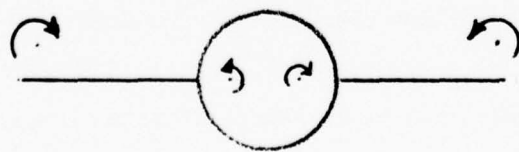
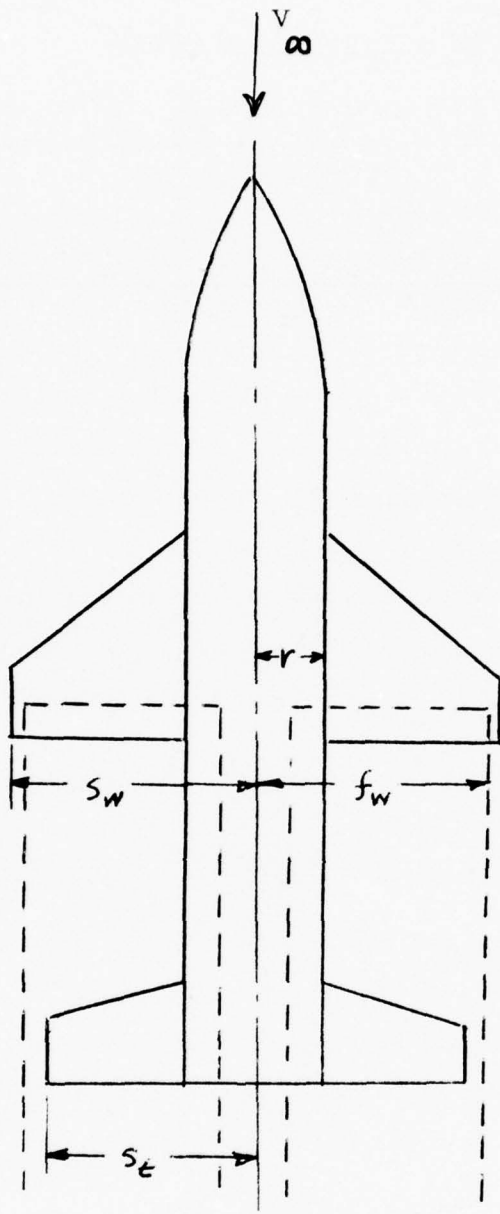


FIGURE 8 WING VORTICES GEOMETRY

$$f = r + (s-r) \left\{ \frac{\pi}{4} (1-\xi^2) - \frac{r}{s} + \frac{(1+\xi^2)^2}{2(1-\xi^2)} \sin^{-1} \left[\frac{1-(\frac{r}{s})^2}{1+\xi^2} \right] \right\} \\ 2 \left(1 - \frac{r}{s} \right)$$

For low angles of attack and zero deflection of the forward surface, the vertical location of the wing trailing vortex is assumed to lie near the plane of the wing. The tail interference factor "i" is evaluated in terms of the two external and two internal or "image" vortices as defined in Reference 14. Appendix B of Reference 13 describes the use of strip theory to obtain the tail interference factor from integration of the lift contribution of the vortex system on the tail panels. The lift on the tail section due to wing vortices is computed from the relation

$$C_{L_{\infty T}(w)} = \frac{C_{L_{\infty w}} C_{L_{\infty T}} K_{W(B)} i (x_T - r_T)}{2\pi A_T (f_w - r_w)}$$

5.4 Center of Pressure

All Mach Numbers

Lifting surface center of pressure at $\alpha = 0$ is obtained from data of Reference 11.

$$CP = f(A, \lambda, \tan A_{1/2}, \beta)$$

Table XXVIII presents lifting surface center of pressure data in percent of mean geometric chord as a function of aspect ratio, taper ratio, tangent of the midchord sweep.

5.5 List of Symbols

<u>Symbol</u>	<u>Description</u>
A	Aspect ratio, exposed
b	Surface span, 2 panels, no body
C_D	Drag coefficient
C_{D_i}	Induced drag coefficient
C_{D_o}	Zero-lift drag coefficient
C_F	Skin friction coefficient
C_{D_p}	Pressure drag coefficient
$C_{L_{\infty}}$	Lift curve slope

<u>Symbol</u>	<u>Description</u>
CP	Center of pressure
f	Lateral location of wing trailing vortex
i	Tail interference factor
K	Airfoil section constant
K_A	Correction factor for $C_{L\alpha}$ of low aspect ratio surfaces
$K_{B(S)}$	Lifting carryover factor due to angle of attack, surface in presence of body
$k_{B(S)}$	Lifting carryover factor due to surface incidence, body in presence of surface
K_F	Lifting surface arrangement factor
K_M	Correction factor for $C_{L\alpha}$ of low aspect ratio surfaces
$K_{S(B)}$	Lift carryover factor due to angle of attack, surface in presence of body
$k_{S(B)}$	Lift carryover factor due to surface incidence, surface in presence of body
r	body radius
s	Surface semi-span
S_P	Planform area of 1 exposed panel
S_R	Reference area
(t/c)	Thickness ratio)
α	Angle of attack
β	$\sqrt{M^2 - 1}$
Λ_{LE}	Leading edge sweep angle, measured from perpendicular to root chord
$\Lambda_{1/2}$	Mid-chord sweep angle, measured from perpendicular to root chord
λ	Surface taper ratio
τ	Semispan - radius ratio

TABLE XXVIII
CENTER OF PRESSURE OF LIFTING SURFACE(SUBSONIC)

```

TRI=TAFFER RATIO
DATA YAC781/0.000, 0.250, 0.500, 1.000,
      ATNS2I=ASPECT RATIO TIMES TANGENT OF MIDCHORD SWEEP
1    0.000, 1.000, 2.000, 3.000, 4.000,
      BARI=ASPECT RATIO TIMES BETA
2    0.000, 0.500, 1.000, 1.500, 2.000,
3    3.000, 4.000, 5.000, 6.000, 7.000,
      XMAC=SURFACE CP IN PERCENT MEAN GEOMETRIC CHORD
      TRI=0.0 ATNS2I=0.0
4    0.250, 0.259, 0.265, 0.269, 0.272,
5    0.274, 0.273, 0.271, 0.270, 0.267,
      TRT=0.0 ATNS2I=1.0
6    0.377, 0.360, 0.345, 0.333, 0.322,
7    0.310, 0.300, 0.291, 0.285, 0.283,
      TRT=0.0 ATNS2I=2.0
8    0.500, 0.445, 0.417, 0.395, 0.373,
9    0.350, 0.332, 0.321, 0.315, 0.311,
      TRT=0.0 ATNS2I=3.0
A    0.501, 0.469, 0.443, 0.421, 0.403,
B    0.377, 0.360, 0.351, 0.343, 0.339,
      TRT=0.0 ATNS2I=4.0
C    0.502, 0.478, 0.460, 0.445, 0.432,
D    0.410, 0.393, 0.380, 0.375, 0.368/
      TRT=0.25 ATNS2I=0.0
DATA YAC782/0.145, 0.173, 0.197, 0.212,
1    0.223, 0.240, 0.246, 0.250, 0.250,
2    0.250,
      TRI=0.25 ATNS2I=1.0
3    0.260, 0.262, 0.265, 0.266, 0.267,
4    0.268, 0.269, 0.270, 0.270, 0.268,
      TRT=0.25 ATNS2I=2.0
5    0.383, 0.354, 0.333, 0.317, 0.305,
6    0.291, 0.286, 0.282, 0.281, 0.281,
      TRT=0.25 ATNS2I=3.0
7    0.394, 0.371, 0.354, 0.340, 0.330,
8    0.314, 0.303, 0.299, 0.295, 0.294,
      TRT=0.25 ATNS2I=4.0
9    0.404, 0.388, 0.383, 0.375, 0.364,
A    0.344, 0.325, 0.316, 0.306, 0.303/

```

BEST AVAILABLE COPY

BEST AVAILABLE COPY

TABLE XXVIII (Continued)

TRI=0.50 ATNS2I=0.0
DATA YAC783/0.070, 0.136, 0.185, 0.213,
1 0.226,
2 0.235, 0.238, 0.245, 0.247, 0.248,
TRI=0.50 ATNS2I=1.0
3 0.179, 0.203, 0.218, 0.229, 0.238,
4 0.245, 0.245, 0.245, 0.245, 0.245,
TRI=0.50 ATNS2I=2.0
5 0.285, 0.260, 0.248, 0.241, 0.243,
6 0.248, 0.252, 0.252, 0.250, 0.250,
TRI=0.50 ATNS2I=3.0
7 0.305, 0.280, 0.269, 0.260, 0.257,
8 0.255, 0.255, 0.255, 0.255, 0.255,
TRI=0.50 ATNS2I=4.0
9 0.319, 0.300, 0.286, 0.280, 0.275,
A 0.270, 0.270, 0.270, 0.270, 0.270/
TRI=1.00 ATNS2I=0.0
DATA YAC784/0.000, 0.117, 0.176, 0.207,
1 0.225,
2 0.239, 0.243, 0.245, 0.246, 0.246,
TRI=1.00 ATNS2I=1.0
3 0.085, 0.093, 0.108, 0.135, 0.164,
4 0.208, 0.222, 0.225, 0.230, 0.231,
TRI=1.00 ATNS2I=2.0
5 0.166, 0.167, 0.168, 0.169, 0.170,
6 0.180, 0.198, 0.206, 0.211, 0.214,
TRI=1.00 ATNS2I=3.0
7 0.194, 0.193, 0.190, 0.190, 0.190,
8 0.191, 0.191, 0.198, 0.201, 0.203,
TRI=1.00 ATNS2I=4.0
9 0.201, 0.200, 0.200, 0.197, 0.194,
A 0.190, 0.191, 0.196, 0.198, 0.198/

TABLE XXVIII (Continued)

CENTER OF PRESSURE OF LIFTING SURFACE(SUPERSONIC)

TRI=TAPER RATIO
 DATA XAC791/0.000, 0.250, 0.500, 1.000,
 ATNS2I=ASPECT RATIO TIMES TANGENT OF MIDCHORD SWEET
 1 0.000, 1.000, 2.000, 3.000, 4.000,
 RARTE=ASPECT RATIO TIMES BETA
 2 0.000, 0.500, 1.000, 1.500, 2.000,
 3 3.000, 4.000, 5.000, 6.000, 7.000,
 XMAC=SURFACE CP IN PERCENT MEAN GEOMETRIC CHORD
 TRT=0.0 ATNS2I=0.0
 4 0.250, 0.299, 0.348, 0.400, 0.450,
 5 0.465, 0.475, 0.480, 0.482, 0.485,
 TRI=0.0 ATNS2I=1.0
 6 0.377, 0.420, 0.470, 0.470, 0.470,
 7 0.470, 0.481, 0.485, 0.490, 0.491,
 TRI=0.0 ATNS2I=2.0
 8 0.500, 0.500, 0.500, 0.500, 0.500,
 9 0.500, 0.500, 0.500, 0.500, 0.500,
 TRT=0.0 ATNS2I=3.0
 A 0.501, 0.518, 0.538, 0.538, 0.538,
 B 0.538, 0.538, 0.538, 0.527, 0.520,
 TRI=0.0 ATNS2I=4.0
 C 0.502, 0.518, 0.539, 0.561, 0.580,
 D 0.580, 0.580, 0.580, 0.580, 0.556/
 TRT=0.25 ATNS2I=0.0
 DATA XAC792/0.145, 0.225, 0.300, 0.370,
 1 0.450,
 2 0.475, 0.483, 0.490, 0.493, 0.495,
 TRT=0.25 ATNS2I=1.0
 3 0.260, 0.307, 0.349, 0.392, 0.435,
 4 0.470, 0.480, 0.488, 0.490, 0.490,
 TRI=0.25 ATNS2I=2.0
 5 0.383, 0.417, 0.445, 0.445, 0.445,
 6 0.445, 0.490, 0.500, 0.500, 0.500,
 TRI=0.25 ATNS2I=3.0
 7 0.394, 0.417, 0.441, 0.465, 0.480,
 8 0.480, 0.480, 0.532, 0.529, 0.522,
 TRI=0.25 ATNS2I=4.0
 9 0.404, 0.417, 0.432, 0.450, 0.469,
 A 0.525, 0.525, 0.525, 0.570, 0.558/

TABLE XXVIII (Continued)

BEST AVAILABLE COPY

TRI=0.50 ATNS2I=0.0
 DATA XAC793/0.070, 0.163, 0.257, 0.355,
 1 0.450,
 2 0.479, 0.485, 0.490, 0.492, 0.492,
 TRI=0.50 ATNS2I=1.0
 3 0.179, 0.256, 0.329, 0.389, 0.415,
 4 0.459, 0.475, 0.480, 0.485, 0.485,
 TRI=0.50 ATNS2I=2.0
 5 0.285, 0.325, 0.356, 0.385, 0.385,
 6 0.422, 0.479, 0.485, 0.490, 0.490,
 TRI=0.50 ATNS2I=3.0
 7 0.305, 0.330, 0.353, 0.371, 0.400,
 8 0.438, 0.462, 0.510, 0.508, 0.506,
 TRI=0.50 ATNS2I=4.0
 9 0.319, 0.320, 0.323, 0.331, 0.333,
 A 0.460, 0.490, 0.510, 0.540, 0.538/
 TRI=1.00 ATNS2I=0.0
 DATA XAC794/0.000, 0.000, 0.330, 0.412,
 1 0.443,
 2 0.465, 0.471, 0.483, 0.485, 0.485,
 TRI=1.00 ATNS2I=1.0
 3 0.085, 0.202, 0.298, 0.366, 0.404,
 4 0.440, 0.456, 0.465, 0.470, 0.470,
 TRI=1.00 ATNS2I=2.0
 5 0.166, 0.270, 0.340, 0.374, 0.399,
 6 0.430, 0.449, 0.457, 0.465, 0.473,
 TRI=1.00 ATNS2I=3.0
 7 0.194, 0.275, 0.344, 0.390, 0.412,
 8 0.440, 0.456, 0.465, 0.475, 0.475,
 TRI=1.00 ATNS2I=4.0
 9 0.201, 0.295, 0.375, 0.434, 0.458,
 A 0.473, 0.484, 0.490, 0.495, 0.494/

6. INLETS

Three types of inlets are used for the airbreathing configurations synthesized in the CM-CCSM; two-dimensional side mounted (2 or 4) inlets, and a single belly line mounted inlet. The side mounted inlets are flat sided and mounted symmetrically with the internal compression surfaces at the top. Belly mounted inlets are mounted beneath the missile body with the internal compression ramp at the top. A wedge type boundary layer diverter system is provided for both inlet types. Figure 5 illustrates the inlet geometry for both side mounted and belly mounted inlets. The model defines the incremental drag, lift, and pitching moment associated with each inlet type. The model accounts for internal (momentum) lift, but does not account for internal drag which is included in the net thrust computation.

6.1 Drag

The incremental drag of the inlet consists of a friction drag, pressure drag, and drag due to lift.

$$C_{D_I} = C_{D_F} + C_{D_P} + C_{D_i}$$

6.1.1 Zero Lift Drag

Subsonic

Zero lift drag coefficient of the inlet subsystem at subsonic Mach numbers consists of friction drag only. The net friction drag increment is based on the inlet surface area minus the skin area of the main body masked by the inlet and fairing. The number of inlets is accounted for by the factor N_{INL} .

$$C_{D_O} = C_F \frac{S_{WET}}{S_{REF}} N_{INL}$$

The skin friction coefficient is based on the Prandtl-Schlichting relationship for turbulent boundary layers corrected for compressibility effects. Reynolds number is based on the total inlet length.

$$C_F = \frac{0.482}{(\log_{10} R_N)^{2.62}} \cdot \frac{C_F}{C_{F_I}}$$

Transonic, M = 1

At transonic speeds the drag consists of friction drag, forward fairing drag, and aft fairing drag.

$$C_{DO} = (C_F \cdot \frac{S_{WET}}{S_{REF}} + C_{DPF} + C_{DPA})$$

The forward fairing drag coefficient is based on a conical fairing with an equivalent conical nose fineness ratio of 3. If the inlet fairing extends forward of the non-tangency point, the fairing length is limited to the length available between the nose tangency point and the inlet leading edge. The diameter of the equivalent body of revolution is based on the total projected frontal area of the inlet. Equivalent cone half angle is based on the relation

$$\theta_c = \tan^{-1} (1. / (FR + FR))$$

The forward fairing pressure drag at M=1 is based on curve fit data of Reference 3 presented in tabular form in Table VII.

Afterbody pressure drag is based on an equivalent body of revolution defined by the length of the aft fairing and the equivalent diameter discussed above. Empirical data of Reference 4 is used to estimate the fairing pressure drag at M=1

$$C_{DPA} = 0.233 / (L/D)^2 * \theta_{BT}$$

Supersonic

At supersonic speeds below the ramjet take-over Mach number the inlets are covered by the conical fairings discussed above. Zero-lift drag coefficient consists of the skin friction drag of the inlet, pressure drag of the forward fairing, and pressure drag of the aft fairing.

$$C_{D_O} = C_F \frac{S_{WET}}{S_{REF}} + C_{DPF} + C_{DPA}$$

Skin friction drag is computed in the manner described in the previous sections. Pressure drag on the forward fairing is based on the data of Table XII for an equivalent conical body of revolution with a maximum cross-sectional area defined by the total projected frontal area of the inlet. Afterbody drag is computed from data of Table XV for an equivalent body of revolution defined by the length of the aft fairing and the equivalent diameter of the inlet.

At supersonic speeds greater than the ramjet take-over Mach number, the inlet fairing is jettisoned and the inlet cowl and boundary layer diameter are exposed. The boundary layer diverter height is equal to 75 percent of the turbulent boundary layer thickness at the inlet leading edge at the design Mach number and altitude. A 10 degree half angle wedge is assumed for the boundary layer diverter system. Diverter system projected area consists of the frontal area of the wedge plus an additional projected area due to the curvature of the body. Boundary layer diverter wedge drag is based on data of Reference 2.

$$C_{D_{DIV}} = [C_{D_O} \left(\frac{M}{t/c} \right)^{2/3}] / (\frac{882 M}{t/c})^{2/3}$$

The term $C_{D_O} \left(\frac{M}{t/c} \right)^{2/3}$ is obtained from a curve fit to data of Figure 8, page 17-9 of Reference 2. Mach number used in the equation is reduced to 88 percent of the free stream value to account for losses in the boundary layer. Friction drag of the diverter system is based on the wetted area of the wedge side panels and the friction coefficient is based on Reynolds number computed at the diverter station based on body length to that point.

Cowl pressure drag is defined by the average pressure coefficient acting on the cowl projected frontal area. Cowl lip pressure coefficients are computed as a function of Mach number, and the angle of the oblique shock waves generated by the external compression ramp of the inlet system.

Pressure coefficient on the cowl lip when the oblique shock lies inside the lip is based on the following relation:

$$C_{P_{LIP}} = \frac{5}{3} \frac{M_\infty^2 \sin^2 \theta_w - 1}{M_\infty^2}$$

If the shock pattern formed by the multiple compression ramps lie outside the cowl lip, a maximum of 4 shocks may be encountered by the flow before reaching the lip. Oblique shock relations derived in Reference 15 are used to define flow angle, Mach number and pressure downstream of each shock wave. For cases when an oblique shock is not possible, normal shock relationships are used for the case of an oblique shock

$$\frac{p_2}{p_1} = \frac{7M_1^2 \sin^2 \theta_w - 1}{6}$$

Pressure coefficient is computed from the relation

$$C_p = \frac{p_2}{p_1} - 1. / .7 M^2$$

Mach number downstream of an oblique shock is based on the shock wave angle and the upstream Mach number

$$M_2^2 = \frac{36M_1^4 \sin^2 \theta_w - 5(M_1^2 \sin^2 \theta_w - 1)(7M_1^2 \sin^2 \theta_w + 5)}{(7M_1^2 \sin^2 \theta_w - 1)(M_1^2 \sin^2 \theta_w + 5)}$$

If the flow conditions create a normal shock pressure ratio across the shock wave is computed by the following

$$\frac{p_2}{p_1} = \frac{7M_1^2 - 1}{6}$$

Pressure coefficient on the lip is computed as above. The average pressure coefficient acting on the cowl surface is assumed to be equal to 1/2 of the pressure coefficient acting on a wedge with a constant angle equal to the lip initial angle. Pressure drag coefficient on the cowl lip is based on the relation

$$CD_{COWL} = CP_{LIP} * S_{PROJ}/S_{REF}$$

Pressure drag coefficient on the aft fairing of the inlet is based on an equivalent body of revolution defined by the length of the fairing and its equivalent diameter. The data of Table XV is used for fairings with an equivalent fineness ratio of at least 2 to 1. Inlet fairing pressure drag for inlet fairings with fineness ratio less than 2 to 1 is computed from the data for conical boattails from Reference 3. If the pressure drag coefficient computed for the short afterbody fairing is greater than the full base drag on the inlet projected area, base drag is used for the drag of the afterbody fairing.

6.1.2 Induced Drag

Induced drag is equivalent for the complete configuration as described in Section 5.1.2.

6.2 Lift Curve Slope

The two-dimensional side mounted inlets are treated as a low aspect ratio lifting surface and the lift curve slope is computed in the manner described in Section 5.2. Span of the equivalent lifting surface is equal to the total width of the side mounted inlets. Effective area of the equivalent lifting surface is based on the total platform area of the inlet plus one-half of the platform area of the aft fairing. Aspect ratio of the equivalent surface is based on the exposed span and the effective area of the inlet. A momentum lift term based on slender body theory is used when the inlet fairing is removed

$$C_{L\alpha M} = \frac{2.0 A}{57.3 S_{REF}}$$

The momentum lift term is the only lift contribution for single belly mounted inlets.

6.3 Center of Pressure

Center of pressure for the side mounted inlets is located at the centroid of the effective planform area at all Mach numbers. Center of pressure for the belly mounted inlet is assumed to be at the inlet leading edge.

List of Symbols

<u>Symbol</u>	<u>Description</u>
A_c	Inlet capture area
$C_{D_{DIV}}$	Boundary layer diverter pressure drag coefficient
C_{D_F}	Friction drag coefficient
C_{D_i}	Induced drag coefficient
C_{D_P}	Pressure drag coefficient
C_F	Skin friction coefficient
$\frac{C_F}{C_{F_i}}$	Compressibility correction factor
C_P	Pressure coefficient
C_{L_M}	Lift curve slope due to turning of the flow at the inlet
FR	Fineness ratio of inlet fairing
L/D	Length to diameter ratio of inlet aft fairing
M	Mach number
$\frac{P_2}{P_1}$	pressure ratio across shock
S_{REF}	Reference area
S_{WET}	Wetted area of inlet and fairings
t/c	Thickness ratio of wedge diverter
θ_{BT}	Boattail fairing angle
θ_w	Oblique shock wave angle

7. EXTERNAL BOOSTER

The external booster model used for surface launched missiles is shown in Figure 8. The booster case is a non-boattailed, right circular cylinder with a 25 degree half angle nose cone with a bluntness ratio of 25 percent. Booster diameter is an input variable, booster length is a function of the propellant required to achieve a desired flight condition.

7.1 Drag

Drag coefficients for the external boosters are based on isolated body coefficients corrected to the coefficient reference area for the complete configuration.

7.1.1 Zero-Lift Drag

External booster zero-lift drag consists of nose cone pressure drag, base drag, and skin friction drag. Skin friction drag coefficient is computed in the manner previously described. Reynold's number computations are based on the booster length. Nose cone pressure drag coefficient for a 25 degree half angle blunted cone is presented in Figure 9. Base pressure drag coefficient is based on the base pressure coefficients presented in Table V. Effective base area is 50 percent of maximum cross sectional area of the booster.

7.1.2 Induced Drag

Induced drag is evaluated for the total configuration as described in Section 4.1.2.

7.2 Lift Curve Slope

Lift curve slope for the external booster is based on a correlation of empirical data on cone-cylinder bodies. Lift curve slope for the cone-cylinder configuration used in the external booster model is shown in Figure 10. Lift data for the external boosters are based on isolated body coefficients corrected to the coefficient reference area for the complete configuration.

7.3 Center of Pressure

Center of pressure data for the external boosters is based on a correlation of empirical data on cone-cylinder bodies. Center of pressure of the isolated booster is presented in Figure 11 as a function of Mach number.

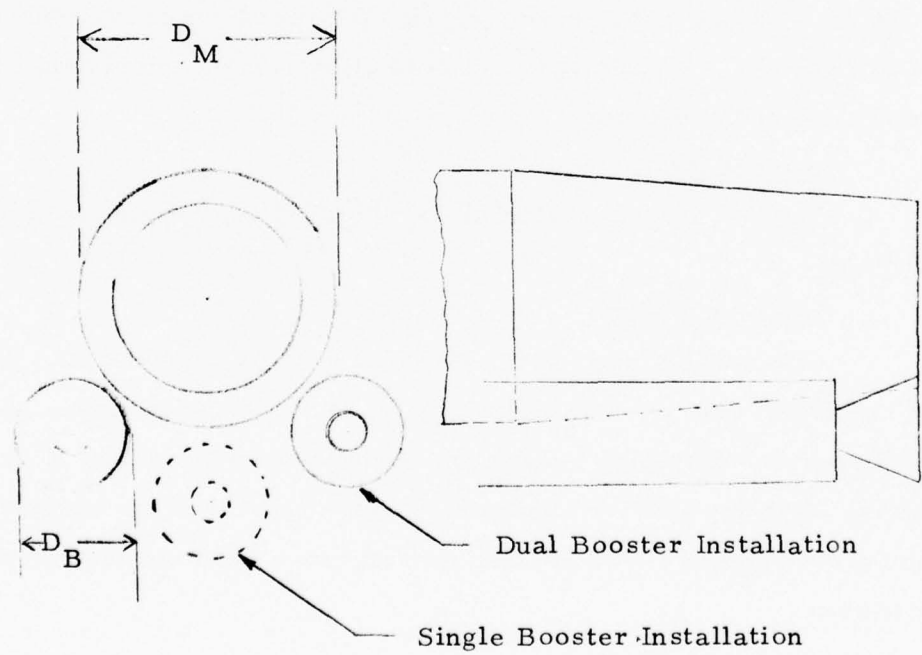
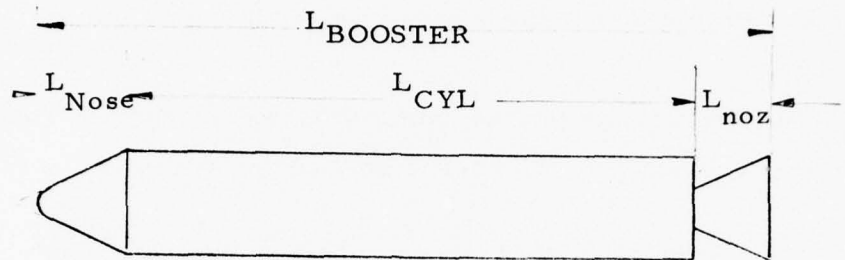
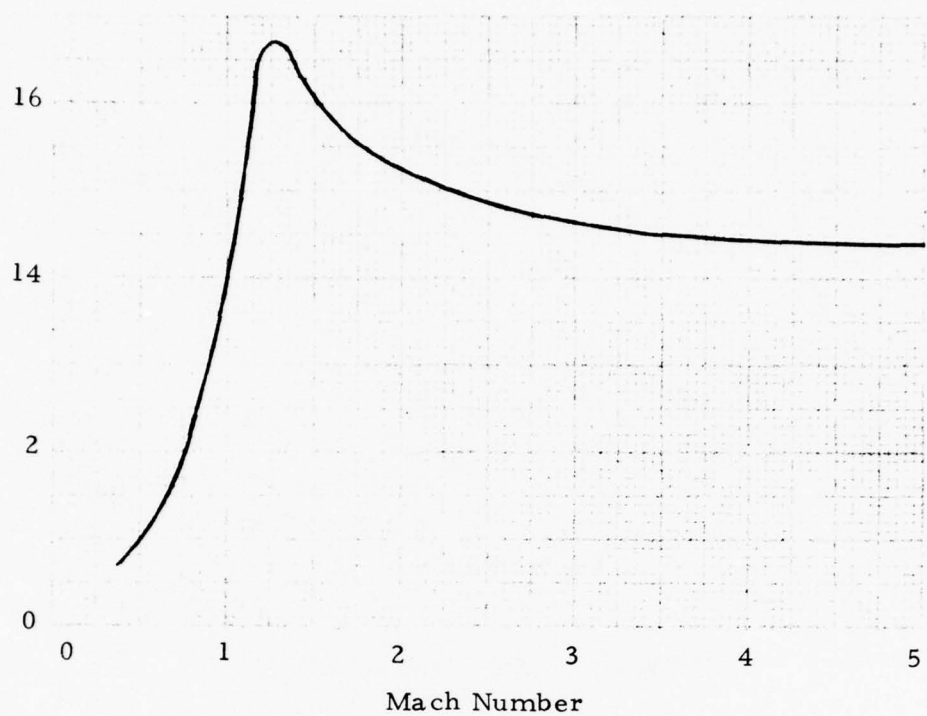


FIGURE 8 EXTERNAL BOOSTER MODEL

Nose Wave Drag
Coefficient - C_{DN}



Base Pressure
Coefficient - C_{PB}

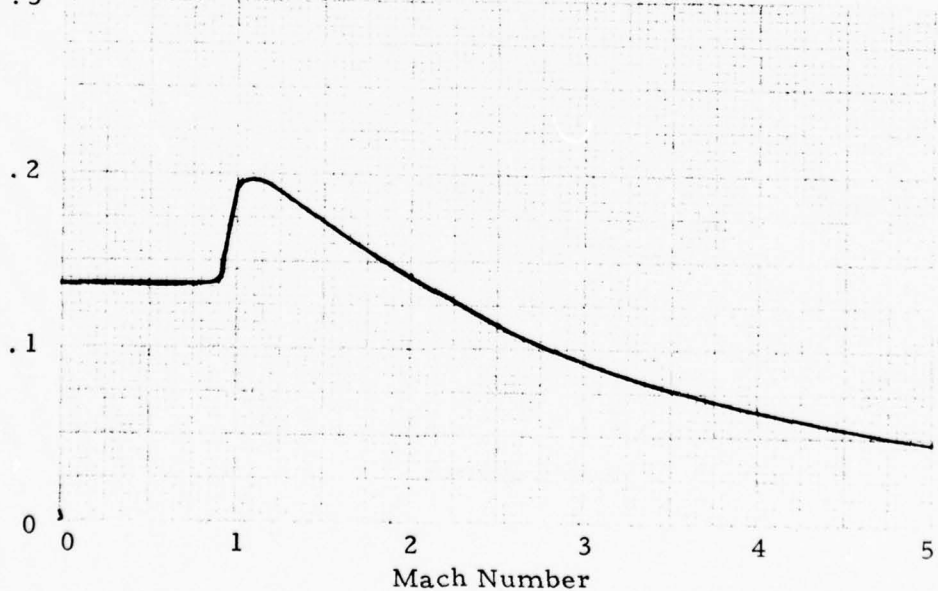


FIGURE 9 NOSE CONE PRESSURE DRAG COEFFICIENT

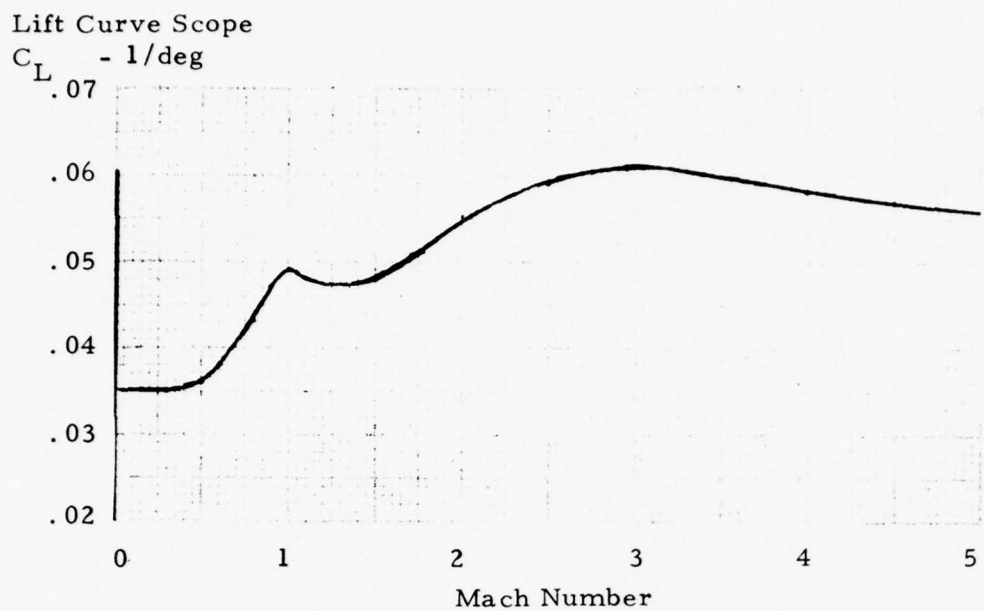


FIGURE 10 LIFT CURVE SLOPE

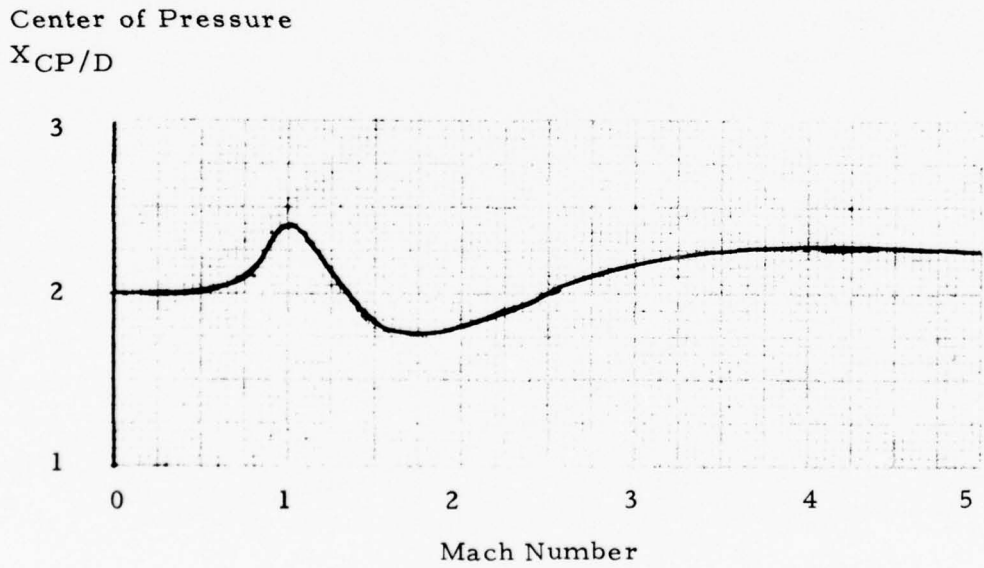


FIGURE 11 CENTER OF PRESSURE

REFERENCES

1. Hook, D. E., "USAF Stability and Control DATCOM", McDonnell Douglas Corporation, Douglas Aircraft Division, Revised September 1970.
2. Hoemer, S. F., "Fluid-Dynamic Drag", published by the author.
3. Journal of the Aerospace Sciences, July 1961
4. Silhan, F. V., and Cubbage, Jr., J. M., "Drag of Conical and Circular-Arc Boattail Afterbodies at Mach Numbers from 0.6 to 1.3", HALA RM L56 K22, January 22, 1957.
5. Jernell, L. J., "Effects of Nose Bluntness on Aerodynamic Characteristics of Cruciform - Finned Missile Configuration at Mach 1.50 to 2.86", NASA TMX-2031, June 1970.
6. Avery, J. T., "A Study of Zero-Lift Drag Characteristics of Various Walleye Components and Configurations in the Subsonic, Transonic, and Supersonic Flight Regions", U. S. Naval Ordnance Test Station, IDP-2598, September 1966.
7. Perkins, E. W., and Jorgensen, L. H., "Investigation of the Drag of Various Axially Symmetric Nose Shapes of Fineness Ratio 3 for Mach Numbers from 1.24 to 3.67". NACA RM A52H28, November 1952.
8. Djordjevic, Branimir D., "Aerodynamic Force Analysis, Volume II", U.S. Army Missile Command, June 1966.
9. Spring, D. V., "The Effect of Nose Shape and Afterbody Length on the Normal Force and Neutral Point Location of Axisymmetric Bodies at Mach Numbers from 0.80 to 4.50", U.S. Army Missile Command, Report No. RF-TR-64-13, 15 July 1969.

10. Koshar, M. M., and Cobb, E. R., "Missile Synthesis and Performance Computer Program Final Report, Vol. II, Missile Subsystem Design Formulation and Methodology", Martin Marietta OR11245, August 1971.
11. "Royal Aeronautical Society Data Sheets", Fifteenth Issue, August 1964.
12. Spearman, M. L., and Trescot, Jr., C. D., "Effects of Wing Planform on the Static Aerodynamics of a Cruciform Wing-Body Missile for Mach Numbers up to 4.63, NASA TM-X1839.
13. Pitts, W., Nielsen, J., and Kaatari G., "Lift and Center of Pressure of Wing-Body-Tail Combinations at Subsonic, Transonic, and Supersonic Speeds," NACA TR-1307, 1957.
14. Nielsen, J. N., "Missile Aerodynamics", McGraw-Hill, 1960.
15. National Advisory Committee for Aeronautics, "Equations, Tables, and Charts for Compressible Flow", Ames Research Staff, 1953.

APPENDIX B
VEHICLE PERFORMANCE SUBMODEL
(VEHPER)

<u>TITLE</u>	<u>Appendix B</u>
VEHICLE PERFORMANCE SUBMODEL (VEHPER)	<u>NO.</u> _____
	<u>DATE</u> _____

TABLE OF CONTENTS

<u>Section</u>		<u>Page</u>
	ABSTRACT.....	B-2
1.	INTRODUCTION	B-3
2.	FLIGHT PATH EQUATIONS	B-7
3.	NUMERICAL METHODS	B-23
4.	SUBMODEL STRUCTURE.....	B-28
5.	REFERENCES.....	B-32

LIST OF ILLUSTRATIONS

<u>Figure</u>		
1	Typical Mission Profile.....	B-4
2	Flight Path Variables.....	B-9
3	Submodel Functional Flow.....	B-31

LIST OF TABLES

<u>Table</u>		
1	Variables of Integration.....	B-26
2	VEHPER Subroutines.....	B-29

PREPARED BY

J. H. Everett

Page 1 of 33

APPROVED BY

L. D. Gregory *L.D.G.*

ABSTRACT

This appendix describes the SEATIDE VEHPER sub-model. In its present state, VEHPER computes the trajectory of a cruise missile powered by rocket, turbojet or ramjet propulsion systems. The description includes math models for the vehicle characteristics and its geophysical environment, numerical techniques, and a top-level block diagram.

1. INTRODUCTION

The role of the VEHPER submodel is to compute the performance of atmospheric cruise missiles synthesized by the SEATIDE Concept Generation and Screening Model. The submodel is capable of analyzing a wide variety of missions and configurations. The vehicle may be surface or air-launched, and it may fly high altitude, low altitude, or split-level missions. Propulsion systems represented include a rocket booster and throttleable rocket, ramjet, and turbojet sustainers.

The basic approach to computing the performance of the missile is to numerically integrate two degree-of-freedom, point mass equations of motion. The integration subroutine utilizes a fourth order, variable step size Runge-Kutta method which controls the integration step size to maintain an approximately constant truncation error. Seven first-order differential equations of motion are integrated simultaneously. Variables integrated include flight path variables, weight, and ideal velocity.

The trajectory is divided into phases for computational and user convenience. At the start of each phase, the vehicle characteristics and its flight path control method may be specified in order that the vehicle can fly through a sequence of configurations and maneuvers. Figure 1 illustrates a typical sequence. Initial conditions define a low-altitude air launch. In the first phase, the missile is accelerated to a desired Mach number by a rocket booster. In the second phase, aerodynamics are re-defined, weights associated with the boost phase are dropped, and the sustainer propels the missile during a climb. The third phase is a maneuver for leveling the climb path at the cruise altitude. Phase 4 is the cruise phase. Phase 5 is a descent. Phase 6 is a pull-out at a low altitude. The 7th and final phase is a low-altitude run-in to the target.

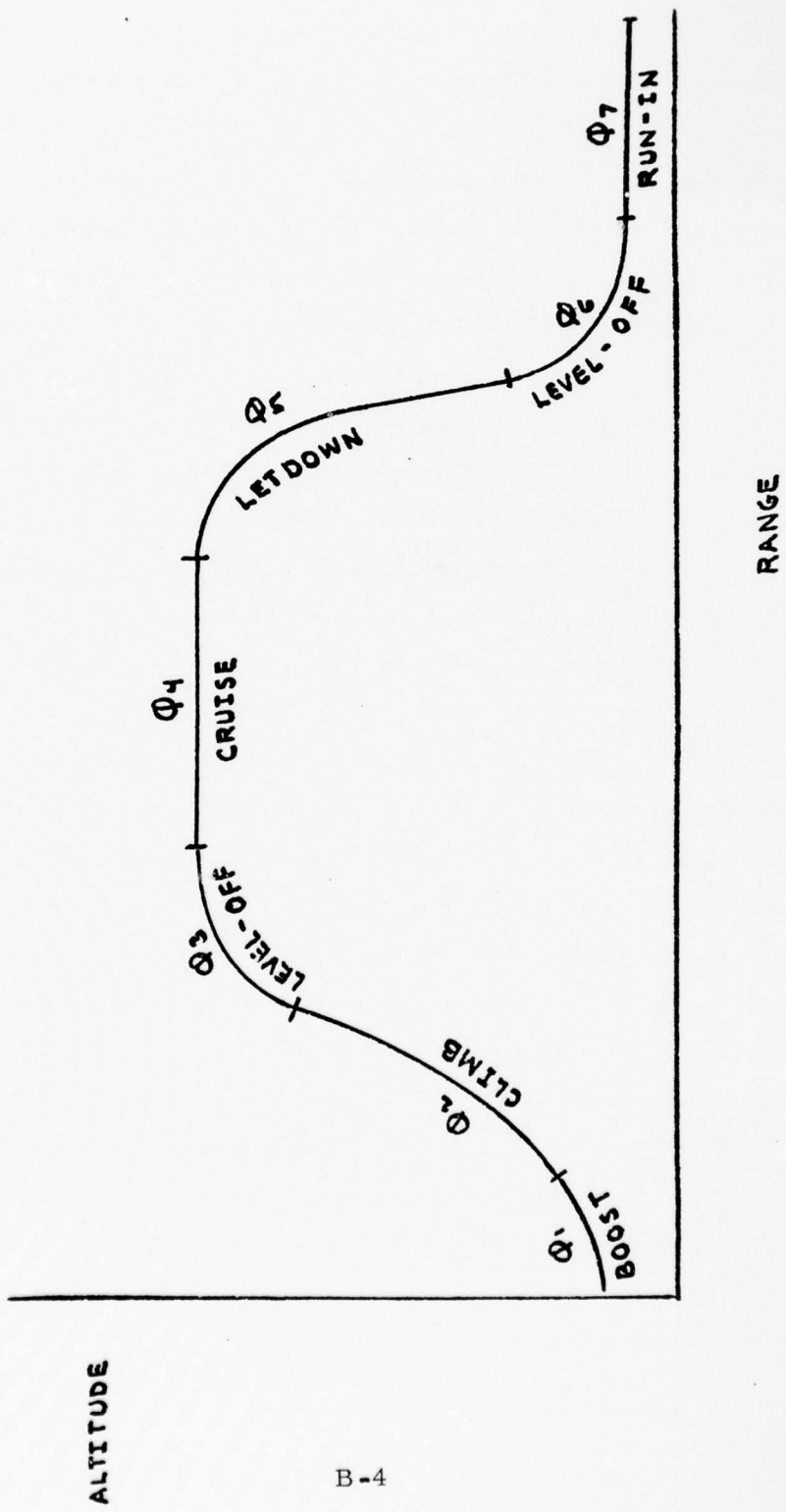


FIGURE 1 TYPICAL MISSION PROFILE

From a propulsion standpoint, a phase may be one of three types. The phase may be unpowered, (thrust and fuel flow are zero) and the vehicle is in "coasting" flight affected only by aerodynamic and gravity forces. A coast phase might be utilized to provide a realistic time delay between booster burnout and air-breathing sustainer ignition or an unpowered descent to target encounter. A second type of propulsion in a phase is boost. A boost phase is one in which an unthrottled rocket propels the vehicle. A boost phase would typically be used to accelerate a ramjet from a subsonic (or zero) velocity to a supersonic ramjet take-over Mach number. The third category is one in which the vehicle is propelled by a sustainer. The sustainer is characterized as being capable of throttled operation in order to satisfy a desired velocity requirement, e.g., a cruise Mach number. At the present state of development, the sustainer may be either a rocket, ramjet, or turbojet. For the duration of a phase, the sustainer may be operated in one of three modes: throttleable, maximum thrust, or minimum thrust.

Some important optional capabilities have been added to the basic trajectory program to relieve the user of tedious "hunt and try" procedures for finding acceptable flight paths.

In assessing a missile design, the analyst must be able to compute its maximum range. For the mission profile of Figure 1, maximum range can be achieved by increasing the length of the cruise leg of the mission until fuel is exhausted at the end of the low altitude run-in. The VEHPER submodel allows the analyst to designate a particular phase as a variable length cruise phase, and the computer program will perform an iterative search for the cruise leg length which exhausts fuel at the end of the last phase.

Another requirement placed on the routine is that the climb to altitude be performed efficiently, as experience has shown that a climb path angle which is too great or too small can have a drastic

effect on total range. Rather than require the user to guess at the proper climb angle, provision has been made to generate a climb schedule, consisting of a Mach number versus altitude table. Just before the climb phase is begun, the table is constructed by searching for the best climb speed for each of several different altitudes. Aerodynamics and propulsion characteristics are utilized to determine excess thrust at each velocity and altitude combination considered.

A third capability designed to ease the user's task is the incorporation of a novel level-off navigation law. During climbs or descents to a cruise altitude, the level-off maneuver must be initiated at a point on the path which allows for the time to change the path angle to zero while the cruise altitude is being achieved. The altitude change during the level-off maneuver can be several miles for a Mach 4 ramjet. The point of level-off initiation could be found through the "hunt and try" process of running several level-off trajectories starting at different times on the climb or descent path. The VEHPER eliminates the need for such iterative techniques by employing a simple, approximate analytical expression relating level-off load factor, altitude error with respect to desired cruise altitude, and vertical speed. The climb or descent phase is stopped when the load factor required to level off at the cruise altitude becomes equal to the level-off load factor desired by the user. From the climb or descent stopping point until reaching the cruise altitude, the path is controlled by the level-off navigation law. At each integration step along the trajectory, the load factor required is computed from the altitude error and vertical speed. A constant velocity during the level-off will result in a near-constant load factor.

2. FLIGHT PATH EQUATIONS

2.1 EQUATIONS OF MOTION

Two dimensional flight path equations of motion define the missile's velocity rate and path angle rate with respect to a non-rotating, spherical earth model:

$$\dot{v} = \frac{T \cos(\alpha + \eta) - D}{m} - g \sin \delta \quad (\text{ft/sec}^2) \quad (2-1)$$

$$\dot{\delta} = \frac{1}{V} \left[\frac{T \sin(\alpha + \eta) + L}{m} + \left(\frac{V^2}{r} - g \right) \cos \delta \right] \quad (\text{rad/sec}^2) \quad (2-2)$$

Rates of change of altitude and down range distance are respectively

$$\dot{h} = V \sin \delta \quad (\text{ft/sec}) \quad (2-3)$$

$$\dot{R} = V \frac{R_E}{r} \cos \delta \quad (\text{ft/sec}) \quad (2-4)$$

Initial conditions for the differential equations of motion are:

$$V(0) = \text{MAX}(V_0, 0.1) \quad (\text{ft/sec})$$

$$\delta(0) = \delta_0 \times \pi/180 \quad (\text{rad})$$

$$h(0) = h_0 \quad (\text{ft})$$

$$R(0) = R_0 \times 6076.115 \quad (\text{ft})$$

where V_0 , γ_0 , h_0 , R_0 are inputs. Path variables used in the equations of motion are illustrated in Figure 2 and are defined as follows:

V	= velocity (ft/sec)
T	= net thrust force (lbf)
α	= angle of attack (rad)
D	= aerodynamic drag force (lbf)
m	= mass (slugs)
g	= gravity force per unit mass (ft/sec ²)
γ	= flight path elevation angle (rad)
L	= aerodynamic lift force (lbf)
r	= geocentric radial distance to vehicle (ft)
η	= thrust cant angle for boost phases (radians)

Vehicle mass is determined by integrating its time rate,

$$\dot{m} = -m_f \quad (\text{lbm/sec}) \quad (2-5)$$

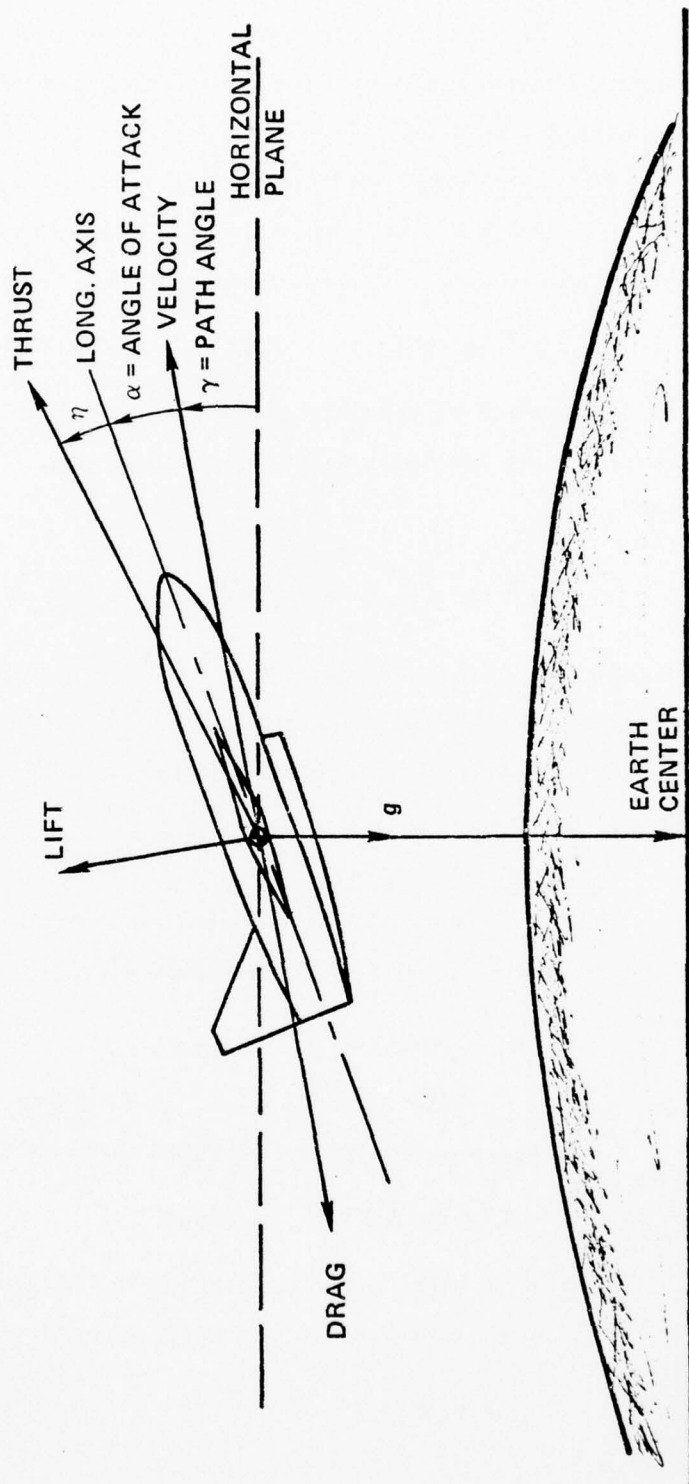
and m_f is the fuel flow rate computed by the propulsion math model.

The missile angle of attack is the control variable used to determine the flight path; its value is constrained to an input maximum value such that

$$|\alpha| \leq \alpha_{\text{MAX}} * \pi/180$$

where α_{MAX} is the input maximum in degrees. Subsequent paragraphs will indicate the several options for computing angle of attack.

The missile flight path is computed by simultaneously integrating five first-order differential equations, Eq. (2-1), (2-2), (2-3), (2-4), and (2-5). The numerical integration procedure is a fourth order variable step size technique described in Section 3.0.



B-9

FIGURE 2 FLIGHT PATH VARIABLES

2.2 PATH CONTROL OPTIONS

The missile angle of attack is the final output of each of the flight path control options. The cruise and level-off options also determine thrust required.

2.2.1 Option 1: $\gamma(t)$ Path Angle Control

An input table of flight path angle versus time determines the desired angle of attack. The commanded path angle is

$$\gamma^* = \gamma(t) \quad (\text{rad})$$

where γ^* is bounded by tabular values, γ_{N+1} and γ_N , and t is likewise bounded by tabular values t_{N+1} and t_N . A computed path angle rate is

$$\dot{\gamma}^* = (\gamma_{N+1} - \gamma_N)/(t_{N+1} - t_N) + (\gamma^* - \gamma) \quad (\text{rad/sec})$$

The angle of attack required to achieve $\dot{\gamma}^*$ is determined by an iterative solution of the $\dot{\gamma}$ equation of motion, Eq. (2-2). Subroutine XALPH1 performs this function. The variation in thrust with angle of attack, if any, is considered in XALPH1.

2.2.2 Option 2: Not Used

2.2.3 Option 3: $\theta(t)$ Attitude Control vs. Time

Angle of attack is computed directly from

$$\alpha = \theta(t) - \gamma \quad (\text{rad})$$

2.2.4 Option 4: $\theta(h)$ Attitude Control vs. Altitude

Angle of attack is computed directly from

$$\alpha = \theta(h) - \gamma \quad (\text{rad})$$

2.2.5 Option 5: $\theta(M)$ Attitude Control vs. Mach No.

Angle of attack is computed directly from

$$\alpha = \theta(M) - \gamma \quad (\text{rad})$$

2.2.6 Option 6: $\alpha(t)$ Angle of Attack Control vs. Time

Angle of attack is determined by a table look-up

$$\alpha = \alpha(t) \quad (\text{rad})$$

2.2.7 Option 7: $\alpha(h)$ Angle of Attack Control vs. Altitude

Angle of attack is determined by a table look-up

$$\alpha = \alpha(h) \quad (\text{rad})$$

2.2.8 Option 8: $\alpha(M)$ Angle of Attack Control vs. Mach No.

Angle of attack is determined by a table look-up

$$\alpha = \alpha(M) \quad (\text{rad})$$

2.2.9 Option 9: $N_z(t)$ Load Factor Control vs. Time

Load factor is determined by a table look-up

$$N_z = N_z(t) \quad (G's)$$

Path angle rate as a function of load factor is

$$\dot{\gamma} = [g_0 N_z + \left(\frac{V^2}{r} - g \right) \cos \gamma] / V \quad (\text{rad/sec})$$

The angle of attack to achieve the path angle rate is computed in subroutine XALPH1 which iteratively solves Eq. 2-2 for α .

2.2.10 Option 10: $N_z(h)$ Load Factor Control vs. Altitude

Load factor is determined by a table look-up

$$N_z = N_z(h) \quad (G's)$$

Path angle rate and angle of attack are computed as in Option 9.

2.2.11 Option 11: $N_z(M)$ Load Factor Control vs. Mach No.

Load factor is determined by a table look-up

$$N_z = N_z(M) \quad (G's)$$

Path angle rate and angle of attack are computed as in Option 9.

2.2.12 Option 12: M(h) Mach Number Climb or Descent Schedule

This is the primary path control option for performing the climb and descent phases on a mission profile. The **M(h)** table is optionally input to VEHPER or internally computed within the VEHPER MAINS subroutine. The engine is assumed to be operating at maximum thrust; hence the schedule is maintained by controlling the path elevation angle.

The path control equation to achieve the desired schedule is

$$\dot{\gamma} = K_v (v - v^*) + K_\gamma (\gamma^* - \gamma) \quad (\text{rad/sec})$$

where

K_v, K_γ are input gains

v^* is the desired velocity (ft/sec);

$$v^* = M(h) * a \quad (\text{ft/sec})$$

a = sound speed at altitude (ft/sec)

γ^* is a computed desired path angle (rad)

The desired path angle is based on the slope of the **M(h)** curve, thrust, and drag:

$$\gamma^* = \sin^{-1} \left[\frac{T^* \cos \alpha^* - D}{m(v \frac{dv}{dh} + g)} \right] \quad (\text{rad}) \quad (2-6)$$

α^* is the angle of attack on the desired path (radians)

D^* is the drag on the desired path (lbf)

T^* is the thrust on the desired path (lbf)

$\frac{dv}{dh}$ = rate of change of velocity on the **M(h)** schedule

Since there are two unknowns, γ^* and α^* , in Eq. (2-6) an additional consideration must be introduced to permit the solution. An assumption that $\dot{\gamma}^* = 0$ yields

$$\alpha^* = -m \left(\frac{v^*}{r} - g \right) \cos \gamma^* / (T^* + C_{L\alpha} \frac{a}{g} S) \quad (\text{rad}) \quad (2-7)$$

Equations (2-6) and (2-7) are solved simultaneously for γ^* and α^* in an iterative procedure.

2.2.13 Option 13: Cruise

During cruise flight the vehicle is flown at constant altitude (if the angle of attack constraint permits), and sustainer engine thrust is controlled to satisfy the desired cruise Mach number.

The concept of accelerations normal and tangent to the flight path are introduced for the cruise path control option (and also the Option 14 level-off path control). Accelerations normal and tangent to the path are respectively

$$a_N = \frac{v \dot{\gamma}}{g_0} = \frac{1}{g_0} \left[\frac{T \sin \alpha + L}{m} + \left(\frac{v^2}{r} - g \right) \cos \gamma \right] \text{ (G's)} \quad (2-8)$$

$$a_T = \frac{\dot{v}}{g_0} = \frac{1}{g_0} \left[\frac{T \cos \alpha - D}{m} - g \sin \gamma \right] \text{ (G's)} \quad (2-9)$$

During cruise flight,

$$a_N = 0 \quad (\text{G's}) \quad (2-10)$$

$$a_T = K_{CRU} (M^* a - v) \quad (\text{G's}) \quad (2-11)$$

K_{CRU} is a gain on the velocity error ($\text{G's}/\text{ft/sec}$)

M^* is the desired (cruise) Mach

a is the speed of sound (ft/sec)

v is the missile velocity (ft/sec)

Subroutine XALPH2 solves equations (2-8) and (2-9) for required thrust T and angle of attack α which satisfy cruise conditions specified by equations (2-10) and (2-11). If thrust required is not available for the sustainer engine, then maximum thrust is commanded, and angle of attack is recomputed based on maximum thrust. If angle of attack required for $a_N = 0$ exceeds the maximum, the vehicle is flown at maximum angle of

attack and a descent to a lower altitude will occur. Maximum angle of attack flight continues until the flight path angle becomes zero, and thereafter the vehicle is flown at $\alpha_N = 0$.

2.2.14 Option 14: Level-Off

The level-off maneuver is used as a transition maneuver between a climb or descent phase and a constant altitude, (zero path angle) cruise phase. A load factor is computed which will cause the path angle to become zero at the same time that cruise altitude is attained. The sustainer propulsion system is throttled to maintain a desired Mach number.

The level-off navigation law relates acceleration normal to the path, α_N , to altitude error and altitude rate:

$$\alpha_N = -\frac{\dot{h}}{2g_0} \left| \frac{\dot{h}}{\Delta h} \right| \quad (\text{G's})$$

Δh = altitude error; cruise less current altitude (ft)

The singularity at cruise altitude is circumvented by holding α_N constant during the last 20 feet of altitude change. The law yields a constant normal acceleration if the missile velocity, V , is constant.

Tangential acceleration during level-off is computed from the same expression used for cruise:

$$\alpha_T = K_{CRU} (M^* a - v) \quad (\text{G's})$$

Just as in the cruise option, subroutine XALPH2 solves for angle of attack and thrust which satisfy the required normal and tangential acceleration. If thrust required is greater than maximum available, the sustainer is operated at maximum thrust.

2.3 AERODYNAMICS FORCES

Aerodynamic lift and drag forces on the vehicle are respectively

$$L = C_{L\alpha} \alpha q_s S \quad (1bF)$$

$$D = (C_{D0} + C_{D\alpha} \alpha^2) q_s S \quad (1bF)$$

where

- $C_{L\alpha}$ is the slope of the lift curve and is an input tabular function of Mach number (radians⁻¹)
- α is the angle of attack (radians)
- q is the dynamic pressure; $q = \frac{1}{2} \rho V^2$;
 ρ is the atmospheric density in slugs/ft³ (lbf/ft²)
- S is the aerodynamic reference area (ft²)
- C_{D_0} is the zero angle of attack drag coefficient; an input tabular function of Mach number and altitude.

2.4 PROPULSION

At the present state of development, the VEHPER submodel considers rocket, turbojet, or ramjet propulsion. The rocket may be either a constant thrust booster or a throttleable sustainer. The ramjet and turbojet sustainers may be operated in a throttleable mode or at maximum or minimum thrust.

2.4.1 Rocket Booster

Both liquid and solid rocket thrust and fuel flow are modeled with the following relationships:

$$T = T_{VAC} - A_e p \quad (\text{lbf})$$

$$w_f = T / I_{sp} \quad (\text{lbf sec/lbm})$$

- T is net thrust (lbf)
- T_{VAC} is the input constant vacuum thrust (lbf)
- A_e is the rocket nozzle exit area (ft²)
- p is the ambient atmospheric pressure (lbs/ft²)
- w_f is fuel flow rate (lbm/sec)
- I_{sp} is the input constant vacuum specific impulse (lbf sec/lbm)

2.4.2

Rocket Sustainer

During throttled operation, thrust required, T^* , is computed to satisfy trajectory requirements during each integration step. The vacuum thrust required is

$$T_{vac}^* = T^* + A_e p \quad (\text{lbf})$$

and is bounded according to

$$(T_{vac})_{\min} \leq T_{vac}^* \leq (T_{vac})_{\max} \quad (\text{lbf})$$

where

$(T_{vac})_{\min}$, $(T_{vac})_{\max}$ are input maximum and minimum values of vacuum thrust (lbf)

The throttle fraction is the ratio of the thrust increment used to the thrust increment available:

$$R = \frac{T_{vac}^* - (T_{vac})_{\min}}{(T_{vac})_{\max} - (T_{vac})_{\min}}$$

Fuel flow is computed from a vacuum specific impulse which is an input tabular function of throttle fraction:

$$w_f = \frac{T_{vac}^*}{I_{sp}(R)} \quad (\text{lbm/sec})$$

Net thrust force is

$$T = T_{vac}^* - A_e p \quad (\text{lbf})$$

2.4.3

Ramjet Sustainer

The source of ramjet performance data is subroutine PROP11. The equations are based on compressible flow laws of gas dynamics and thermodynamics. The math models employed by PROP11 are those detailed for PROPL in Appendix F. Because the computations produce lengthy computer execution times, the representation of ramjet characteristics has been linearized to reduce the number of times the PROP11 subroutine must be executed. In the course of trajectory

calculations, linear relationships for ramjet performance characteristics are utilized in the equations of motion. The PROP11 subroutine is used only to produce partial derivatives for the linear relationships. Partial derivatives are computed by finite differences.

Ramjet performance linearization is based on the assumptions that performance characteristics are linear functions of flight conditions within a flight condition region. A region is established at the beginning of ramjet powered flight and thereafter is re-established each time a flight condition exceeds a bound of the previous region.

Maximum or minimum thrust engine operation is utilized respectively for climbs or descents. Ramjet thrust coefficient, specific fuel flow, and combustion temperature are represented as linear functions of angle of attack, altitude, and Mach number. Thus for maximum or minimum thrust flight (designated by an input flag),

$$T = \left[C_{F_0} + \frac{\partial C_F}{\partial \alpha} (\alpha - \alpha_0) + \frac{\partial C_F}{\partial h} (h - h_0) \right. \\ \left. + \frac{\partial C_F}{\partial M} (M - M_0) \right] q S$$

$$\omega_F = \left[S_{F_0} + \frac{\partial S_F}{\partial \alpha} (\alpha - \alpha_0) + \frac{\partial S_F}{\partial h} (h - h_0) \right. \\ \left. + \frac{\partial S_F}{\partial M} (M - M_0) \right] q S$$

$$T_{T_4} = T_{T_{4_0}} + \frac{\partial T_{T_4}}{\partial \alpha} (\alpha - \alpha_0) + \frac{\partial T_{T_4}}{\partial h} (h - h_0) \\ + \frac{\partial T_{T_4}}{\partial M} (M - M_0)$$

where performance characteristics are

- T net thrust (lbf)
 C_F net thrust coefficient
 w_f fuel flow (lbm/sec)
 S_F specific fuel flow
 T_{T_4} combustion temperature ($^{\circ}$ R)

and flight conditions are

- α angle of attack (rad)
 h altitude (ft)
 M Mach number

Nominal values of the performance characteristics and flight conditions (values at the "center" of the flight condition region) are denoted by the "0" subscript.

Throttled engine operation is utilized during cruise or during the level-off maneuvers to achieve a desired Mach number. For this case, the required thrust coefficient is an independent variable, and we have

$$w_f = \left[S_{F_0} + \frac{\partial S_F}{\partial \alpha} (\alpha - \alpha_0) + \frac{\partial S_F}{\partial h} (h - h_0) + \frac{\partial S_F}{\partial M} (M - M_0) + \frac{\partial S_F}{\partial C_F} (C_F^* - C_{F_0}) \right] g s$$

$$T_{T_4} = T_{T_{4_0}} + \frac{\partial T_{T_4}}{\partial \alpha} (\alpha - \alpha_0) + \frac{\partial T_{T_4}}{\partial h} (h - h_0) + \frac{\partial T_{T_4}}{\partial M} (M - M_0) + \frac{\partial T_{T_4}}{\partial C_F} (C_F^* - C_{F_0})$$

AD-A048 344

LTV AEROSPACE CORP DALLAS TEX VOUGHT SYSTEMS DIV
SEATIDE ANALYSIS PROCESS. VOLUME IIIB. CRUISE MISSILE - CONCEPT--ETC(U)
JAN 74

F/G 15/7
DAAB09-72-C-0062

NL

UNCLASSIFIED

VSD-00.1636-VOL-3B

2 OF 2
ADI
A048 344

END
DATE
FILMED
2-78
DDC

where C_F^* is the desired thrust coefficient as determined by trajectory considerations, and C_{F_0} is the nominal values for the established flight condition region. Bounds on desired thrust coefficient, which are used to represent maximum and minimum thrust available, are

$$0 \leq C_F^* \leq C_{F_{MAX}}$$

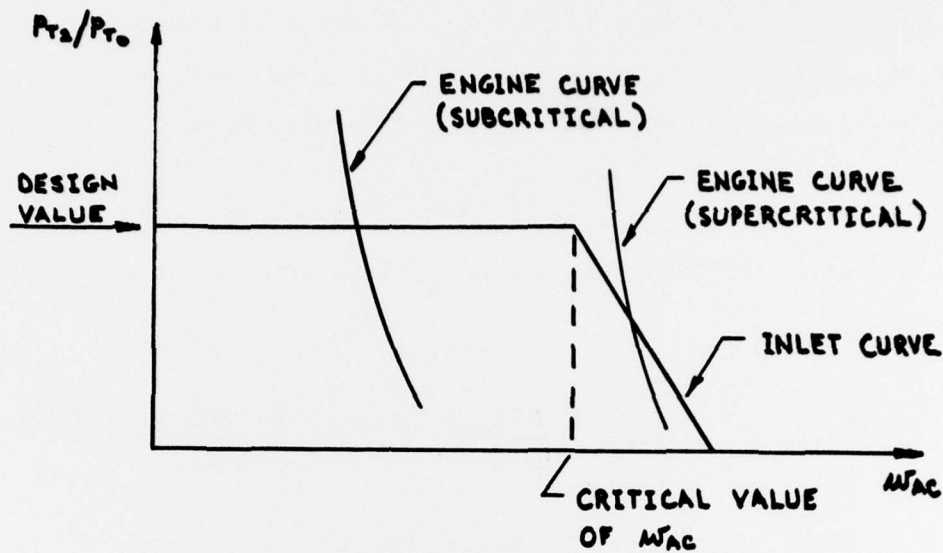
The maximum thrust coefficient must also be represented as a function of flight conditions:

$$C_{F_{MAX}} = C_{F_{MAX_0}} + \frac{\partial C_{F_{MAX}}}{\partial \alpha} (\alpha - \alpha_0) + \frac{\partial C_{F_{MAX}}}{\partial h} (h - h_0) \\ + \frac{\partial C_{F_{MAX}}}{\partial M} (M - M_0)$$

The zero lower limit on net thrust coefficient is generally not representative of the minimum available; negative values are usually achievable during ramjet operation at minimum fuel flow. However, the difference in the zero limit and the achievable negative value should not affect the trajectory to a significant degree for foreseeable applications. The use of a zero limit serves to reduce computer execution time and to ease PROPI convergence difficulties associated with negative thrust coefficients.

2.4.4 Turbojet Sustainer

The calculation of thrust and fuel flow for a turbojet sustainer entails the computation of pressure recovery and corrected airflow which satisfy both the inlet and the engine requirement. For a given engine design, a specified turbine inlet temperature, and flight conditions (Mach number, altitude, and angle of attack), the relationships between pressure recovery ρ_{t2}/ρ_{t0} , the corrected airflow M_{AC} are illustrated in the sketch.



It is seen that if flight conditions and the turbine inlet temperature result in subcritical corrected airflow, the inlet can deliver any corrected air flow less than the critical value at the design pressure recovery. (Critical flow conditions result in a normal shock at the inlet throat; subcritical flow means that the shock is upstream of the throat; and supercritical flow means that the shock is downstream of the throat.) If the engine demands a supercritical corrected airflow, then the engine and inlet relationships must be solved simultaneously for pressure recovery and corrected air flow. The algorithm for the engine corrected air flow requirement as a function of pressure recovery is embodied in GENENG, a subroutine version of the computer program documented in Reference 2. The inlet algorithm is contained in subroutine INLET and is described in Appendix E. Subroutine TJPER controls the calculations performed by INLET and GENENG.

2.5 GRAVITY

The gravitational force per unit mass, acting at the vehicle mass center and directed toward the center of the spherical earth model, is

$$g = g_0 \left(\frac{r_0}{r_0 + h} \right)^2 \quad (\text{ft/sec}^2)$$

- g_0 is zero-altitude standard gravity;
 $32.17405 \text{ ft/sec}^2$
 r_0 is the radius of the spherical earth model;
 $20.9 \times 10^2 \text{ ft}$
 h is vehicle altitude (ft)

2.6 ATMOSPHERIC PROPERTIES

A time and location invariant U.S. Standard 1962 model atmosphere is used to define atmospheric properties including density, pressure, temperature and speed of sound. The standard atmosphere equations are contained in Reference (1).

2.7 ROCKET ENGINE IDEAL VELOCITY

Rocket engine ideal velocity is computed in the course of trajectory computations in order that velocity losses can be quantified. Ideal velocity, the velocity which the vehicle would attain in the absence of atmospheric, gravity, and turning losses, is

$$\Delta V_{ID}(t) = \int_{t_1}^{t_2} \frac{T_{vac}}{m} dt \quad (\text{ft/sec})$$

where

- t_1, t_2 are respectively the rocket engine ignition
 and burnout times (sec)
 T_{vac} is vacuum thrust (lbf)
 m is vehicle mass (slugs)

Total velocity loss may be computed from

$$\Delta V_{loss} = \Delta V_{ID} - [V(t_2) - V(t_1)] \quad (\text{ft/sec})$$

where $V(t_2) - V(t_1)$ is the actual velocity change during rocket engine operation.

2.8

CLIMB SCHEDULE GENERATION

A climb schedule can be generated just before the start of a climb phase if the user selects this optional capability. The climb schedule, which consists of a table of Mach number versus altitude, is part of the phase initialization process accomplished in the MAINS subroutine.

The principal relationships utilized are the equation of motion, Eq. (2-1) and (2-2). The assumptions are made that missile velocity rate \dot{V} , path angle rate $\dot{\gamma}$, and thrust cant angle η are zero and that mass is constant during the climb. The forms of the equations of motions utilized are obtained by solving Eq. (2-1) for $\sin\gamma$ and Eq. (2-2) for α :

$$\sin\gamma = \frac{1}{g} \cdot \frac{T \cos\alpha - D}{m} \quad (2-12)$$

$$\alpha = m \left(g - \frac{V^2}{r} \right) \cos\gamma / (T + C_L \alpha g s) \quad (\text{rad}) \quad (2-13)$$

Maximum rate of climb is obtained by maximizing the quantity $V \sin\gamma$ at each altitude of an array of altitudes encompassing the expected climb path. At each velocity-altitude combination, Eqs. (2-12) and (2-13) are solved simultaneously for the angle of attack and path angle by means of an iterative successive substitutions technique. The search for climb speed, V_{cl} , is limited according to

$$V_{MIN} \leq V_{cl} \leq V_{MAX} \quad (\text{ft/sec})$$

where

V_{cl} = the climb speed (ft/sec)

V_{MAX} = $M_{REF} \times a$ (ft/sec)

M_{REF} is an input reference Mach number
for the phase

a is the local speed of sound (ft/sec)

and

$$V_{MIN} = \text{MAX}(V_1, V_{MAX}/2)$$

V_1 is the speed at the start of the climb phase
(ft/sec)

When the search for climb speed has converged, climb Mach number and the altitude are computed and stored in the climb schedule table.

Because of the assumptions made in formulating the climb schedule generation, limitations on its use should be observed. Obviously a vehicle with a high thrust to weight ratio would not be consistent with the assumption that $\dot{V} = 0$, and in fact thrust-to-weight ratios greater than unity can cause Eq. (2-12) to yield a value for $\sin \gamma$ which is greater than one, a mathematical impossibility. The assumption of constant mass is not normally significant, but it could be significant if a large percentage of the initial mass is consumed during the climb (e.g. a low thrust to weight ratio rocket with an extended climb) or if weight is jettisoned during the climb. For vehicles where these modeling limitations preclude internal climb schedule generation, a climb schedule (Mach No. vs. altitude) can be provided by the user through Option 12 path control (see Section 2.2.12).

3. NUMERICAL METHODS

3.1 RUNGE-KUTTA INTEGRATION WITH ERROR CONTROL

The Runge-Kutta formula used is of fourth-order accuracy in step size h . It is of the form

$$X]_1^2 = X_2 - X_1 = \frac{1}{6} (K_1 + 2K_2 + 2K_3 + K_4)$$

where

X = a dependent variable

$X]_1^2$ = increment in the dependent variable

h_2 = increment in the independent variable t

$$K_1 = h_2 \dot{x}_2(t_1, X_1)$$

$$K_2 = h_2 \dot{x}_2(t_1 + \frac{h_2}{2}, X_1 + \frac{K_1}{2})$$

$$K_3 = h_2 \dot{x}_2(t_1 + \frac{h_2}{2}, X_1 + \frac{K_2}{2})$$

$$K_4 = h_2 \dot{x}_2(t_1 + h_2, X_1 + K_3)$$

A lower-order formula may be found by utilizing the three derivatives at $t = t_0$, t_1 , and t_2 . If $h_1 = t_1 - t_0$ and $h_2 = t_2 - t_1$, the following Lagrangian interpolation formula gives the derivative at any time $t_0 \leq t \leq t_2$:

$$\begin{aligned} \dot{x} &= \frac{\dot{x}_0(t-t_1)(t-t_2)}{h_1(h_1+h_2)} - \frac{\dot{x}_1(t-t_0)(t-t_2)}{h_1 h_2} \\ &+ \frac{\dot{x}_2(t-t_0)(t-t_1)}{h_2(h_1+h_2)} \end{aligned}$$

Integration of this equation from t_1 to t_2 yields

$$X'_1 = \frac{1}{6} \left[\left(\frac{h_2}{h_1} \right)^2 \left(\frac{-h_2}{1+h_2/h_1} \right) \dot{X}_0 + \frac{h_2}{h_1} (h_2 + 3h_1) \dot{X}_1 \right. \\ \left. + \left(2h_2 + \frac{h_2}{1+h_2/h_1} \right) \dot{X}_2 \right]$$

The difference in the increments over the interval h_2 between the Runge-Kutta scheme and the low-order scheme may be divided by a nominal value of the dependent variable \bar{X} to obtain the relative error δ_2 . Thus,

$$\delta_2 = \left| \frac{X'_1 - X'_1}{\bar{X}} \right|$$

The error is expected to vary as approximately the fifth power of h , which leads to

$$\delta = A h^5$$

(where A is a suitable coefficient) or in the logarithmic form

$$\log \delta = A' + 5 \log h$$

where

$$A' = \log A$$

Let it be assumed that A' will vary linearly with t , the variable of integration. Then A' at a time corresponding to t_3 can be found from A' at two previous points t_1 and t_2 as

$$A'_3 = A'_2 + \frac{A'_2 - A'_1}{t_2 - t_1} (t_3 - t_2)$$

and if $h_3 = t_3 - t_2$ and $h_2 = t_2 - t_1$,

$$A'_3 = A'_2 + (A'_2 - A'_1) \frac{h_3}{h_2}$$

and on this basis δ_3 would be predicted to be $A'_3 + 5 \log h_3$.

It is desired that δ_3 should approximate $\bar{\delta}$, the reference error; therefore,

$$\log h_3 = \frac{1}{5} (\log \bar{\delta} - A'_3)$$

Each dependent variable has an associated relative error and would lead to computation of a different step size for each variable; however, the maximum relative error of all variables may be selected for δ . Obviously, inaccurate predictions of step size can occur when the maximum relative error shifts from one variable to another or when any sudden change occurs. When a step size produces an excessively large error ($\delta > \delta_{\text{limit}}$), a reduced step size must be used. It may be obtained from the reference error $\bar{\delta}$ as

$$h_3 = \exp \left[\frac{1}{5} \log \bar{\delta} - A'_2 \right]$$

3.1.1 Starting the Integration

The Runge-Kutta scheme is simple to start, since integration from X_n to X_{n+1} requires no knowledge of X prior to X_n . Since the error control coefficient A has no value at $t=0$, however, a prediction of the second step size is difficult. To overcome this difficulty, two equal size first steps may be made before checking the error. The A for the first step may be arbitrarily set equal to the A for the second step so that h_3 may be predicted. The low-order integration scheme equation in this case becomes, with $h_2 = h_1$,

$$X'_1 = \frac{h_1}{3} (\dot{X}_0 + 4\dot{X}_1 + \dot{X}_2)$$

3.1.2 Failures

Should two consecutive predictions of the same step fail to produce an error δ less than δ_{limit} , a return to the starting procedure will be made with a third prediction on step size, which is no larger than one-half of the second estimate. The step-size control described here will operate stably with nearly constant error per step only for a well-behaved function. For most problems it will repeat a step occasionally to

reduce a large error, and on sharp corners it will restart. This action is not regarded as objectionable. The objective is to attain a desired level of accuracy with a minimum total number of steps.

3.1.3 Variables of Integration for This Application

The array of variables of integration \mathbf{X} and their normalization values \bar{X} are shown in Table 1. The numbers identifying the variable locations in the array correspond to the column headed by NERR in the trajectory time history output. Thus NERR identifies the variable having the maximum normalized truncation error.

TABLE 1 VARIABLES OF INTEGRATION

Location In X Array	Variable	Definition	Normalization Value \bar{X}
1	t	time (sec)	1,000.0
2	γ	flight path angle (rad)	1.0
3	v	velocity (ft/sec)	5,000.0
4	h	altitude (ft)	100,000.0
5	R	range (ft)	1,000,000.0
6	w	mass (lbm)	1,000.0
7	V_{ID}	ideal velocity (ft/sec)	1,000.0

3.2 NEWTON-RAPHSON PROCEDURE

A Newton-Raphson procedure is used in several instances to solve a non-linear equation for the independent variable. Specifically, the Newton-Raphson method is used to:

- (a) Find the time at which a phase should terminate when a dependent variable stop is employed.
(RUNGE K subroutine)
- (b) Find the angle of attack required to satisfy a given path angle rate. (XALPH1 subroutine)

(c) Find the angle of attack required to satisfy a given normal acceleration. (XALPH2 subroutine)

(d) Find the angle of attack required to satisfy a path angle rate which varies during the iteration.

(DERIV subroutine, ICONT = 2 option)

Let the independent variable be denoted by x , and let the non-linear function of x be $y(x)$. The condition to be satisfied is

$$f(x) = y^* - y(x) = 0$$

where y^* is the desired value of y . The derivative of $f(x)$ is found by finite differences to be

$$f'(x) = \frac{f(x_n) - f(x_{n-1})}{x_n - x_{n-1}}$$

The next guess for x is

$$x_{n+1} = x_n - \frac{f}{f'}$$

The process is repeated until f is within a given tolerance of zero.

4. SUBMODEL STRUCTURE

The principal subroutines, their primary functions, and the flow between them are illustrated in Figure 3. All subroutines are not shown; e.g., subroutines XALPH1 and XALPH2 used for angle of attack iterative solutions by DERIV, subroutines used in support of PROP1, the ramjet performance subroutine, and FORTRAN supplied subroutines are omitted.

All subroutines used which are not FORTRAN supplied are listed and briefly described in Table 2.

TABLE 2 VEHPER SUBROUTINES

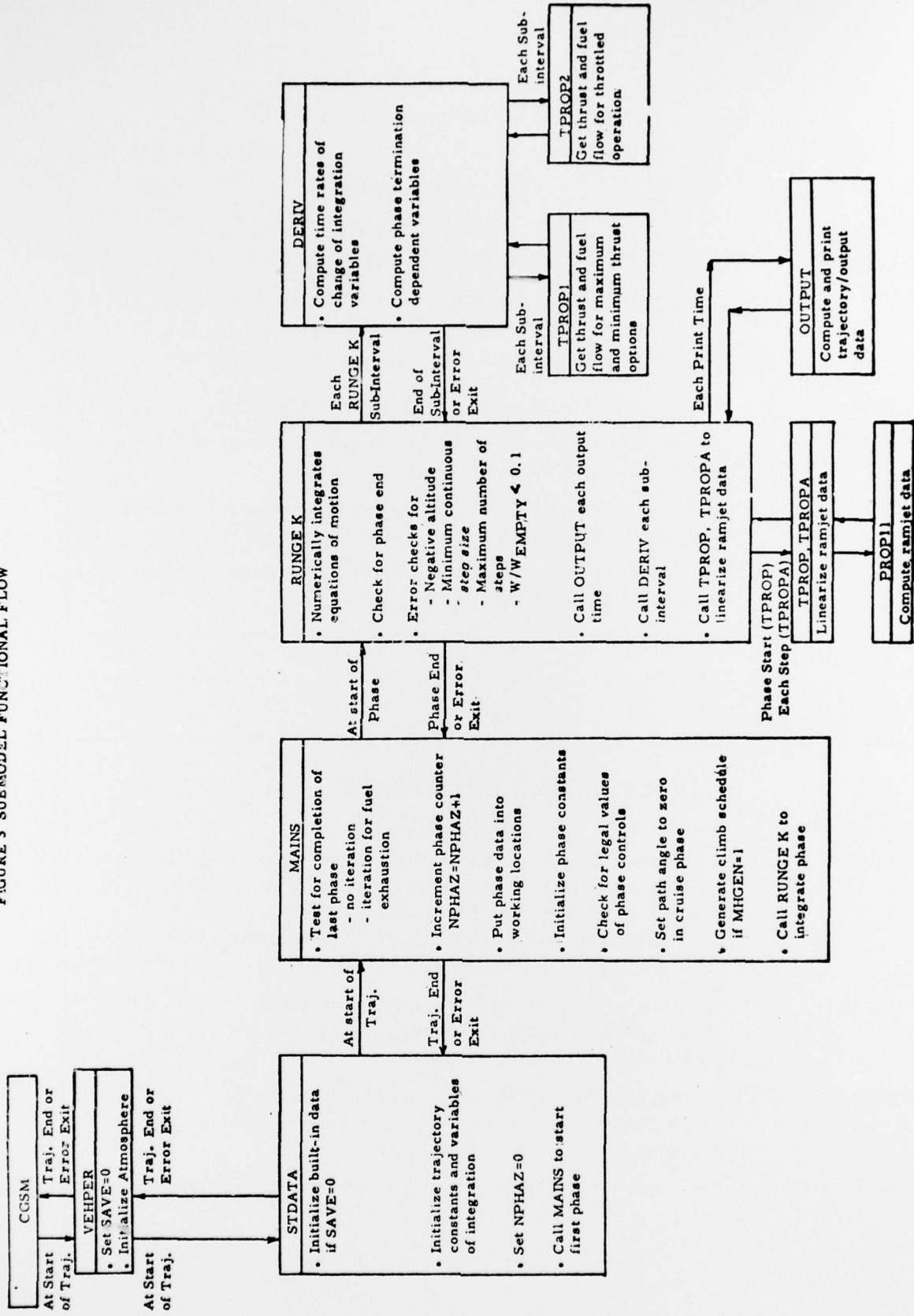
<u>Trajectory Related Subroutines</u>	
<u>NAME</u>	<u>DESCRIPTION</u>
AIR1	Initializes atmosphere computations
AIR	Gets atmospheric properties on trajectory (an AIR1 entry point)
DERIV	Computes derivatives of integration variables
DSLINE	Linear interpolation for functions of two independent variables
ERROUT	Not Used
MAINS	Initializes phase
OUTPUT	Prints trajectory time history
RUNGEK	Integrates simultaneous first-order differential equations
STDATA	Initializes trajectory
SLINE	Linear interpolation for functions of a single independent variable
TPROP	TPROP has four entry points. TPROP entry point initializes linearized ramjet model.
TPROPA	Entry point tests flight conditions for region bounds
TPROP1	Entry point gets maximum or minimum thrust engine performance
TPROP2	Entry point gets throttleable engine performance
XALPH1	Uses Newton-Raphson method to get angle of attack
XALPH2	Finds angle of attack and thrust required to satisfy normal and tangential accelerations
VEHPER	Starts trajectory computation by calling STDATA

TABLE 2 (Continued)

<u>Ramjet Propulsion Subroutines</u>	
<u>NAME</u>	<u>DESCRIPTION</u>
DTRGET	Determine temperature rise by table look-up
ISEN	Determines real gas total temperature and pressure from static temperature and pressure
MACHNO	Determine Mach No. from area ratio change
PROP11	Principal ramjet performance subroutine
RGAMER	Determines ratio of specific heats (gamma) and gas constant from table look-up
TLU1	Performs linear interpolation for functions of a single independent variable
TLU2	Performs linear interpolation for functions of two independent variables

<u>Turbojet Propulsion Subroutines</u>	
<u>NAME</u>	<u>DESCRIPTION</u>
TJPER	Computes turbojet off-design performance (thrust and fuel flow) as a function of flight conditions (angle-of-attack, altitude, and Mach No.) and thrust required. The principal function of TJPER is to match inlet airflow and pressure recovery to the engine requirement.
GENENG	A package of subroutines which for given flight conditions and pressure recovery, computes thrust, fuel flow, and corrected airflow
INLET	A package of subroutines which for given flight conditions and corrected airflow, computes inlet pressure recovery

FIGURE 3 SUBMODEL FUNCTIONAL FLOW



5. REFERENCES

1. "U. S. Standard Atmosphere, 1962," U. S. Government Printing Office
2. National Aeronautics and Space Administration NASA TN D-6552, "GENENG - A Program for Calculating Design and Off-Design Performance for Turbojet and Turbofan Engines", by R. W. Koenig and L. H. Fishbach, February 1972.